Alfred Wegener Institute for Polar and Marine Research, Research Unit Potsdam
Working Group "Periglacial Dynamics"

Characterisation and evolution of periglacial landscapes in Northern Siberia during the Late Quaternary – Remote sensing and GIS studies

Dissertation
zur Erlangung des akademischen Grades
„doctor rerum naturalium"
(Dr. rer. nat.)
in der Wissenschaftsdisziplin „Geologie"

eingereicht an der
Mathematisch-Naturwissenschaftlichen Fakultät
der Universität Potsdam

von
Guido Grosse

Potsdam, März 2005

Table of contents

Abstract

About 24 % of the land surface in the northern hemisphere are underlayed by permafrost in various states. Permafrost aggradation occurs under special environmental conditions with overall low annual precipitation rates and very low mean annual temperatures. Because the general permafrost occurrence is mainly driven by large-scale climatic conditions, the distribution of permafrost deposits can be considered as an important climate indicator. The region with the most extensive continuous permafrost is Siberia. In northeast Siberia, the ice- and organic-rich permafrost deposits of the Ice Complex are widely distributed. These deposits consist mostly of silty to fine-grained sandy sediments that were accumulated during the Late Pleistocene in an extensive plain on the then subaerial Laptev Sea shelf. One important precondition for the Ice Complex sedimentation was, that the Laptev Sea shelf was not glaciated during the Late Pleistocene, resulting in a mostly continuous accumulation of permafrost sediments for at least this period. This shelf landscape became inundated and eroded in large parts by the Holocene marine transgression after the Last Glacial Maximum. Remnants of this landscape are preserved only in the present day coastal areas.

Because the Ice Complex deposits contain a wide variety of palaeo-environmental proxies, it is an excellent palaeo-climate archive for the Late Quaternary in the region. Furthermore, the ice-rich Ice Complex deposits are sensible to climatic change, i.e. climate warming. Because of the large-scale climatic changes at the transition from the Pleistocene to the Holocene, the Ice Complex was subject to extensive thermokarst processes since the Early Holocene.

Permafrost deposits are not only an environmental indicator, but also an important climate factor. Tundra wetlands, which have developed in environments with aggrading permafrost, are considered a net sink for carbon, as organic matter is stored in peat or is syn-sedimentary frozen with permafrost aggradation. Contrary, the Holocene thermokarst development resulted in permafrost degradation and thus the release of formerly stored organic carbon. Modern tundra wetlands are also considered an important source for the climate-driving gas methane, originating mainly from microbial activity in the seasonal active layer.

Most scenarios for future global climate development predict a strong warming trend especially in the Arctic. Consequently, for the understanding of how permafrost deposits will react and contribute to such scenarios, it is necessary to investigate and evaluate ice-rich permafrost deposits like the widespread Ice Complex as climate indicator and climate factor during the Late Quaternary. Such investigations are a pre-condition for the precise modelling of future developments in permafrost distribution and the influence of permafrost degradation on global climate.

The focus of this work, which was conducted within the frame of the multi-disciplinary joint German-Russian research projects “Laptev Sea 2000“ (1998-2002) and “Dynamics of Permafrost“ (2003-2005), was twofold. First, the possibilities of using remote sensing and terrain modelling techniques for the observation of periglacial landscapes in Northeast Siberia in their present state was evaluated and applied to key sites in the Laptev Sea coastal lowlands. The key sites were situated in the eastern Laptev Sea (Bykovsky Peninsula and Khorogor Valley) and the western Laptev Sea (Cape Mamontovy Klyk region). For this task, techniques using CORONA satellite imagery, Landsat-7 satellite imagery, and digital elevation models were developed for the mapping of periglacial structures, which are especially indicative of permafrost degradation. The major goals were to quantify the extent of permafrost degradation structures and their distribution in the investigated key areas, and to establish techniques, which can be used also for the investigation of other regions with thermokarst occurrence. Geographical information systems were employed for the mapping, the spatial analysis, and the enhancement of classification results by rule-based stratification. The results from the key sites show, that thermokarst, and related processes and structures, completely re-shaped the former accumulation plain to a strongly degraded landscape, which is characterised by extensive deep depressions and erosional remnants of the Late Pleistocene surface. As a results of this rapid process, which in large parts happened within a short period during the Early Holocene, the hydrological and sedimentological regime was completely changed on a large scale. These events resulted also in a release of large amounts of organic carbon. Thermokarst is now the major component in the modern periglacial landscapes in terms of spatial extent, but also in its influence on hydrology, sedimentation and the development of vegetation assemblages.

Second, the possibilities of using remote sensing and terrain modelling as a supplementary tool for palaeo-environmental reconstructions in the investigated regions were explored. For this task additionally a comprehensive cryolithological field database was developed for the Bykovsky Peninsula and the Khorogor Valley, which contains previously published data from boreholes, outcrops sections, subsurface samples, and subsurface samples, as well as additional own field data. The period covered by this database is mainly the Late Pleistocene and the Holocene, but also the basal deposits of the sedimentary sequence, interpreted as Pliocene to Early Pleistocene, are contained. Remote sensing was applied for the observation of periglacial strucures, which then were successfully related to distinct landscape development stages or time intervals in the investigation area. Terrain modelling was used for providing a general context of the landscape development. Finally, a scheme was developed

describing mainly the Late Quaternary landscape evolution in this area. A major finding was the possibility of connecting periglacial surface structures to distinct landscape development stages, and thus use them as additional palaeo-environmental indicator together with other proxies for area-related palaeo-environmental reconstructions. In the landscape evolution scheme, i.e. of the genesis of the Late Pleistocene Ice Complex and the Holocene thermokarst development, some new aspects are presented in terms of sediment source and general sedimentation conditions. This findings apply also for other sites in the Laptev Sea region.

Kurzfassung

Etwa 24 % der Landoberfläche der Nordhemisphäre sind von Permafrost in verschiedenem Zustand unterlagert. Permafrost bildet sich unter besonderen Umweltbedingungen mit prinzipiell geringen Jahresniederschlägen und sehr niedrigen mittleren Jahrestemperaturen. Da die generelle Verbreitung von Permafrost hauptsächlich von großräumigen Klimabedingungen bestimmt ist, kann Permafrost als wichtiger Klimaindikator betrachtet werden. Sibirien ist die größte zusammenhängende Region mit kontinuierlichem Permafrost. Besonders in Nordostsibirien sind als Eiskomplex bezeichnete eis- und organikreiche Permafrostablagerungen weit verbreitet. Diese Ablagerungen bestehen größtenteils aus schluffigen bis feinsandigen Sedimenten, die während des Spätpleistozäns in einer ausgedehnten Ebene auf dem in dieser Zeit subaerischen Laptevsee-Schelf akkumuliert wurden. Die fehlende Vergletscherung des Laptevsee-Schelf während des Spätpleistozäns ermöglichte in diesem Zeitraum eine weitestgehend ununterbrochene Sedimentation und war damit eine wichtige Vorraussetzung für die Eiskomplexakkumulation. Nach dem Letzten Glazialen Maximum wurde diese Schelflandschaft größtenteils von der holozänen marinen Transgression überschwemmt und erodiert. Überreste dieser Landschaft sind nur noch in den heutigen Küstengebieten erhalten.

Der Eiskomplex enthält eine Reihe von Paläoumwelt-Indikatoren, die ihn zu einem exzellenten Paläoklimaarchiv für das Spätquartär in der Region machen. Die eisreichen Eiskomplexablagerungen reagieren überdies sensibel auf Klimaveränderungen, insbesondere auf Klimaerwärmung. Durch die weitreichenden Klimaveränderungen während des Übergangs vom Pleistozän zum Holozän war der Eiskomplex seit dem frühen Holozän intensiven Thermokarstprozessen ausgesetzt.

Permafrostablagerungen sind aber nicht nur ein Klima- und Umweltindikator, sondern auch ein wichtiger Klimafaktor. Tundrenfeuchtgebiete, die sich in Permafrostgebieten entwickelten, werden als Nettosenke für Kohlenstoff angesehen, da organisches Material in

Form von Torf oder durch synsedimentäres Einfrieren mit der fortschreitenden Permafrostaggradation gebunden wird. Die beschriebene holozäne Thermokarstentwicklung führte zu umfangreicher Permafrostdegradation und damit zu einem Freisetzen des vorher gebundenen organischen Kohlenstoffs. Moderne Tundrenfeuchtgebiete werden ebenfalls als wichtige Quelle für das Treibhausgas Methan angesehen, das hauptsächlich von mikrobiellen Aktivitäten in der saisonalen Auftauschicht des Permafrosts gebildet wird.

Die meisten Szenarios zu zukünftigen Klimaentwicklungen sagen einen starken Erwärmungstrend besonders in der Arktis voraus. Für das Verständnis, wie Permafrostablagerungen darauf reagieren und selbst zu solchen Szenarien beitragen, ist es deshalb notwendig, eisreiche Permafrostablagerungen (wie den weit verbreiteten Eiskomplex) zu untersuchen und ihre Bedeutung als Klimaindikator und Klimafaktor während des Spätquartärs einzuschätzen. Solche Untersuchungen sind eine Vorraussetzung für das genaue Modellieren zukünftiger Entwicklungen in der Permafrostverbreitung und des Einflusses von Permafrostdegradation auf das globale Klima.

Diese Arbeit, die im Rahmen der multidisziplinären Deutsch-Russischen Verbundprojekte „Laptevsee 2000“ (1998-2002) und „Dynamik des Permafrost“ (2003-2005) erstellt wurde, konzentrierte sich auf zwei Schwerpunkte. Zum einen wurden die Möglichkeiten der Nutzung von Fernerkundung und Geländemodellierung für die Untersuchung periglazialer Landschaften in Nordostsibirien in ihrem gegenwärtigen Zustand evaluiert und auf zwei Schlüsselgebiete im Küstentiefland der Laptevsee angewandt. Die betreffenden Studiengebiete befanden sich in der östlichen Laptevsee (Bykovsky-Halbinsel und Khorogor-Tal) und in der westlichen Laptevsee (die Region um das Kap Mamontov Klyk). Für diese Aufgabe wurden Techniken für die Nutzung von CORONA und Landsat-7 Satellitenbildern sowie von Geländemodellen zur Kartierung periglazialer, Permafrostdegradation-anzeigender Strukturen entwickelt. Hauptziele waren die Quantifizierung von Ausmaß und Verbreitung dieser Permafrostdegradations-Strukturen, sowie die Entwicklung von Techniken, die die Untersuchungen auch auf andere Gebiete mit Thermokarsterscheinungen ausdehnen lassen. Geographische Informations-Syteme wurden für die Kartierung, die räumliche Analyse und die Verbesserung von Klassifikationsergebnissen durch regelbasierte Stratifizierung angewandt. Die Ergebnisse aus den Schlüsselgebieten zeigen, dass Thermokarst und damit verbundene Prozesse und Strukturen die ehemalige Akkumulationsebene zu einer stark degradierten Landschaft umgeformt haben, die durch ausgedehnte Thermokarstsenken und erosive Überreste der ehemaligen Spätpleistozänen Oberfläche charakterisiert ist. Als Ergebnis dieser hauptsächlich innerhalb einer kurzen Periode im Frühholozän abgelaufenen

Prozesse wurde das hydrologische und sedimentäre Regime vollkommen und in großem Maßstab verändert. Diese Ereignisse führten auch zur Freisetzung großer Mengen organischen Kohlenstoffs. Thermokarst ist heute bezüglich des Flächenanteils die Hauptkomponente dieser Periglaziallandschaften, aber auch in seinem Einfluss auf die Hydrologie, Sedimentation und die Entwicklung von Vegetationskomplexen.

Der zweite Schwerpunkt der Arbeit lag in der Auslotung der Möglichkeiten, Fernerkundung und Geländemodellierung als unterstützende Methode für die Paläoumweltrekonstruktion zu nutzen. Dafür wurde zusätzlich für die Region Bykovsky-Halbinsel und Khorogor-Tal eine umfangreiche cryolithologische Felddatenbank entwickelt, die bereits veröffentlichte Daten zu Bohrlöchern, Aufschlussprofilen, Schurfen und Oberflächenproben, sowie zusätzliche eigene Felddaten enthält. Mit dieser Datenbank wird hauptsächlich der Sedimentationszeitraum des Spätpleistozän abgedeckt, doch sind auch in Bohrungen aufgeschlossene basale Ablagerungen der Sedimentsequenz enthalten, die als Pliozän-Frühpleistozän interpretiert werden.

Fernerkundung wurde für die Untersuchung periglazialer Strukturen angewandt, die danach erfolgreich bestimmten Landschaftsentwicklungsphasen im Untersuchungsgebiet oder Zeitintervallen zugeordnet werden konnten. Geländemodellierung wurde für die Bereitstellung eines generellen Kontexts für die Landschaftsentwicklung genutzt. Letztendlich wurde ein Schema entwickelt, das die spätquartäre Landschaftsentwicklung in dieser Region beschreibt. Ein Hauptergebnis dieser Studie belegt, das es möglich ist, periglaziale Oberflächenstrukturen mit bestimmten Landschaftsentwicklungsstadien in Verbindung zu bringen, und diese damit als zusätzlich Paläoumweltindikator zusammen mit anderen Indikatoren für eine flächenbezogene Paläoumweltrekonstruktion zu nutzen. Mit dem Landschaftsentwicklungsschema werden einige neue Aspekte in Bezug auf Sedimentursprung und genereller Sedimentationsbedingungen insbesondere für die Genese des spätpleistozänen Eiskomplex und der holozänen Thermokarstentwicklung präsentiert. Diese Ergebnisse lassen sich auch auf weitere Lokalitäten in der Laptevsee-Region anwenden.

1. Introduction

1.1 Scientific background

1.1.1 Permafrost and permafrost distribution

Periglacial environments are non-glacial landscapes dominated by frost-action and permafrost-related processes (French, 1996). Permafrost is defined as any ground, which experiences temperatures at or below 0°C for at least two or more consecutive years (Everdingen, 1998). According to this definition, about 24 % of the exposed landsurface of the northern hemisphere is underlain by permafrost (Zhang et al., 1999). The distribution of permafrost is classified into regions of continuous, discontinuous, isolated or sporadic permafrost occurence, depending mainly on latitude, altitude and local conditions (Figure 1-1) (Everdingen, 1998). On the northern hemisphere, continuous lowland permafrost is widely distributed especially at the high latitude regions of Siberia, Canada, and Alaska.

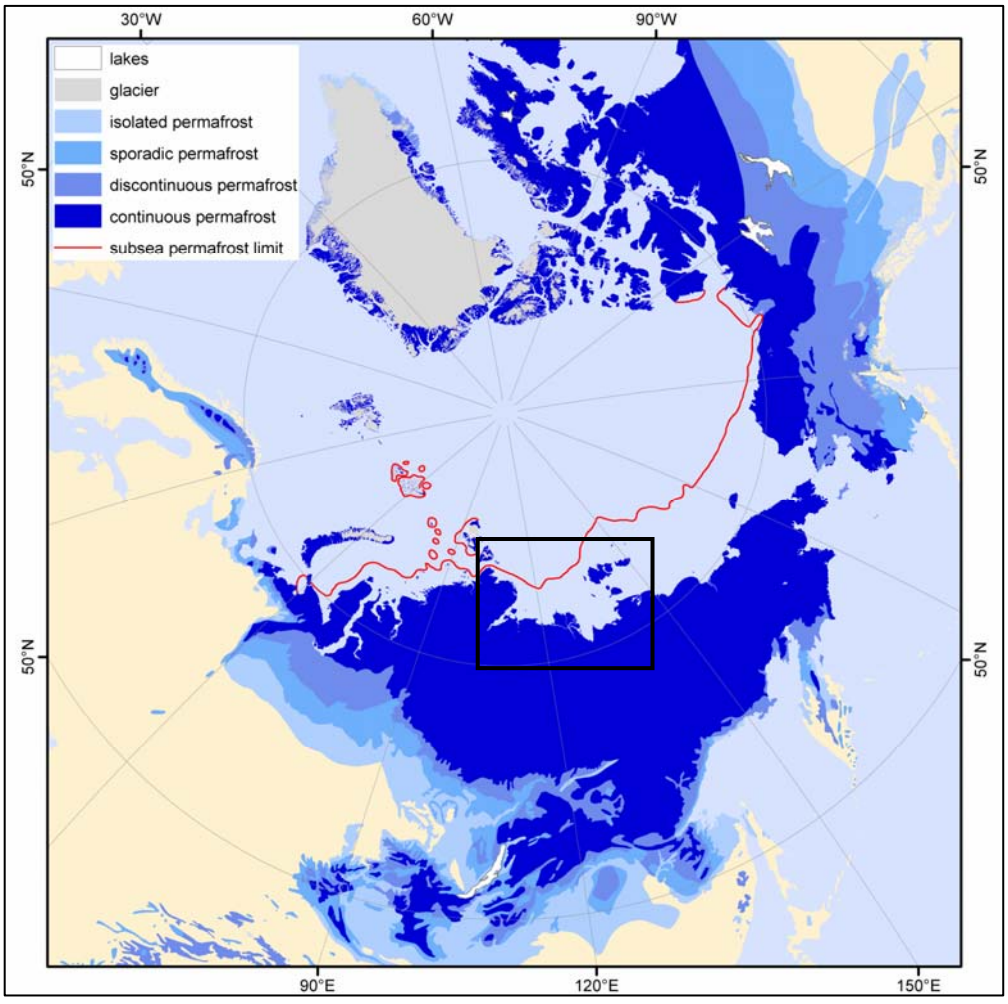

Figure 1-1: Distribution of different permafrost types on the northern hemisphere and location of the Laptev Sea region (black rectangle) (map produced with data from Brown et al., 1998b).

By its definition, permafrost is also a climate indicator (Washburn, 1980; French, 1999). The existence of permafrost is connected to relatively low precipitation rates and air temperatures below zero for about 75 % of the year (Washburn, 1979). The large scale spatial and temporal variation of permafrost distribution is mainly driven by climatic conditions. The existence of deep permafrost is an evidence for long-term, cold climatic conditions in a region. The region with the most extensive occurrence of continuous permafrost is Siberia, where permafrost depths of up to 1500 m are known (Yershov, 1998) and the oldest permafrost indications in the form of ground wedges and ice wedge pseudomorphs are assigned to Pliocene deposits in the Kolyma basin (Kaplina, 1981). Permafrost deposits often contain high amounts of ground ice, which occurs in the form of segregated ice, ice bands, ice wedges or other massive ice bodies. Especially from Siberia permafrost deposits are known, which have extreme high ice contents and form ice-supersaturated permafrost deposits, the so-called “Ice Complex” (IC).

1.1.2 Permafrost in the Quaternary

Arctic permafrost regions are highly sensitive geosystems. Whereas continuous low precipitation and extremely low winter temperatures lead to an aggradation of permafrost, a change in these climatic frame conditions can rapidly result in the degradation of permafrost. This happened repeatedly in many Arctic and Subarctic regions during the recurring climatic changes of the Quaternary (e.g. Kondratjeva et al., 1993; Vandenberghe & Pissart, 1993; Rozenbaum & Shpolyanskaya, 1998; Yershov, 1998; Eissmann, 2002). Large areas of the non-glaciated parts of the northern hemisphere were dominated by permafrost during the glacial stages. The climate driven cooling of the upper lithosphere led to permafrost formation in the marginal regions of the continental ice shields and to permafrost aggradation even in lower latitudes of central North America, central Europe, the Russian Plain and the Siberian Lowlands. During the interglacials, the climate warming caused a temperature disequilibrium in many of the extensive permafrost grounds, forcing permafrost into the state of degradation. Permafrost dominated areas were strongly reduced in extent, and retreated to regions in high latitudes and high altitudes, where cold conditions remained. Thermally controlled degradation processes like thermokarst, thermo-erosion and thermo-abrasion of ice-rich permafrost deposits are dominant during such transition periods. These periglacial processes are strongly and rapidly changing the local and regional geocryology, geomorphology, and hydrology, which again results in changes of biocoenoses as well as energy and matter fluxes (e.g. Czudek & Demek, 1970; Are, 1999; Romanovskii et al., 2000; Jorgenson et al., 2001). The information about such climate controlled transformations of permafrost landscapes is often well preserved in frozen deposits.

1.1.3 Permafrost as palaeoclimate archive

The impacts of drastic environmental changes and interactions between individual processes in high latitudes during the Quaternary are still poorly understood. Therefore, it is necessary to investigate past climatic variations and their consequences on permafrost in the Arctic.

Many of the sedimentary permafrost deposits in these regions are excellent multi-proxy palaeo-environmental archives (e.g. Vasil'chuk, 1991; Kienel et al., 1999; Andreev, 2001; Brigham-Grette, 2001; Eisner et al., 2005). In north-central Siberia, ice-rich permafrost deposits of the Ice Complex are widely distributed (Romanovskii, 1993) and provide detailed information about the regional environmental history of the Late Pleistocene. The genesis and palaeo-environmental information contained in Ice Complex deposits in these regions is investigated since about 50 years by russian researchers (e.g. Romanovskii, 1958a, b; Grigoriev, 1966; Tomirdiaro, 1970, 1980; Ivanov, 1972; Kaplina, 1981; Konishev & Kolesnikov, 1981; Tomirdiaro et al., 1984; Kaplina & Lozhkin, 1985; Tomirdiaro & Chernenky 1987; Grigoriev, 1993; Fartychev, 1993; Slagoda, 1991, 1993; Kunitsky 1989, 1998; Nikolsky et al., 1999). Since several years multi-disciplinary Russian-German projects are focussing on this topic (Andreev et al., 2002; Kunitsky et al., 2002; Meyer et al., 2002a, b; Schirrmeister et al., 2002a, b; Siegert et al., 2002; Schwamborn et al., 2002a; Schirrmeister et al., 2003a; Sher et al., 2005). In some locations the permafrost records cover at least the last 200.000 years (Schirrmeister et al., 2002c; Andreev et al., 2004). Important climate proxies found in these deposits are sedimentary and geocryologic facies conditions, the isotopic composition of ground ice and a wide variety of palaeontological records. The fossil remains, like pollens, plant macro remains, aquatic microfossils, insect remains, rodent remains, as well as mammal bones and soft tissues are often excellently preserved in the frozen sediments. The possibility of a multi-proxy approach for palaeoenvironmental reconstructions, which is delivering a wide range of environmental parameters, makes these deposits unique climate archives for Siberia. Although permafrost deposits do not have a high resolution like the classical records, their environmental records are supplementing the Eurasian high latitude archives consisting of marine records from the Pacific, Atlantic and Arctic Ocean, the glacial records of the Greenland, Svalbard and Severnaya Zemlya ice caps and the lacustrine records of e.g. the lakes Baikal and Elgygytgyn.

1.1.4 Permafrost and changing climate

Climatic changes can have an enormous influence on the distribution and state of permafrost. This is verified by palaeo-records covering the phases of transition between glacials and interglacials as shown above and by studies of recent interactions between climatic changes and permafrost landscapes (e.g. Pavlov, 1994; Allard, 1996; Fedorov, 1996; Li et al., 1998; Osterkamp & Romanovsky, 1999; Payette et al., 2004). But the main processes and mechanisms of the interaction between permafrost, atmosphere and climate are still insufficiently explained.

The recently published report on Arctic Climate Impact Assessment (ACIA, 2004) summarises major findings of Arctic change research over the last decades and illustrates future climatic trends. Generally, a trend towards a warmer Arctic within the next decades is predicted. The report demonstrates possible consequences of a global warming scenario on high latitude environments and the resulting social and economical impacts. Supported by studies covering the last decades or centuries, the main predictions affecting permafrost are:

- Annual mean temperatures increase with higher rates than in lower latitudes.
- Precipitation increases and winters become shorter and warmer.
- Snow cover extent and duration decreases.
- Vegetation zones migrate northward.
- Permafrost temperatures, active layer depth and thermokarst activity increases.
- Wetlands will shift due to changing hydrological conditions.
- The southern permafrost boundary will migrate northward by several 100 km.

Additionally, permafrost is not only reacting on climate changes, it is also a major agent in climate forcing. Tundra wetland ecosystems with underlying permafrost are considered to be a net sink for carbon, as organic matter is stored as peat, or is syn-sedimentary frozen and removed from the active carbon cycle (Smith et al., 2004). Contrary, modern permafrost landscapes, which are subject to thermo-denudation and changing hydrological conditions, are an important source of methane (Christensen, 1993; Semiletov et al., 1996; Zimov et al., 1997; Smith et al., 2004). This methane is mainly produced by microbial activity, decomposing the organic remains in thawing permafrost deposits, especially in the wet and anaerob parts of the active layer (e.g. Conrad, 1989; Wagner et al., 2003). It is important to determine the contribution of such processes under scenarios of further climate warming and intensified permafrost thawing (Gorham, 1991; Christensen, 1995; Chapin et al., 2000;

Callaghan et al., 2004). Therefrom some questions arise: How much permafrost has degraded since the Last Glacial Maximum, how much organic matter was released by permafrost thawing? And how will permafrost areas be influenced by predicted future climate warming? Especially the balance of energy and matter fluxes for these landscapes is still a big variable in global climate modelling.

1.2 Aims and approaches

1.2.1 Basic ideas

The development of the modern landscapes in the North Siberian permafrost regions was and is determined mainly by climatic parameters. The permafrost deposits and the periglacial landscapes contain information on climatic changes in the past, and their analysis is necessary for understanding the past changes and useful for the prediction of future climate-induced trends in periglacial environments. Whereas the ice-rich permafrost deposits and lacustrine deposits of North Siberia are investigated with classical methods of palaeo-environmental reconstuction at key locations, it is desirable to use additional techniques for the up-scaling of these local results, for the extraction of environmental information preserved in the landscape morphology itself, and for providing a regional context of the results. Such tasks require techniques and methods for area-related analyses. Adequate techniques include remote sensing (RS) and geo-information systems (GIS). The application and combination of these techniques is just in the beginning for Arctic periglacial landscapes, since qualified sensors and software became available in the last years only. Recent methodical approaches for the application of RS or GIS in Arctic periglacial environments include mapping and modelling of vegetation (Joria & Jorgenson, 1996; Walker, 1999; Brook & Kenkel, 2002; Hope et al., 2003; Stow et al., 2004; Virtanen et al., 2004), geology (Etzelmüller et al., 2001; Bartsch et al., 2004; Lorenz, 2004), geomorphology (Ermolin et al., 2002; Luoto & Seppälä, 2003), hydrology (Sellmann, 1975; Yoshikawa & Hinzman, 2003), and permafrost or thermokarst features (Pollard & French, 1980; Morrissey et al., 1986; Lewkowicz & Duguay, 1999; Hinkel et al., 2003; Jorgenson et al., 2001; Beaulieu & Allard, 2003).

Because of the wide extent and the characteristics of periglacial tundra landscapes in Northern Siberia, RS provides an ideal tool for large scale observations of various periglacial phenomena. The modern thermo-denudation relief is easily visible in imagery from optical satellite sensors and a variety of periglacial structures can be identified.

Using GIS as integrator for various data types (raster, vector) and sources (satellite data, field data, elevation data, thematic maps), the periglacial phenomena of large regions can be

analysed in detail in terms of their surface and subsurface properties, spatial extent, morphometry, distribution or relations to each other. Additionally, temporal changes can be observed, when using multi-temporal data. Hence, applying these techniques, it is possible to make conclusions on quality and quantity of periglacial phenomena and their role in periglacial landscape development. These analyses form a basis for the characterisation and a comprehensive perception of periglacial landscape evolution in North Siberia, as well as for balancing energy and matter fluxes and landscape change.

There are three general research topics, for which this thesis provides basic information:

- Characterisation of periglacial terrain and surfaces types in key areas and determination of their spatial distibution as a basis for balancing energy and matter fluxes
- Quantification of landscape change due to rapid geological and geomorphological processes like thermokarst or thermo-erosion
- Reconstruction of the evolution of periglacial landscapes in key areas of the Laptev Sea during the Late Quaternary

To support these general aims, several individual research objects are accounted for in this thesis:

- Development and application of remote sensing techniques for the analysis of periglacial landscapes in North Siberia, using spatially high-resolution satellite data (CORONA) and multispectral satellite data (Landsat-7 ETM+)
- Analysis of the satellite data for two key areas in the Laptev Sea coastal lowland, with a focus on terrain that is affected by thermo-denudation
- Development of appropriate elevation models (DEM) for terrain analysis in both key areas
- Spatial analysis of the resulting data with GIS, focussing on morphology, distribution, and quantification of Holocene thermokarst
- Collection of ground data, focussing on surface properties of periglacial landscape units and cryo-lithological composition of the key areas
- Application of the resulting data for supplementation, enhancement, and regionalisation of local palaeo-environmental reconstructions derived from Late Pleistocene and Holocene deposits in the key areas, and derivation of a landscape genesis model

1.2.2 Field work

The field work was part of the Russian-German research cooperation “System Laptev Sea”. This multi-disciplinary research cooperation mainly focuses on the modern and palaeo-environmental conditions in marine and terrestrial parts of the Laptev Sea region. Several major research projects have been conducted within this frame, such as LAPTEV SEA SYSTEM (1994-1997), TAYMYR (1994-1997) (both: Kassens et al., 1999), SYSTEM LAPTEV SEA 2000 (1998-2002) (Rachold, 2002; Bauch & Kassens, in press), and DYNAMICS OF PERMAFROST (2003-2005). Own field work for his thesis was conducted in two field seasons during the summers 2002 and 2003. The region of Tiksi, including the Khorogor Valley and the Bykovsky Peninsula, was investigated during the Expedition “Lena - New Siberian Islands 2002” (Grigoriev et al., 2003). The region of Cape Mamontov Klyk was investigated during the expedition “Lena – Anabar 2003” (Schirrmeister et al., 2004).

1.3 Study area

1.3.1 Geography of the Laptev Sea region

The study areas are located in the coastal lowlands of the Laptev Sea (Figure 1-2). The Laptev Sea is situated at the northern Eurasian continental margin of Russia (Figure 1-1). The region encompasses some coastal mountain ranges, the coastal lowlands and a shallow shelf sea between the Taymyr Peninsula in the west, the Yakutian-Siberian mainland in the south and the New Siberian Islands in the east (Figure 1-2). The region belongs to the zone of continuous permafrost and mean annual ground temperatures vary between –9 °C to –11 °C (Yershov 1998). The thickness of permafrost in the coastal lowlands ranges from 300-700 m below surface. Usually, the active layer has a thickness of less than 30-60 cm in July-August. On the Laptev Sea shelf subsea permafrost occurs (Figure 1-1).

The region is part of the arctic tundra zone of the northern hemisphere (Treshnikov, 1985). Because of S and SE dominated wind directions, the climate of the region is relatively continental despite the geographic location at the Arctic Ocean. Mean annual precipitation rates are rather low with less than 300 mm. Monthly mean temperatures for January are between –36 °C and –30 °C, for July between +2 °C and +10 °C (Treshnikov, 1985). Positive temperatures commonly occur from end of June to end of August only.

Some of the largest Siberian rivers like the Khatanga, Anabar, Olenek, Lena, and Yana discharge into the Laptev Sea, whereas the Lena forms the largest river delta of the Arctic. The coastal mountains of the Pronchishchev Range, the Chekanovsky Ridge and the

Karaulakh Range have elevations of about 200-500 m above sea level. The coastal lowlands are formed by arctic tundra plains at about 10-70 m above sea level. The very low inclined plains are moderately drained by strongly meandering rivers. Ponds and lakes occur frequently due to the lacking drainage in the frozen ground. The modern landscape is shaped mainly by periglacial processes, which control erosion, transport and accumulation. The relief of the lowland plains is dominated by thermo-denudation structures, like thermokarst depressions and thermo-erosional valleys. At shores with ice-rich permafrost deposits, the modern coast rapidly retreats with an average of 2-6 m per year due to thermo-abrasion (Rachold et al., 2000; Romanovskii et al., 2004).

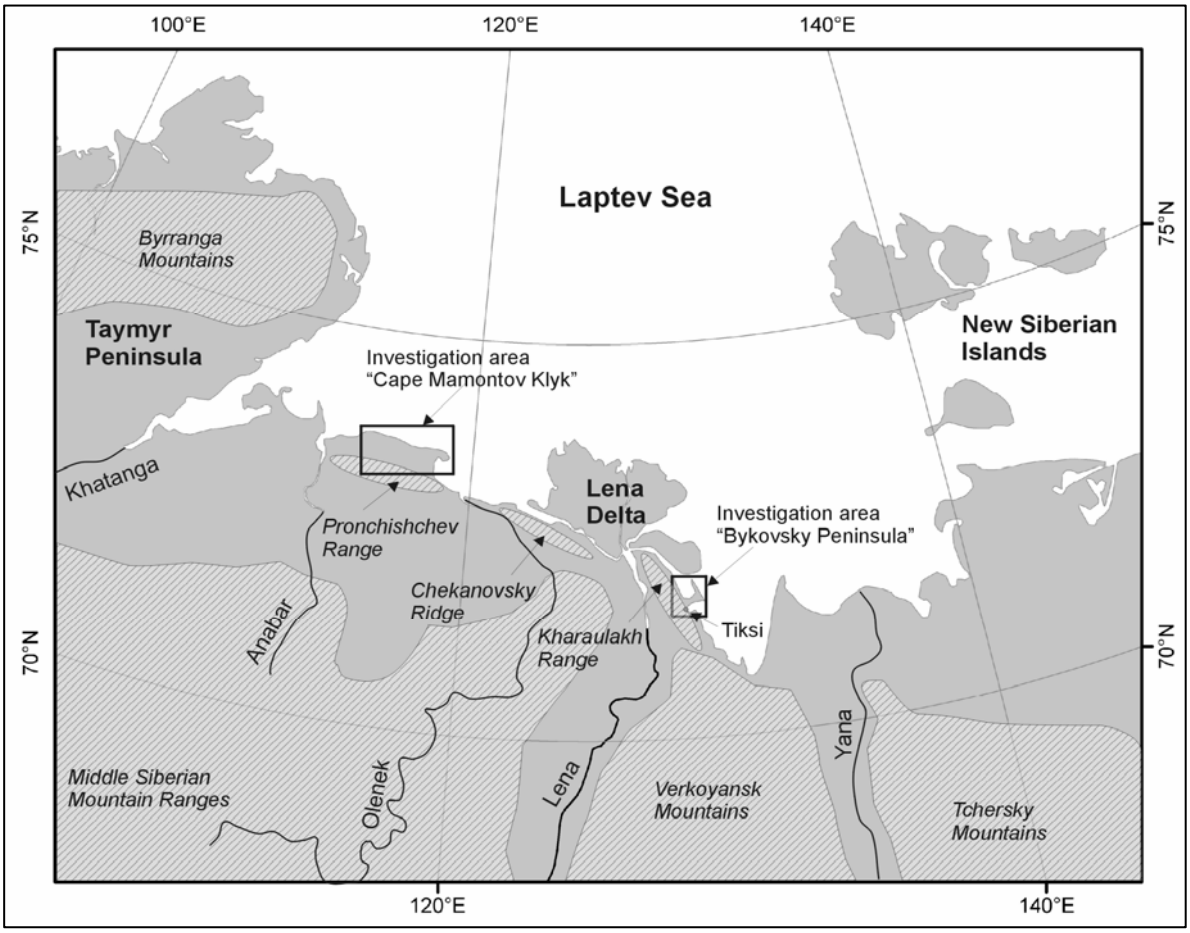

Figure 1-2: Location of the study areas and geographic situation in the Laptev Sea region

1.3.2 Geology and tectonics (Figure 1-3)

In the western part of the region the Siberian Craton and the Early Mesozoic Taymyr fold belt are the dominant structural elements. The eastern part is dominated by the Verkhoyansk-Kolyma fold belt and the New Siberian-Chukchi fold belt, which are separated by the ophiolitic Lyakhov-South Anyui Suture. The Laptev shelf is characterised by a rift system, which is a SE directed branch of the Nansen-Gakkel Ridge in the Arctic Ocean (Drachev et al., 1998, Franke et al., 2001). This Laptev Rift system is divided into several rift basins and uplift blocks. There are three main parts: the Ust‘ Lena rift, the Stolbovoi and East Laptev uplift and the Bel’kov-Svyatoi-Nos rift (from W to E). The rift system is filled with sediments, which increase in thickness from E (4-5 km) to W (10-12 km) (Drachev et al., 1999). The rift is filled with terrigenous and carbonatic sediments of the Pre-Vendian, Vendian and Lower Carboniferous, followed by terrigenous deposits of the Upper Carboniferous, Upper Cretaceous and Palaeocene. The latter partially have coal-bearing horizons. Alternating sequences of marine and terrigenous sediments occur in the rift from the lower Eocene to the Holocene. Neotectonic activity is recorded mainly the eastern Laptev Sea region with its distinctive rift systems. Grigoriev et al. (1996) assume young and still active vertical block tectonics due to the occurrence of different base levels for Late Pleistocene and Holocene deposits in the Lena Delta and strong seismic activities. Are et al. (2000) supposes, that tectonic processes played and still play a major role in the formation of the Lena Delta and the orientation of its main channels. Franke et al. (2001) also identify the Lena Delta as a key region for the interaction between the Verkhoyansk Fold Belt and the Laptev Rift.

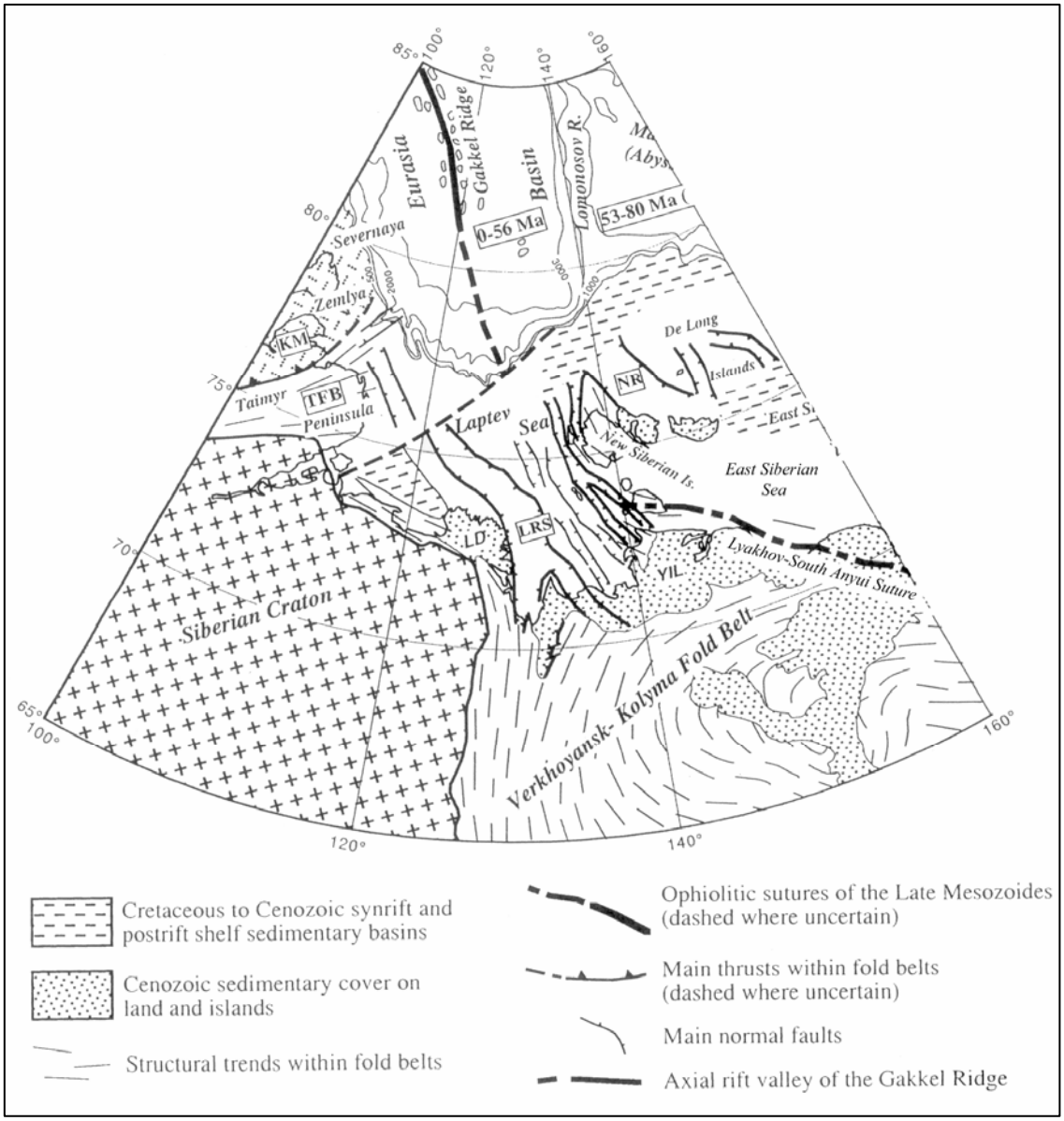

Figure 1-3: Tectonic setting in the Laptev Sea region (subset of a map from Drachev et al., 1999) (KM – Kara Massif, LD – Lena Delta, LRS – Laptev Rift System, NR – New Siberian Rift, TFB – Taymyr Fold Belt, YIL – Yana-Indigirka Lowland)

1.3.3 Palaeogeography during the Late Pleistocene (Figure 1-4)

Due to a very continental climate, the Laptev Sea region was not glaciated at least since the Late Saalian (Hubberten et al., 2004; Svendsen et al., 2004). During the Last Glacial Maximum (LGM, *c.* 21 ky BP[*]), the global sea level was lowered approximately 120 m (Fairbanks, 1989) and the Laptev Sea coast was located several 300-800 km further north (Romanovskii et al., 2004). The region is situated at the northwesternmost edge of the Late

[*] *c.* – circa; ky BP – 1000 years before present

Quaternary Beringia landscape system (e.g. Pisaric et al., 2001; Sher et al., 2005). Large parts of the huge shallow shelf were exposed to subaerial periglacial conditions during the Late Pleistocene and wide accumulation plains were formed in front of the mountain ranges. Fluvial processes also played an important role for the Pleistocene shelf sedimentation (e.g. Kleiber & Niessen, 1999; Schwamborn et al., 2002a). The landscape was dominated by tundra-steppe biomes (e.g. Yurtsev, 2001; Sher et al., 2005) with extreme seasonal differences. Furthermore, the extreme climatic conditions led to the formation of polygonal tundra due to frost cracking and growth of large ice wedges in ice-rich deposits. During summers, enough vegetation was available to feed herds of large grazing mammals of the mammoth fauna (Vereshchagin & Baryshnicov, 1982; Guthrie, 2001, Sher et al., 2005). With the end of the Last Glacial Maximum, the rapidly transgressing sea inundated large parts of the shallow shelf area (Romanovskii et al., 2000). With the rising sea level after the LGM and the climatic amelioration in the Early Holocene, a widespread thermo-denudation of the ice-rich deposits started. The modern sea level in the region was approximately reached at about 5 ky BP (Bauch et al., 2001). The river estuaries retreated southward during the transgression and with sea level stabilisation the aggradation of the young river deltas like Lena, Yana or Olenek started (e.g. Grigoriev, 1993; Schwamborn et al., 2002a). Thermokarst and thermo-erosion caused extensive destruction of the ice-rich permafrost deposits and large scale surface subsidence. Nowadays, a complex tundra landscape exists in the investigation area, composed of Late Pleistocene accumulation structures and Holocene thermokarst and thermo-erosional features. Remains of the former periglacial landscape of the shelf region are preserved in the permafrost areas of the modern NE-Siberian coastal lowlands and the New Siberian Islands (Romanovskii & Hubberten, 2004).

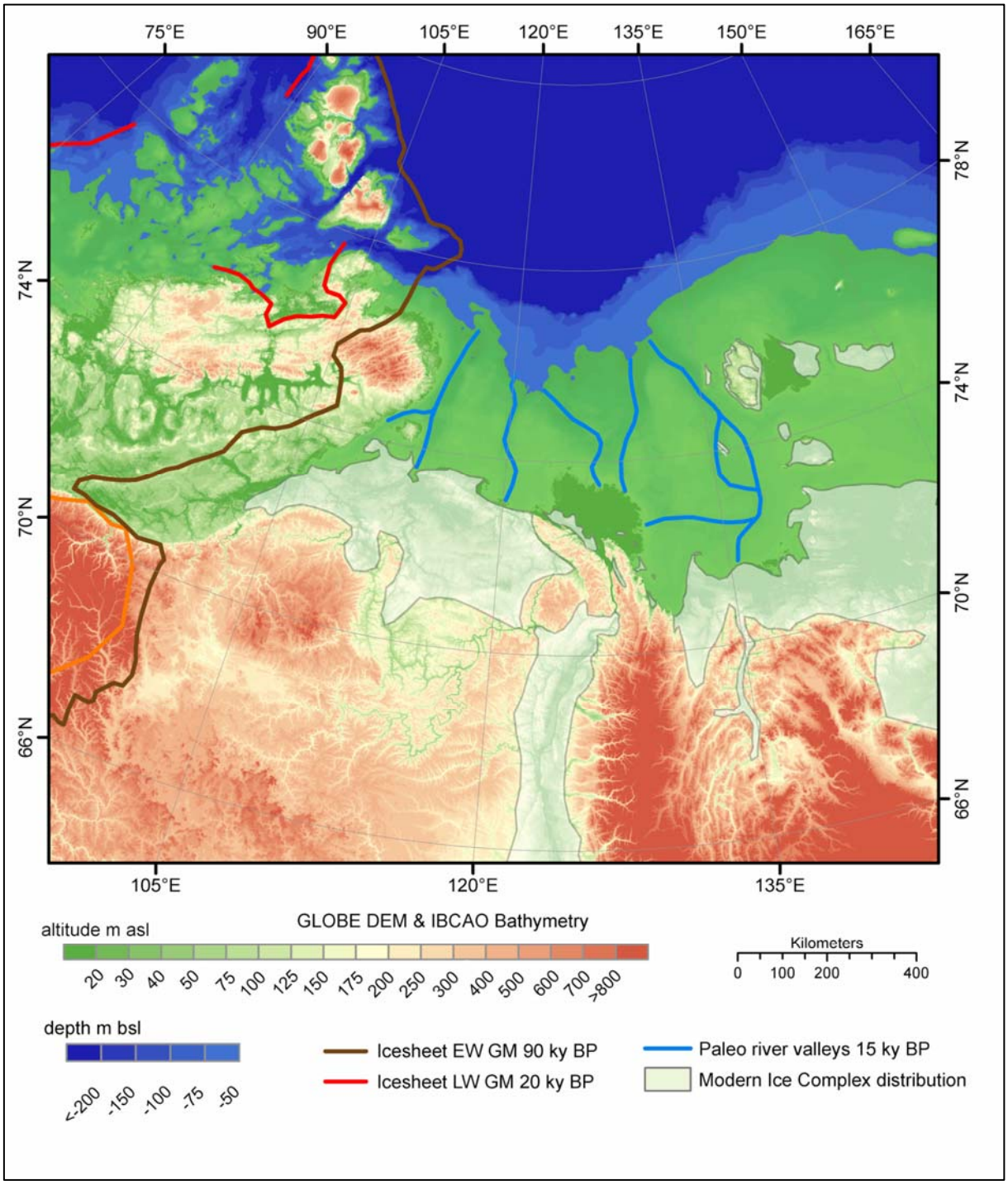

Figure 1-4: Late Pleistocene palaeogeography of the Laptev Sea region, illustrating the extent of the subaerial shelf area at about 11.1 ky BP (green) (-50 m b.s.l.; after Bauch et al., 2001), the course of palaeo-river valleys on the shelf at about 15 ky BP (blue lines) (after Holmes & Creager, 1974), the modern distribution of Ice Complex deposits (greyish green) (after Romanovskii, 1993; with modifications) and the approximate maximum extent of ice sheets during the Early Weichselian glacial (green line) and the Late Weichselian glacial (red line) (after Svendsen et al., 2004). The terrestrial digital elevation data origins from a global DEM (GLOBE Task Team, 1999), the bathymetry origins from the International Bathymetric Chart of the Arctic Ocean (IBCAO) (Jacobsson et al., 2000). Probable Weichselian glaciations in the Verkhoyansk Mountains in the SE of the map are not shown.

1.3.4 Ice Complex and thermokarst

The uppermost permafrost zone in most land areas and on the subaerial shelf was composed of mainly fine-grained, organic-rich sediments of several tens metre thickness. These sediments accumulated more or less continuously during the Late Pleistocene and were synchronously frozen. The deposits, so-called Ice Complex, have an extreme high ice content, which results from the formation of segregated ice and the growth of large syngenetic ice wedges in the sediments (Figure 1-5). The main sources for these sediments were nival and nival-eolian processes (Kunitsky, 1989; Galabala, 1997; Kunitsky et al., 2002), and proluvial processes (Slagoda, 1993), which were very active in nearby mountains during the Late Pleistocene.

The modern permafrost landscape in the North Siberian lowlands is characterised by strong thermo-denudation (Figure 1-6). The main process is thermokarst, which is defined as the thawing of ice-rich permafrost or melting of massive ice, and the subsequent surface subsidence and formation of characteristic landforms (Everdingen, 1998). Especially the ice-rich permafrost deposits of the Ice Complex are vulnerable to extensive thermokarst. Often thermokarst is self-energising by forcing local changes in hydrology and vegetation, which again enhance the further permafrost degradation. Other important processes in these ice-rich permafrost areas are thermo-erosion, thermo-abrasion and slope processes.

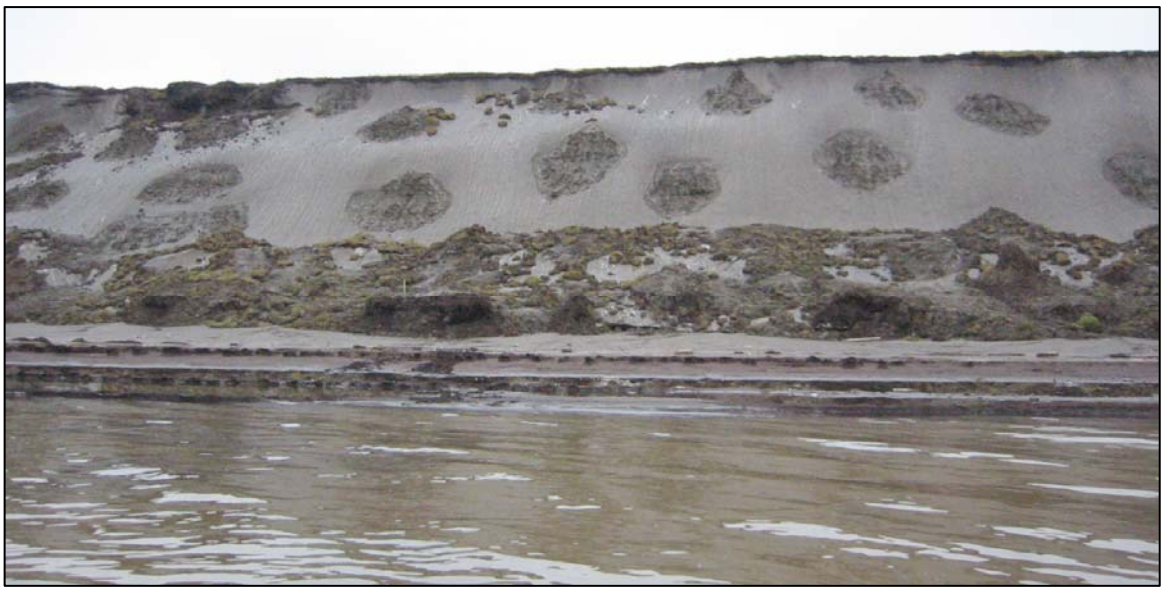

Figure 1-5: Ice Complex at Cape Mamontov Klyk, western Laptev Sea. The about 18 m high coastal cliff has formed due to thermal abrasion. Clearly visible are the patches of fine-grained Late Pleistocene sediments, which were deposited in the centres of ice-wedge polygons (dark grey). Ice wedges (light grey) appear as massive ice wall due to varying viewing angles on to the polygonal net (Photo from 2003).

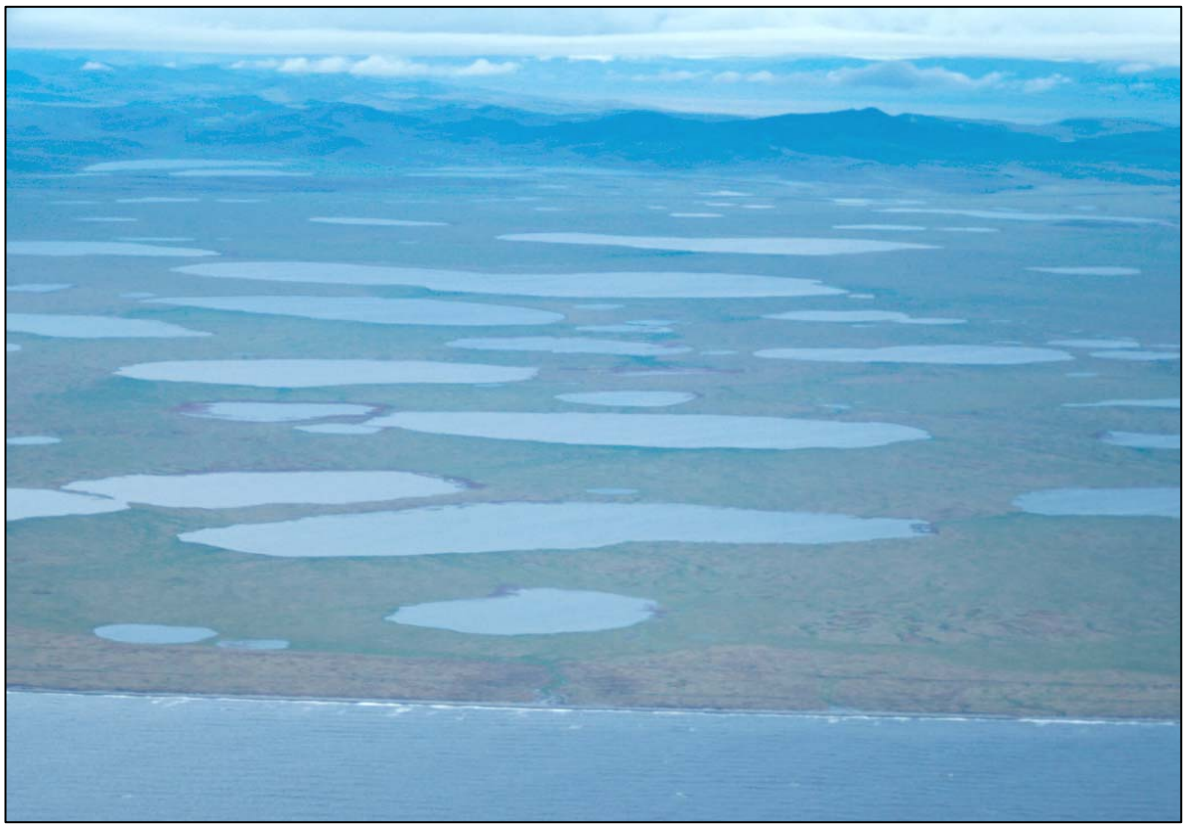

Figure 1-6: Thermo-denudation landscape with thermokarst lakes in an accumulation plain in front of a coastal hill range at the eastern coast of the Buor-Khaya bay, about 180 km east of the Tiksi region (Photo from 1999).

1.4 Synopsis

The thesis is composed of an introduction and three main chapters, followed by a synthesis. The main chapters consist of three independent research papers. One paper is ‘in press’ in an international peer-reviewed journal (Chapter 2: Permafrost and Periglacial Processes), and the other two are already submitted (Chapter 3: Polar Research) or in preparation for submission (Chapter 4: Geomorphology) to such an journal.

The papers, and hence the chapters, represent independent but successive studies on remote sensing techniques and methods for analysing periglacial landscapes in north-central Siberia, and the application of these results for the reconstruction of palaeo-landscape development in the region.

In chapter 2, the application of newly declassified, very high-resolution panchromatic space photography of the CORONA satellite program is demonstrated for the identification and detailed mapping of periglacial surface features on the Bykovsky Peninsula and in the Khorogor Valley, both situated southeast of the Lena Delta. The peninsula is a key site for the

reconstruction of the Late Quaternary palaeo-environment and the observation of modern periglacial processes in the Laptev Sea coastal lowlands of north-central Siberia. In this area, features connected to thermo-denudation and destruction of ice-rich permafrost deposits are the prevalent periglacial surface structures.

In chapter 3, the Lena-Anabar coastal lowland in the western Laptev Sea is investigated with high-resolution multi-spectral satellite data of the Landsat-7 ETM+ satellite. Using semi-automatic supervised classification methods for the detection and analysis of periglacial surface features, the focus is set on thermokarst-affected terrain. Thermokarst is active in this region since the latest Late Pleistocene and Early Holocene. In the investigation area thermo-denudation plays the most important role in transforming the Late Pleistocene landscape of an accumulation plain into the modern thermokarst and thermo-erosion dominated landscape. These processes are strongly influencing regional geomorphology, hydrology, vegetation as well as energy and matter fluxes.

Chapter 4 demonstrates the reconstruction of landscape development for a periglacial tundra environment since the Late Pleistocene. The study region is the Bykovsky Peninsula and the adjacent Khorogor Valley. The reconstruction of this key area focusses on the development of a Late Pleistocene accumulation plain in front of the Kharaulakh mountain range and its denudation by various processes during the Holocene. The reconstruction is based on a variety of information derived from own and other authors field-work, from remote sensing data, and from the incorporation of terrain analysis.

Parts of the data analysis in all 3 main chapters were conducted within a Geographical Information System (GIS) software package (ArcGIS^{TM}), which provided the necessary spatial analysis tools for some tasks. The local GIS that were produced for each investigated region consisted of topographical data, medium-resolution digital elevation models, own field data and that of other authors, and the data derived from the applied remote sensing methods.

The following chapter 5 synthesises the preceding chapters and demonstrates the necessity to use the applied or similar techniques for the reconstruction of Late Quaternary Arctic palaeo-environments, and for the quantitative and qualitative analysis of permafrost deposits in circum-Arctic landscapes under global climate change scenarios. Furthermore, the synthesis points on important open questions and possible directions for future research concerning the application of remote sensing and GIS techniques for arctic periglacial environments and change assessment in these regions. Finally, the references cited in all previous chapters are collected in a reference list.

2. The use of CORONA images in remote sensing of periglacial geomorphology: An illustration from the NE Siberian coast

Guido Grosse[a], Lutz Schirrmeister[a], Viktor V. Kunitsky[b] and Hans-Wolfgang Hubberten[a]
[a] Alfred Wegener Institute for Polar and Marine Research, Research Unit Potsdam
[b] Permafrost Institute, Siberian Branch of Russian Academy of Science, Yakutsk

2.1 Abstract

CORONA images have been used for the mapping of periglacial features on the Bykovsky Peninsula and adjacent Khorogor Valley in NE Siberia. Features, mapped and analyzed within a geographical information system include thermokarst depressions, thermo-erosional valleys, thermo-erosional cirques, thermokarst lakes, thermokarst lagoons and pingos. More than 50% of the area is strongly influenced by thermally-induced subsidence. Thermokarst in the area is probably less active today than in the early-middle Holocene.

2.2 Introduction

Diverse remote sensing methods have been employed in Arctic periglacial research in the last years. These include vegetation mapping (e.g. Walker, 1999; Brook & Kenkel; 2002, Hope et al., 2003; Tommervik et al., 2003), change detection (e.g. Rees et al., 2003; Rigina, 2003; Yoshikawa & Hinzman, 2003; Stow et al., 2004) and mapping of general permafrost properties (e.g. Morrissey et al., 1986; Peddle & Franklin, 1993; Leverington & Duguay, 1997; Lewkowicz & Duguay, 1999; Etzelmüller et al., 2001). Investigations of permafrost and periglacial geomorphology in the Arctic hemisphere were usually associated with the use of high-resolution aerial imagery (e.g. Cabot, 1947; Frost, 1963; Mollard, 2000; Boike & Yoshikawa, 2003). But the spatial and temporal coverage of such imagery is often limited. For the large Russian part of the Arctic, aerial imagery and detailed topographic maps are often still classified or not available. This paper describes the use of easily-available, high-resolution CORONA satellite photography as a substitute for aerial imagery in NE Siberia. The high-resolution mapping of thermokarst features from CORONA imagery is the basic input for any GIS of the investigation area.

2.3 The CORONA program and its satellite images

CORONA satellite imagery became first available in 1995. In 2002, subsequent images similar to imagery from the CORONA program (1963-1980) were declassified. The satellite images of varying ground resolution (0.6m to 150m) are available from the USGS EROS Data Center in Sioux Falls, South Dakota (http://edc.usgs.gov).

CORONA imagery has been used for several years for different scientific purposes and in different regions of the world. Most applications dealt with archaeological research (e.g. Kennedy, 1998; Goossens et al., 2000; Philip et al., 2002) and geoscientific research (Tappan et al., 2000; Altmaier & Kany, 2002). Some worked with this imagery in polar regions (Bindschadler & Vornberger, 1998; Rigina, 2003).

2.4 Investigation area

The Bykovsky Peninsula and adjacent Khorogor Valley are part of the recent coastal lowland of the Laptev Sea (Figure 2-1). They belong to two separate geological regions - the Karaulakh Mountain range in the west (Khorogor Valley) and a Pleistocene accumulation plain in the east (Bykovsky Peninsula).

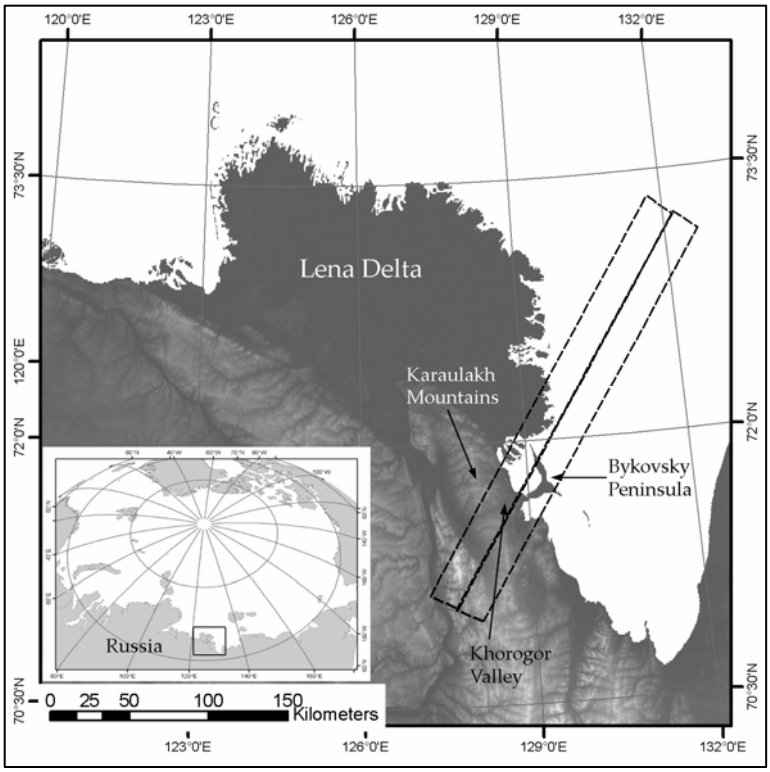

Figure 2-1: Location of the investigation areas of Bykovsky Peninsula and Khorogor Valley. The dashed rectangles mark the coverage of the two CORONA image stripes used in this work (map after GLOBE30 DEM data).

In the Khorogor Valley, the features of interest were mainly situated in the lower valley regions (Figure 2-2). Of the total investigation area of 258.7 km^2, two thirds belonged to the Bykovsky Peninsula and one third to the Khorogor Valley. The permafrost in this region is continuous and reaches depths of 300-500 m. The active layer is up to 30-50 cm thick. The relief of the Bykovsky Peninsula is dominated by flat elevated areas up to 40 m a.s.l., together with thermokarst depressions down to sea level. Coastal erosion, mainly a combination of thermal erosion and coastal abrasion, produces steep cliffs up to 40 m in height.

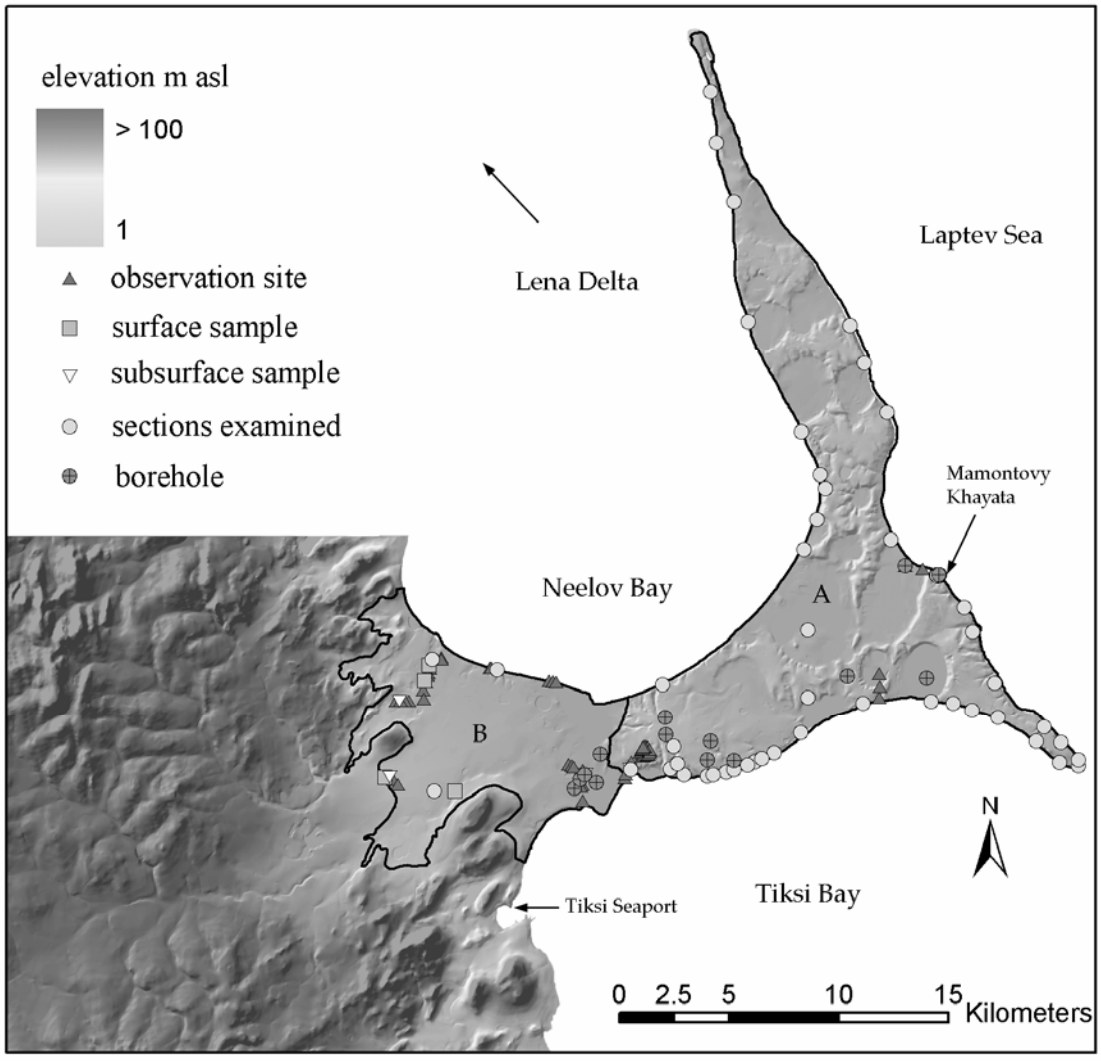

Figure 2-2: Digital elevation model (DEM) of the investigation area, illuminated from the upper left; A – Bykovsky Peninsula, B – Lower Khorogor Valley up to the 50 m elevation contour. The various field sites with geo-cryological ground truth data origin from own fieldwork and fieldwork of other authors (Kunitsky, 1989; Slagoda, 1993; Grigoriev, 1993).

Many authors describe thermokarst and its impacts in Siberia (e.g. Soloviev, 1973; Czudek & Demek, 1970; Romanovskii et al., 2000) and other periglacial regions in North America (e.g. Mackay, 1962; French 1974; French, 1996; Murton, 1996).

Several palaeo-environmental studies with a multi-disciplinary focus have been conducted in the area by Russian and German colleagues during the last few years (Romanovskii et al., 2000; Schirrmeister et al., 2002a, b; Meyer et al., 2002a; Siegert et al., 2002; Andreev et al., 2002). Most have investigated outcrops on the East shore of Bykovsky Peninsula, especially at the Mamontovy Khayata site (Figure 2-2). Some authors published geo-cryological field data from this area in Russian literature (e.g. Kunitsky, 1989; Slagoda, 1993; Grigoriev, 1993). The only previously published work on remote sensing dealing in parts with this area was conducted by Grosswald (1998), who presents geomorphological features on aerial images of the Tiksi region (SE of the Lena Delta).

Fieldwork during the summers 1998, 2000 and 2002 (Siegert et al., 1999; Schirrmeister et al., 2001; Grigoriev et al., 2003), and literature reviews were important tools for the ground validation of the geomorphological structures visible on the CORONA images.

2.5 Image processing

Two cloud-free images where chosen, covering a region of about 5 x 10^3 km^2 (Figure 2-1). The Bykovsky Peninsula and the Khorogor Valley are covered by a small subset of these images of about 1.4 x 10^3 km^2; thus only parts of the image strips were used. Only a tiny area (about 1 km^2) in the southeast of the Bykovsky Peninsula (Cape Muostakh) is not covered by these two images (Figure 2-3). The images were captured as parallel stripes by the CORONA KH-4B satellite system (Table 2-1) in July 1969. The image specifications are given in Table 2-2. The images were ordered as film negatives and scanned with a high-resolution A3 transmitting-light scanner (Type AGFASCAN XY 15) to produce high-quality digital grayscale files. The maximum information return from digitalising CORONA photography is reported to be at a scan resolution of 4 μm by Leachtenauer et al. (1998). They found no substantial loss of information up to a scan resolution of 15 μm, whereas file sizes were significant smaller. Thus, the scan resolution in this work was chosen with 900 dpi and 400% enlargement. This corresponds to a total resolution of 3600 dpi or about 7 μm.

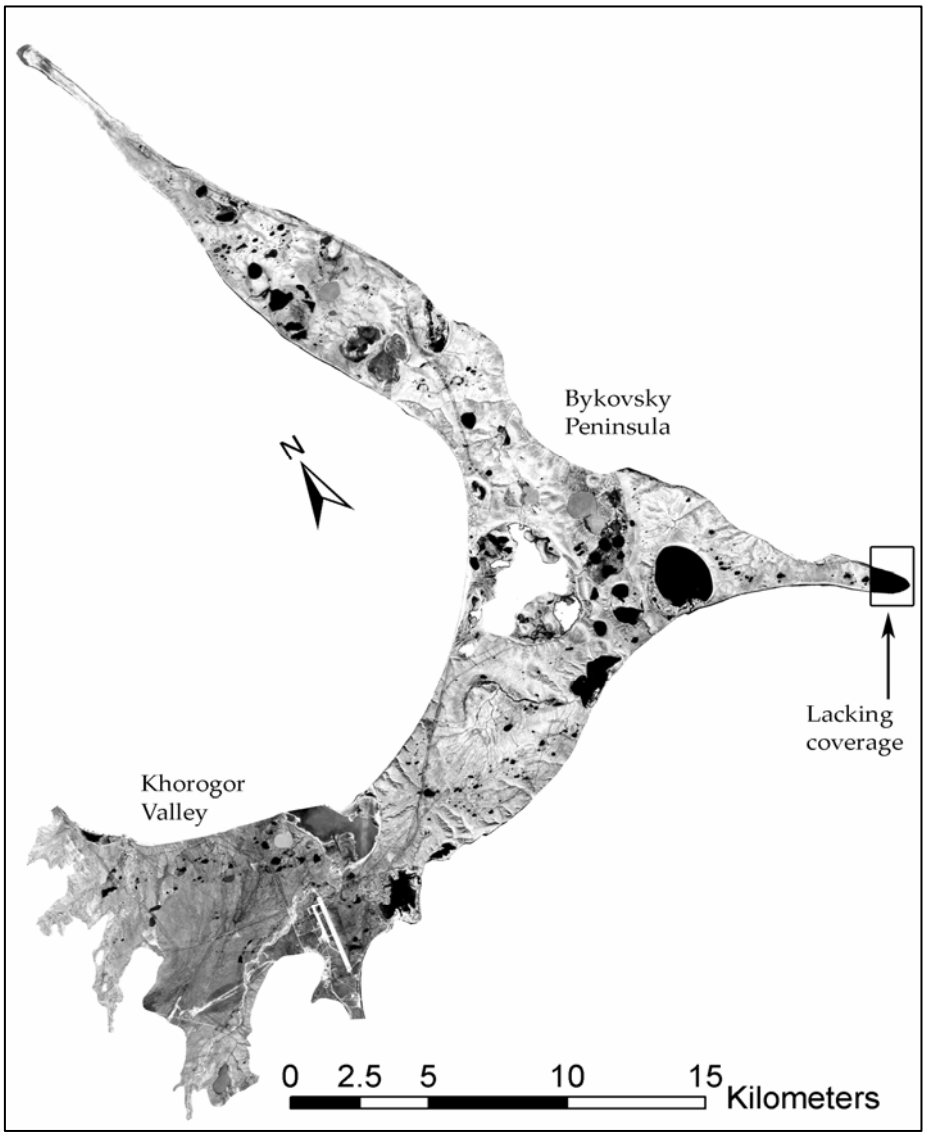

Figure 2-3: Panchromatic CORONA mosaic of the investigation area, based on two images from July 1969.

Table 2-1: Technical characteristics of the CORONA KH-4B camera system.

Satellite KH-4B	
Period of operation	15/09/1967-25/05/1972
Camera type	J-3, panchromatic
Flight altitude	150 km
Focal length	61 cm
Frame format	5.5 cm x 75.7 cm
Film resolution	160 lines / mm
Photo scale of the film	1:247,500
Ground coverage	13.8 km x 188 km
Best ground resolution	1.8 m

Table 2-2: Image characteristics for the 2 satellite scenes used in this work.

CORONA images used	D003003M1107-1AFT D003002M1107-1AFT
Date of acquisition	24th July 1969
Film size per image subset	5.5 x 14 cm
Ground coverage per subset	13.8 x 35 km
Scan resolution	7 μm (3600 dpi)
Ground resolution	2.5 m

The image subsets of each strip have different radiometric behavior. Therefore a radiometric correction was applied with the software ENVI™ version 3.6. Both image subsets were radiometrically corrected relative to each other. Then, by collecting tie points in the slightly overlapping subsets, the images were mosaicked. Finally a linear contrast stretching was employed for the whole mosaic to enhance visual interpretability. The pixels in the digital CORONA images consist of gray values from 0 (black) to 255 (white). Similar to panchromatic aerial imagery, a correlation of gray-scale value and surface reflectance is given, so the interpretation of surface parameters is possible. Coherent dark pixel values stand for low reflection and high absorption, light pixel values for high reflection and low absorption of sunlight. This information can be used for discrimination of water (high absorption) or barren land (high reflection) and the visual differentiation of soil moisture or geological features. Dependent from sun azimuth and altitude, shadows occur in areas with strong relief. The shadows can be used for interpretation of geomorphological features (e.g. depth of valleys or slope inclination).

For geo-referencing, 82 ground control points (GCP) were identified across the CORONA mosaic for co-registration with a previously geo-referenced topographical map mosaic in 1:100,000 scale (0.5 mm = 50 m in reality). The topographical maps are based on aerial and field survey data from 1966-1994. To rectify the image mosaic to the map projection (Gauss-Krueger Pulkovo 1942 zone 22, with datum Pulkovo 1942), a polynomial warping function of third order and bilinear pixel resampling was used. The overall RMS error for rectifying the CORONA mosaic was 16.86 m, whereas the individual errors had a range from 1.98 to 28.83 m. The RMS error of several times a pixel size is caused mainly by the use of medium resolution, poor quality scanned topographical maps for geo-coding and the lack of clearly identifiable GCP's, like buildings or road intersections. The final image is shown in Figure 2-3.

2.6 Mapping of thermokarst and water surfaces

To enhance desktop mapping and spatial analysis, a digital elevation model (DEM) was developed. It is based on manually digitised elevation data from the same topographical maps used for rectification of the CORONA mosaic. Within ArcInfo™ the TOPOGRID tool was used for the generation of a elevation grid with 15 m cell size. A test for vertical accuracy of the DEM interpolation algorithm with 52 original elevation points from the map and their accordant grid cells revealed a mean vertical error of +0.49 m in the DEM. The accuracy of the elevation model is considered useful for this and further work. Additionally, a slope map and a shaded relief map were calculated from the DEM. The DEM, slope map and shaded relief map were separately used as a 50% transparent overlay for the CORONA image to enhance the visual interpretation of geomorphological structures in the panchromatic image.

Thermokarst features that could be discriminated and interactively mapped from the CORONA mosaic within the desktop GIS included lakes, depressions, lagoons, gullies, slumps and pingos (Figure 2-4A-F). Water surfaces were classified with a density-slicing algorithm. For this task we assumed that water surfaces have the lowest reflectance values in the panchromatic images. The density slice separates the gray values in the image according to a threshold value. Several gray value thresholds were tested and finally the one with best visual separation of water from land was applied to classify the image. The result is a binary image containing only water and non-water pixels (Figure 2-5). This classification method for panchromatic imagery has a few weak points. First, due to low sun elevations, shadows are strong in deep valleys or slumps and hence miss-classified as water. Second, due to the acquisition time in July, some large lakes were still covered by highly reflective lake ice, hence miss-classified as non-water. Third, some large lakes were strongly disturbed with sediment suspension, hence miss-classified as non-water. Finally, in small polygonal ponds, vegetation grows in the shallow water and no exact boundary between water and non-water could be drawn.

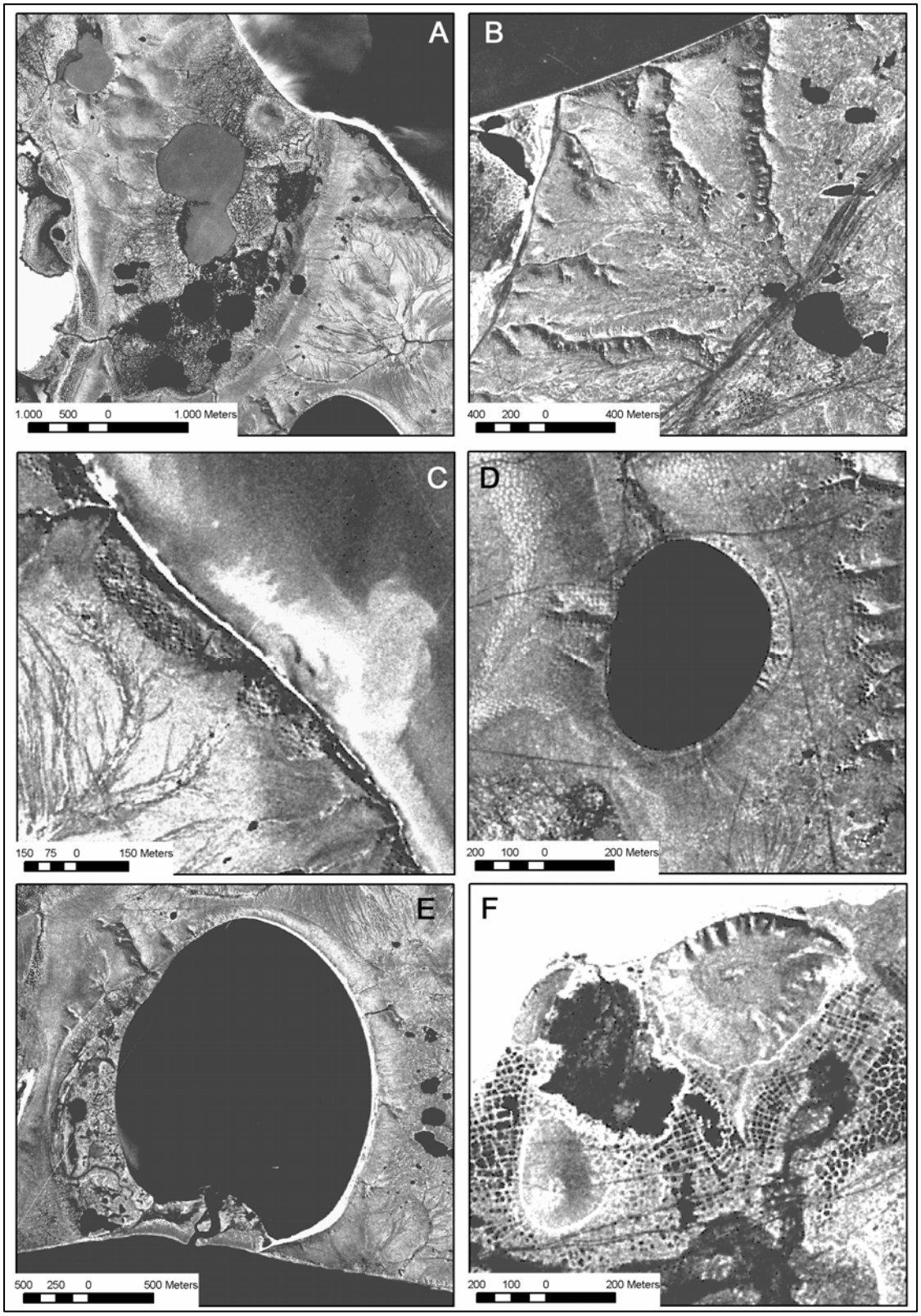

Figure 2-4: Geomorphological features identified from the CORONA images: A – Due to coastal erosion partially drained thermokarst depression with lake remnants and pingo, B – Gullies discharging an upland surface and human-induced vehicle tracks, C – Large thaw slumps along the east shore of Bykovsky Peninsula, D – Thermokarst lake with subsidence features on an upland plain, E – Lagoon in an early stage formed by coastal erosion and drainage of a thermokarst lake (Ivashkina lagoon), F – Pingos and partially drained, low centred ice-wedge polygon terrain.

The first three types of miss-classification were corrected manually. According to the chosen threshold, the classification of lakes with vegetated boundaries results in minimum areas for such ponds. For an estimation of the water-classification accuracy, the classified water surfaces were compared to the manually mapped water surfaces and the digitised water surfaces from the topographical map (Table 2-3). The visually examined and manually corrected classification result is considered the most accurate approximation for water surfaces.

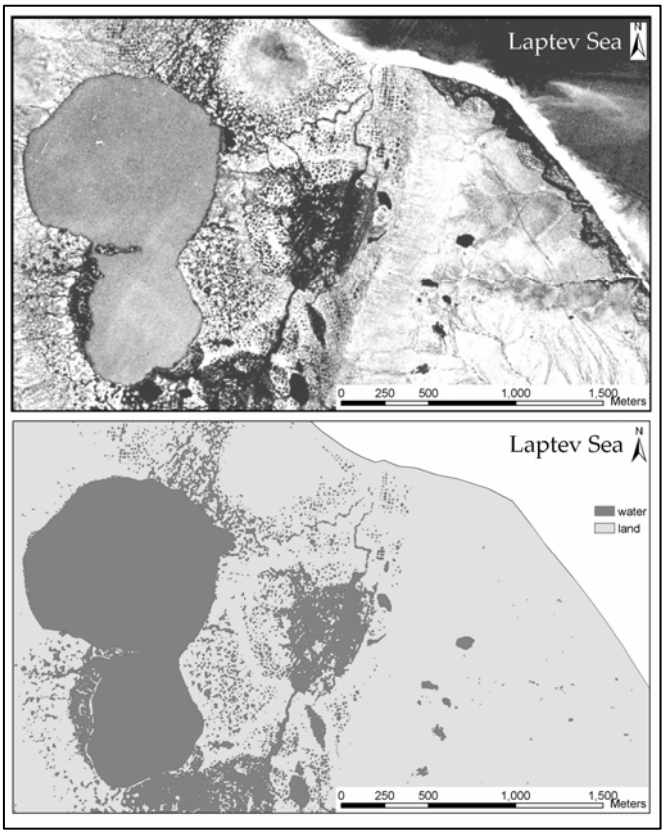

Figure 2-5: Classification of water surfaces in the thermokarst depression of Mamontovy Bysagasa (left part of image) and on the upland of Mamontovy Khayata (right part of image) on the east shore of the Bykovsky Peninsula: upper image – CORONA; lower image – interactively corrected density-slice classification of inland water surfaces.

Table 2-3: The different mapping methods reveal different results for the spatial extent of lakes and lagoons.

Feature	Source	Number	Area (km^2)	% of investigation area
Lakes and lagoons	Topographical map 1:100,000	397	30.143	11.7
Lakes and lagoons	CORONA interactive mapping	569	31.862	12.3
Lakes	CORONA density slice classification	25,050	26.362	10.2
Lagoons		7	10.862	4.2
Overall lakes and lagoons		25,057	37.224	14.4

2.7 Results

The results for the mapping of periglacial structures are shown in Table 2-4. In total, 145 valleys, 16 depressions, 7 slumps, and 6 pingos were mapped. By digitising the 1:100,000 topographic map 397 water bodies were detected, by manual mapping from the CORONA image 569 water bodies were detected and finally, by classification from the CORONA image 25,050 water bodies were detected (Table 2-3).

Table 2-4: Spatial properties and distribution of periglacial features mapped from the CORONA image mosaic.

Geomorphological feature	Number	Area (km^2)	% of overall investigation area	% of Khorogor Valley area	% of Bykovsky Peninsula area
Thermo-erosional valleys	145	11.188	4.3	0.2	6.3
Thermokarst depressions	16	80.713	31.2	-	46.1
Thermo-erosional cirques	7	1.170	0.5	-	0.7
Pingos	6	0.385	0.1	-	0.2

The minimum lake area that has been calculated from the topographic map and the manual CORONA mapping was 278 m^2 and 186 m^2, respectively. The minimum lake size for the classification was one pixel, which is about 6 m^2. This small pond size is not necessary and not useful to implement into topographic maps, but is nevertheless an important factor in arctic tundra geo-ecosystems. The size distribution of the classified water bodies (lakes and lagoons) reveals a strong bias in area towards a few large lakes, but also a strong bias towards the number of very small lakes or ponds (Table 2-5).

Table 2-5: Distribution of the spatial parameter area for lakes detected by density slice classification.

Lake type	Number	Area (km^2)	In % of total lake number	In % of overall lake area
>=10,000 m^2 (large lakes)	186	21.694	0.7	82.3
<10,000 m^2 & >= 400 m^2 (medium-small sized lakes)	2,081	3.104	8.3	11.8
<400 m^2 (polygonal ponds, meteoric ponds)	22,783	1.564	91.0	5.9

Water bodies < 400 m^2 represent shallow polygonal ponds and small pools of meteoric water. The huge amount of such small ponds is responsible for increasing the total water surface in the investigation area for more than 6.5-7.2 km^2 (+2.1-2.7 %) compared to topographic map

and manual mapping. Although 91% of all lakes are represented by small ponds < 400 m^2, they contribute only 5.9 % of the total lake water surface.

Although most ponds are situated in the depressions, many ponds can also be found on the elevated plateaus, where drainage conditions are poorer. Large lakes and lagoons with more than 10,000 m^2 coverage mainly occur in the basins of the central and the northern peninsula and at the isthmus between Khorogor Valley and Bykovsky Peninsula. Only some large lakes have developed in the lower valley, the area of the biggest is less than 0.43 km^2.

The area of the Bykovsky Peninsula occupied by lakes is only one third of the area occupied by thermokarst depressions. This shows that lakes must have been larger in the past. This is supported by the presence of pingos, several situated in the larger basin agglomerates in the central part of the peninsula (e.g. see Figures 2-4A and 2-4F).

2.8 Conclusions

CORONA images are a cheap, efficient and easily available substitute for old aerial imagery. This makes them a valuable tool for preliminary investigations and pre-fieldwork mapping. In this paper we illustrate how the main periglacial surface features of a coastal lowland site in the Laptev Sea region could be distinguished and mapped with a mosaic of high-resolution CORONA satellite images. The DEM data enhanced the mapping process. It was possible to produce high-resolution maps of periglacial features from the CORONA panchromatic imagery.

Quantification of the results within a GIS revealed that thermokarst structures cover more than 50 % of the Bykovsky Peninsula. Their occurrence proves the presence of thick ice-rich deposits. In the Khorogor Valley thermokarst structures occur only in the lowest valley parts, where sedimentary deposits are thick and ice-rich. The pingos of the Bykovsky Peninsula reveal that the taliks below the thermokarst depressions are largely, but not completely, refrozen. According to Schirrmeister et al. (2002b), local climate deterioration started around 4,500 kaBP with decreasing summer temperatures, decreasing pollen contents and increasing ice wedge growth. This suggests that also the silting-up and drainage of many of the thermokarst lakes occurred during the Middle- to Late-Holocene. Using the density slice classification, a fast high-resolution classification of water and non-water was applied successfully. This approach quantified the vast amount of small water bodies in the tundra landscape. Because such lakes play a major role in methane emission in tundra landscapes, detailed mapping can provide basic information for the quantification of trace gas fluxes from tundra landscapes.

3. Application of Landsat-7 satellite data for the quantification of thermokarst-affected terrain types in the periglacial Lena-Anabar coastal lowland

Guido Grosse[a], Lutz Schirrmeister[a] & Timothy J. Malthus[b]
[a] Alfred Wegener Institute for Polar and Marine Research, Research Unit Potsdam
[b] Institute of Geography, School of GeoSciences, University of Edinburgh, Great Britain

3.1 Abstract

Large scale degradation of ice-rich permafrost in the coastal lowlands of the Laptev Sea in North Siberia produces specific subsidence structures, which are not only important factors for local geomorphology, geology and hydrology, but also for regional balances of organic carbon, fresh water and sediment due to re-mobilisation of formerly frozen material. Different types of periglacial terrain surfaces in a tundra landscape, dominated by ice-rich permafrost, were observed with Landsat-7 ETM+ satellite data. A terrain classification approach included a supervised maximum likelihood classification applied to the Landsat data and matched digital elevation data. Class-refinement was achieved with rule-based image stratification that was applied before and after the classification. The overall classification accuracy was 79 %. The 13 final terrain surface classes were characterised and their relevance to thermokarst and the degradation of ice-rich deposits of the Ice Complex in the study region around Cape Mamontov Klyk at the western Laptev Sea coast was described. Classification results were subsequently linked with preliminary results from cryolithological fieldwork, and each class was interpreted in terms of how strong the Ice Complex has degraded below this class. Altogether, only 22 % of the coastal plain investigated is not affected by permafrost degradation due to thermokarst, thermo-erosion or slope denudation. Terrain with signs of permafrost degradation increases from south to north on the gently northward inclined coastal plain. Thermokarst structures dominate the geomorphology of the investigated area, indicating the importance of thermokarst during the Holocene sea level transgression in the region.

3.2 Introduction

About 24 % of the land surface of the northern hemisphere are underlayed by permafrost (Zhang et al., 1999). Permafrost is an ideal indicator of environmental changes, as its stability depends on various environmental (e.g. vegetation, geomorphology, hydrology) and climatic (e.g. temperature, precipitation) factors (e.g. French, 1996). An understanding of permafrost regions in the Arctic land-ocean-atmosphere system has became an increasingly important

objective for the scientific community over the last decade. It is widely accepted that the Arctic environment will react early and to a greater extreme than the global average response under currently estimated climate change scenarios (ACIA, 2004). Researchers have already addressed periglacial processes acting in permafrost-dominated environments in many studies. As periglacial environments are mostly located in remote Arctic regions, the application of remote sensing data for the monitoring of these extensive landscapes is often the most cost-effective tool, and thus a fast growing research area. The wide range of available sensors provides a variety of data for modelling and process studies in the Arctic. By using remote sensing, the science community is able to observe such environments frequently at large scales, observe change, and deliver basic data for the Arctic and global change discussion. Previous approaches in northern tundra landscapes have focused predominantly on land cover analysis and vegetation classification (Joria & Jorgenson, 1996; Walker, 1999; Brook & Kenkel, 2002; Hope et al., 2003; Stow et al., 2004; Virtanen et al., 2004).

Beside these functions, one of the most interesting and important processes to be investigated by remote sensing is the degradation of permafrost. The value of remote sensing in mapping of permafrost or permafrost degradation features has already been demonstrated, but mostly for locally limited studies (Sellmann, 1975; Pollard & French, 1980; Morrissey et al., 1986; Lewkowicz & Duguay, 1999; Ermolin et al., 2002; Hinkel et al., 2003; Grosse et al., 2005). Despite these previous research efforts, and the combination of high spatial detail and large coverage offered by remote sensing data, the extent and distribution of permafrost and permafrost degradation is still a challenge to be met for most remote Arctic areas. The results of such studies would be of significant value for various environmental modelling tasks dealing with permafrost, geomorphology, landscape dynamics and coastal dynamics. As remotely sensed data have been available now for several decades, various change detection approaches concerning permafrost degradation have also been developed (Jorgenson et al., 2001; Beaulieu & Allard, 2003; Yoshikawa & Hinzman, 2003). New attempts for the detection and analysis of permafrost and associated degradation processes combine remote sensing imagery, digital elevation models (DEM) and other thematic data in geographical information systems (GIS) (Joria & Jorgenson, 1996; Etzelmüller et al., 2001; Jorgenson et al., 2001; Bartsch et al., 2004).

The dominating process in permafrost degradation is thermokarst, which is defined as the thawing of ice-rich permafrost or melting of massive ice, and the subsequent surface subsidence and formation of characteristic landforms (Everdingen, 1998). In fact, thermo-

erosive and thermo-abrasive processes are also controlled by thermokarst (French, 1996). Generally, thermokarst is considered as an indicator of severe environmental changes in landscapes dominated by ice-rich permafrost. Thermokarst is strongly interacting with local hydrological changes, and can result in a self-reinforcing process. Many studies on thermokarst have been published since the early 1950's for various regions in Canada (e.g. Mackay, 1963; French 1974; Murton, 1996), Alaska (e.g. Hopkins, 1949; Black, 1969; Osterkamp & Romanovsky, 1999) and Russia (e.g. Romanovskii, 1961; Czudek & Demek, 1970; Soloviev, 1973; Romanovskii et al., 2000; Romanovskii et al., 2004). Further global descriptions of thermokarst and its environmental implications are given by Washburn (1979), French (1996), and Yershov (1998).

This paper demonstrates the use of optical remote sensing and GIS-based integration of digital elevation data for the quantification of different types of periglacial terrain surfaces in the western Laptev Sea coastal lowland, north-central Siberia. The approach particularly focussed on Holocene permafrost degradation features, as thermokarst played a key role in the shaping of the present-day periglacial coastal lowlands. The remote sensing approach, using Landsat-7 ETM+ data, provided the necessary spatial ground resolution and the regional coverage for the large area of investigation. We suggest the application of remote sensing of periglacial terrain surfaces as a supplementary tool for palaeo-environmental and especially for palaeo-geographic reconstruction. Remotely sensed information on geomorphology, geology and land cover, as well as the spatial extent and distribution of thermokarst-affected terrain were achieved as important parameters for the reconstruction of the palaeo-environmental development of these landscapes during the Late Quaternary. The remotely sensed information was used for the upscaling of local cryolithological results to a regional context. The integration of different data types like satellite images, DEM and field data within a GIS and the subsequent analysis with GIS-based spatial analysis tools proved beneficial for the understanding of the distribution of periglacial terrain elements and the impacts of periglacial processes, i.e. thermokarst, on this landscape. Furthermore, the achieved dataset can be used for the quantification of modern environmental dynamics at the investigated key site, e.g. for the estimation and upscaling of the natural greenhouse gas flux from periglacial tundra regions, which is strongly dependent on vegetation and terrain.

The approach presented is part of multidisciplinary joint German-Russian research efforts, aimed at the reconstruction of the Late Quaternary palaeo-environment and the dynamics of permafrost in that region. Detailed palaeo-environmental reconstructions based on proxies from sedimentology, cryolithology, pedology, geochemistry and palaeontology have already

been accomplished for various other key sites in north-central Siberia at the eastern Laptev Sea coast (Andreev et al., 2002; Kunitsky et al., 2002; Meyer et al., 2002a, b; Schirrmeister et al., 2002a, b; Siegert et al., 2002; Andreev et al., 2004) and in the Lena Delta (Krbetschek et al., 2002; Schwamborn et al., 2002a, b; Schirrmeister et al., 2003a). Within these efforts, the investigated area near Cape Mamontov Klyk is the first site situated on the western Laptev Sea coast (Figure 3-1) and forms an interesting location for regional comparison of palaeo-environmental, geomorphological and geological results with the eastern Laptev Sea sites. Also for the first time, these well-established palaeo-environmental studies on permafrost sequences were complemented with remote sensing and GIS studies for the reconstruction on landscape scales. The results from our terrain surface classification for a large region in the Lena-Anabar coastal lowland is also of interest for researchers aiming to model coastal dynamics in ice-rich permafrost coasts, as is proposed in the Arctic Coastal Dynamics project for this site (Are, 1999) and for other sites along the Laptev Sea coast (Rachold et al., 2005).

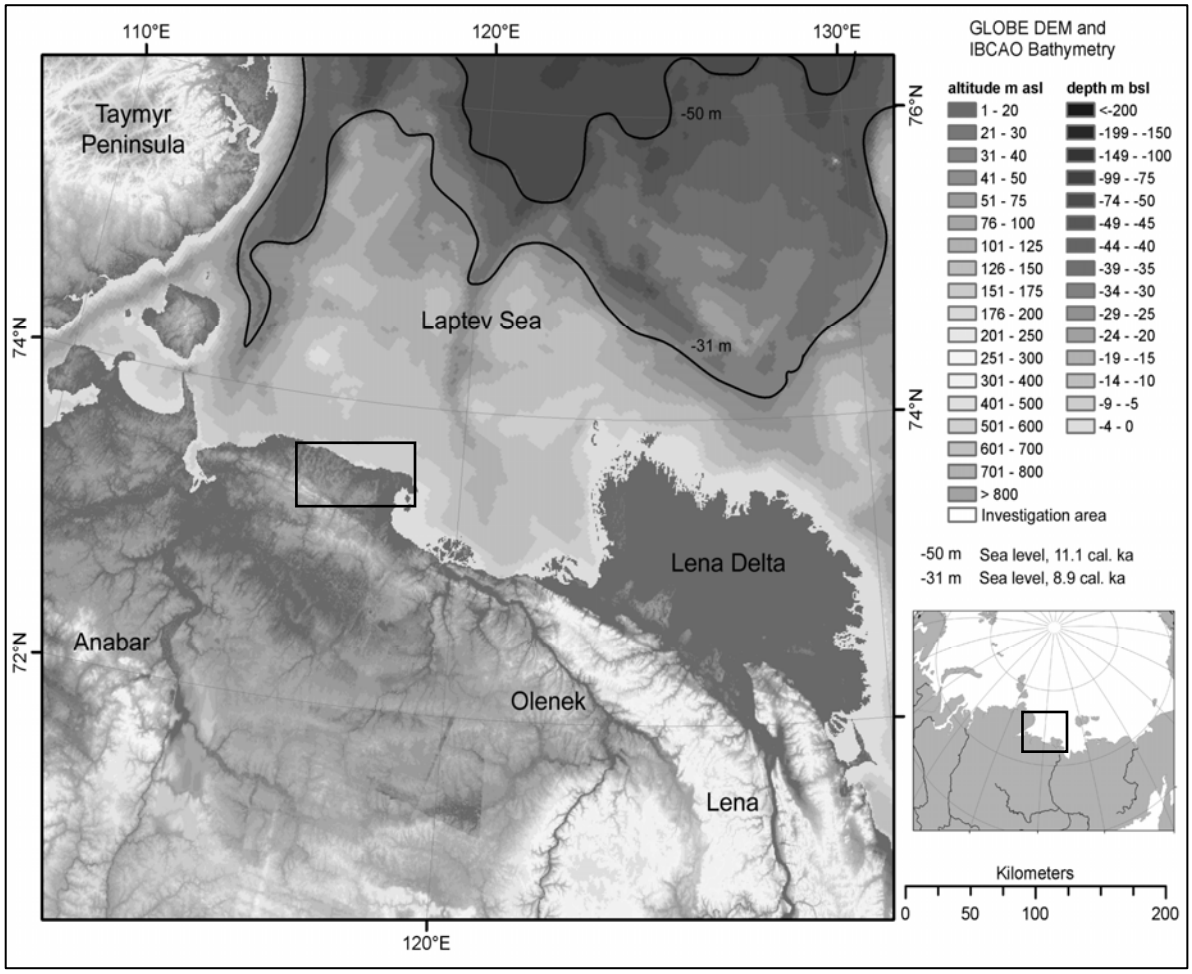

Figure 3-1: Location of the investigation area (black square in the large map) in the western Laptev-Sea coastal lowlands, northern Siberia (small map). Palaeo-sea levels are adapted from Bauch et al. (2001).

3.3 Approach

Thermokarst structures differ in their surface properties from other geomorphological structures in periglacial landscapes. Thermokarst and thermo-erosion result in negative relief forms like deep depressions or valleys, which are straightforward to identify in tundra regions, because of generally minor vegetation cover. These structures either contain large lakes or have a local hydrological regime resulting in high soil moisture at the bottom. The high soil moisture benefits vegetation communities adapted to such very wet conditions. These vegetation communities are quite distinguishable from communities settling in upland positions or on well drained slopes. Their spectral properties are also largely different. Thus, these characteristics enable the discrimination of thermokarst structures from other relief features using both remotely sensed and elevation data. Furthermore, it is possible to deduce the development stages of a periglacial landscape by the analysis of geomorphological units using their spectral properties in combination with morphometric analysis, an approach already applied to thermokarst basins in Alaska by Hinkel et al. (2003). This approach allows for qualitative conclusions on thermokarst development in a region to be made.

To examine the key site at Cape Mamontov Klyk (73.61° N, 117.18° E) and the surrounding coastal plain on the western Laptev Sea coast we used multi-spectral, high-resolution Landsat-7 ETM+ data. The Landsat-7 image was integrated with a digital elevation model (DEM) and a supervised classification was undertaken on the combined dataset. The aim of the classification was the general mapping of terrain surfaces and the quantification of thermokarst-affected surfaces in the investigation area. Additional data layers were used to evaluate the classification results. These layers included field data, a geological map, and high-resolution, panchromatic CORONA satellite images. The analysis resulted in spatial information on the quantity, distribution and quality of the extensive thermokarst processes in the region under investigation.

3.4 Investigation area

The study area covers an extent of 3403 km^2 (*c.* 73.33°-73.66° N, 116.0°-119.0° E) and is situated in the western Laptev Sea coastal lowland between the rivers Anabar and Olenek, in north-central Siberia (Figure 3-1). Its northern boundary is the Laptev Sea, and the southern boundary is formed by the Pronchishchev Ridge about 30 km to the south. The coastal lowland in front of this hill range is a smoothly sloped plain with elevations between 25-55 m a.s.l. (Figure 3-2). Altitudes increase towards the south, to a maximum height of 270 m reached in the hills. The overall inclination of the plain is less than 1° towards NNE. The

study area is part of the arctic tundra zone of the northern hemisphere (Treshnikov, 1985). Long severe winters and short cold summers are typical for the continental Arctic climate in the region. The mean annual air temperature is –14°C. The mean winter temperature is about –22°C, and mean summer temperatures vary from +5 to +10°C (Treshnikov, 1985). There is 230-270 mm of mean annual precipitation in the region, 75% of which precipitates in summer. In general, snow cover starts in the end of September and disappears towards the end of June. The thickness of snow cover is less than 40-50 cm. Aeolian snow removal and re-deposition occurs in extensive areas depending on wind and geomorphological conditions. The study territory belongs to the zone of continuous permafrost reaching 400-600 m in depth (Yershov, 1998). The mean annual ground temperature is –11 to –12°C, and the thickness of the active layer varies between 20-50 cm in July. The permafrost coasts in the investigation area are affected by strong coastal erosion. Are (1999) calculates a mean coastal retreat rate of 2 m y^{-1}.

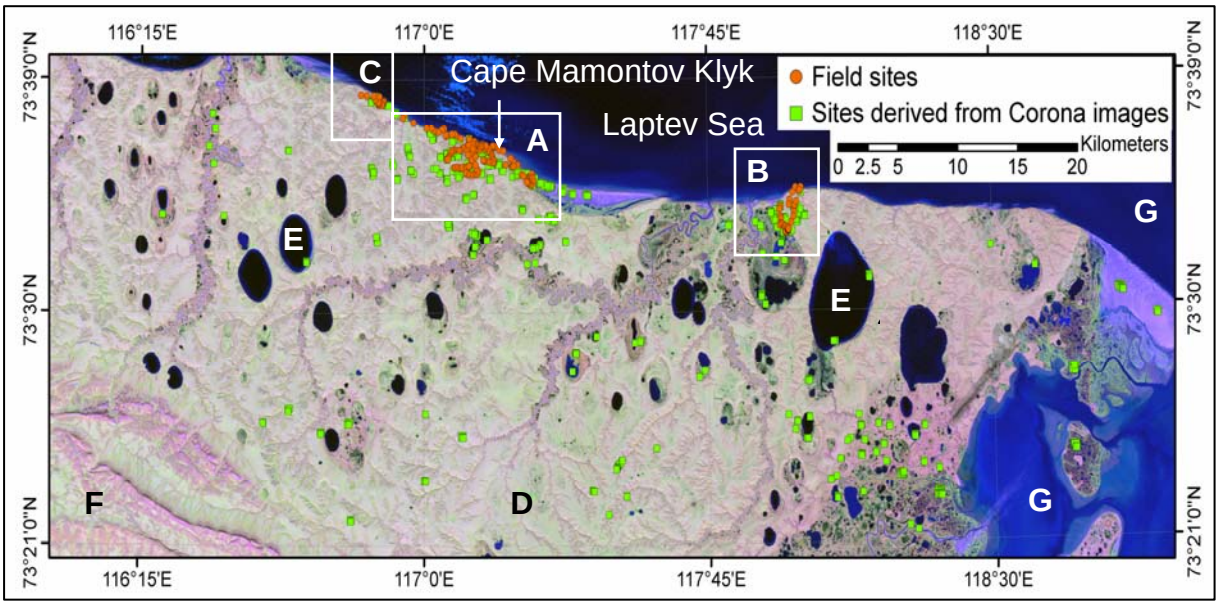

Figure 3-2: Landsat-7 ETM+ image of the investigation area (band combination 5-4-3), showing the location of all 178 field sites, where ground data was collected during the field campaign. The white squares mark the investigated regions around Cape Mamontov Klyk (A), a thermokarst depression east of it (B), and a thermokarst depression west of it (C). Additional evaluation sites derived from high-resolution CORONA images are also indicated. After image stratification only the regions 'plain' (D) and 'inland water bodies' (E) were used for a maximum likelihood classification. The regions 'hill range' (F) and 'marine water' (G) were omitted from the classification process.

The geocryological conditions of the region and the cryolithology of the sediments are still poorly known. Major geomorphological features in the plain are river valleys with meandering streams, discharging towards the N, NE and E (Figure 3-2). The longest streams

originate in the Pronchishchev Ridge. Extensive thermokarst and thermo-erosion structures are also present. Deep thermokarst depressions and thermokarst lakes, most of them ellipsoid and strictly N-S oriented, occur along the river valleys and on the Edomas. The Edoma uplands are elevated surfaces between the river valleys and thermokarst depressions. They are erosional remnants of the Late Pleistocene accumulation plain consisting of ice-rich deposits of the Ice Complex. The whole plain is incised by thermo-erosional valleys which drain the interfluve uplands to the river valleys or the coast. A schematic view of major relief features and the geology in the coastal plain is given in Figure 3-3. The Pleistocene geological evolution of the territory is characterised by several stages of subsidence (Pliocene to Early Pleistocene; Middle Pleistocene to Late Pleistocene) and uplift (Early Pleistocene to Middle Pleistocene; Late Pleistocene to Holocene). The region is neo-tectonically active. Formations outcropping at the surface include Late Pleistocene and Holocene sediments in the plain, and Mesozoic sedimentary bedrocks in the hill range (Geological Map Ulakhan-Yunkyur, 1986).

The Middle to Late Pleistocene (Q_{II} - Q_{III}) deposits consist of limnic-alluvial sands and silts with pebbles and gravels. Peat layers occur in the upper part of this unit. These deposits outcrop in deep river valleys and thermokarst depressions. The sandy deposits have a gravimetric content of segregated ice of 25-40 weight-% (compared to dry sediment mass). Late Pleistocene to Holocene deposits (Q_{III}^{2-4} - Q_{IV}^{1-2}) are the most extensive deposits cropping out at the surface in the region. The Late Pleistocene deposits (Q_{III}^{2-4}) consist of very ice-rich silty to sandy sediments (Ice Complex formation), with high organic content in the form of peat layers, dispersed plant remains, and macrofossils of the Beringian mammoth fauna. The ground ice in these strata consists of massive ice bodies (ice wedges) and segregated ice in the sediment (ice lenses, ice bands). The gravimetric content of segregated ice in these deposits is 50-90 weight-%, whereas in zones with ice bands or peat layers the ice content may exceed far above 100 weight-%. The average thickness of the Ice Complex is 20-30 m, with a thinning towards the hill range. The Holocene (Q_{IV}^{1-2}) consists of fluvial, limnic, thermokarst and marine deposits, mainly defined as sand, silty sand, silt, clayey silt, peat lenses and peat layers. These deposits outcrop in river valleys, thermokarst depressions, thermo-erosional valleys and coastal sites of the region. The gravimetric ice content is up to 130 %, again with the highest ice content occurring in zones with peat inclusions and ice bands. Additionally, in places the Ice Complex is discordantly covered by a relatively thin layer (<2 m) of ice-rich sediments that were probably formed by small-scale initial thermokarst during the Holocene. For the investigation area a few preliminary AMS radiocarbon datings for sediments of drained thermokarst lakes and sediments of a thermo-

erosional valley suggest Early to Late Holocene ages and thus are in general agreement with datings from other thermokarst sites in the Laptev Sea region (datings: L. Schirrmeister, unpublished data). Preliminary AMS radiocarbon datings of peat and wood from a marine terrace suggest historical ages less than 1500 cal y BP for these deposits (cal y BP – calibrated years before present).

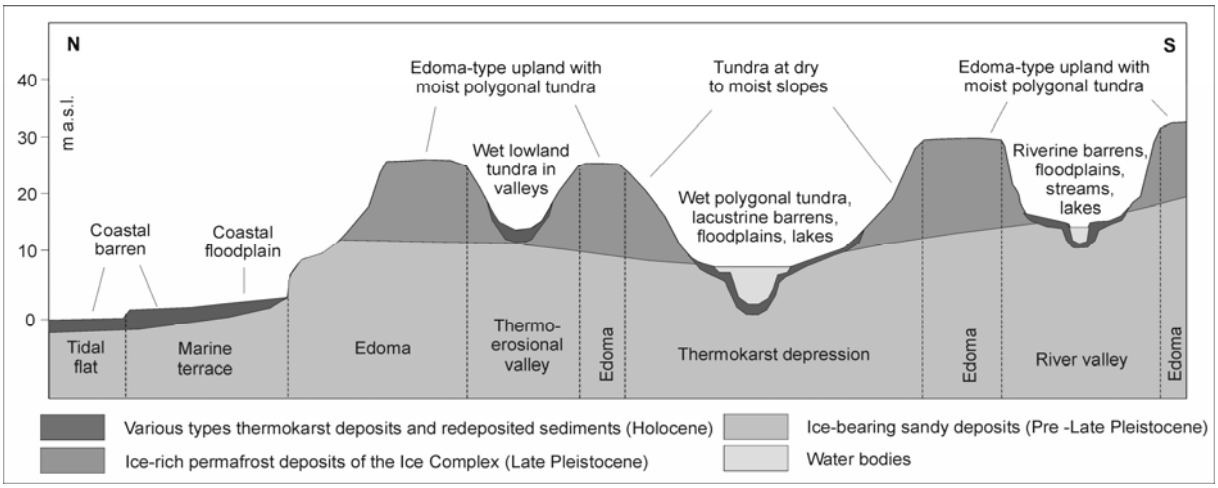

Figure 3-3: Schematic view of major relief features identified in the field (descriptions in the profile), classes associated with them (descriptions above the profile) and the geological situation in the investigation area at Cape Mamontov Klyk (legend).

3.5 Fieldwork

Fieldwork was conducted in the vicinity of Cape Mamontov Klyk (Figure 3-2) within a three - week period during a Russian-German field campaign in August 2003 (Schirrmeister et al., 2004). Beyond sedimentological and cryolithological sampling of outcrops exposed at the up to 30 m high coastal cliff, the hinterland was investigated for ground data acquisition in terms of surface characteristics and geomorphology.

Altogether, surface parameters were observed and described for 178 sites (Figure 3-2). The closer area around Cape Mamontov Klyk contributed 129 sites, and two remote thermokarst depressions contributed another 49 sites. The recorded parameters for each site include relief type, slope inclination, major vegetation composition, estimation of soil moisture, active layer depth, and quantity and type of water bodies. A location was chosen as a site, when these parameters were relatively homogeneous in the surrounding area within a radius of about 25 m. According to the morphological situation and surface characteristics, each location was assigned to one of 7 major terrain surface classes occurring in the plain. A schematic view of these classes is illustrated in Figure 3-3. The field data was used for the verification of the classification results. An image database containing more than 200 detailed photographs from 115 of the sites was also developed.

3.6 Digital elevation data

Elevation models are important tools for the investigation and classification of terrain and surface features. The DEM of the investigation area was calculated from manually digitised elevation information of three scanned and geo-referenced 1:100,000 topographic map sheets, originally produced by the Soviet government in 1977-78. The content was based on aerial imagery and field surveys undertaken in 1971-72. The maps are projected in Gauss-Kruger (Pulkovo 1942, zone 20) projection based on the geodetic ellipsoid Krassovsky 1940. All height information from the maps (contours, elevation points, streams, and lakes) were used for the calculation of the DEM applying the TOPOGRID tool of ArcInfo^{TM}. TOPOGRID is based on an enhanced ANUDEM algorithm after Hutchinson (1989) and calculates a hydrologically correct DEM by using drainage enforcement and removal of spurious sinks. The algorithm produced good results for this type of periglacial landscape, although a small error may be introduced by the removal of natural sinks in some locations. The grid cell size for the output DEM was chosen at 30 m, in agreement with the pixel size of Landsat-7 ETM+ data. The vertical accuracy of the DEM was tested by comparing 304 original elevation points from the map with corresponding DEM grid cells. 286 values (94.1 %) were within an error range from –1 m to +1 m. The mean error was +0.1 m, while isolated extreme values may range to –5.9 m and +10.1 m. These few significant errors were irregularly located at extreme positions like high peaks or at sharp natural boundaries like steep cliffs, where data density was not high enough for correct modelling of the surface. Other independent elevation data was not available for testing the DEM accuracy. Lake bathymetry was not provided with the topographic maps. We concluded, that the DEM had sufficient quality to be used for the supervised classification and further geomorphological analyses of relief structures in the study region.

3.7 Remote sensing data

3.7.1 Basic information

The area of investigation was covered by a subset from a multi-spectral Landsat-7 ETM+ satellite image from 4th August 2000 (path 139, row 8; Figure 3-2). The image was level 1G systematically corrected, including standard radiometric and geometric corrections. For the image classification only the optical bands 1-5 and 7 were used. They have 30 m ground resolution, and cover the visible, near infrared and shortwave infrared wavelengths (e.g. Goward et al., 2001). The panchromatic band 8 and the thermal band 6 were omitted from the analysis. To convert the raw 8-bit digital numbers to reflectance and to correct for

time/location-specific atmospheric conditions, an atmospheric correction was applied based on image values alone using a dark object subtraction approach modified to include a correction for atmospheric transmittance. The approach adopted was that developed by Chavez (1996) and named COST, as the COsine of the Solar zenith angle is used as an approximation for atmospheric Transmittance. Chavez (1996) shows that there is a first order relation between these two values and the resulting atmospheric correction produces good results for a wide range of conditions. For accuracy estimation we compared spectra of surface types (grass, water) derived from the corrected satellite image with standard spectra provided by a spectral library (in this case, the John Hopkins University spectral library). Although Chavez (1996) states that the COST method has not been tested for solar zenith angles greater than 55°, we applied the method to our data (solar zenith angle of 56.2°) and achieved good results, qualifying this approach for the geomorphological application of the Landsat-7 ETM+ data in this work. As a final step, the image was more precisely georectified using 73 ground control points derived from the topographic maps described above. The root mean square error averaged at 0.89, thus a horizontal error of less than 30 m was achieved for most locations.

Additionally, three panchromatic 3 m ground resolution images and one 10 m ground resolution image from the CORONA satellite archive covering large parts of the area of investigation were used for subsequent evaluation of the classification results achieved using the multispectral Landsat data and the DEM. The images were acquired on 20th July 1965 and 14th July 1975. The particular value of high-resolution CORONA images in supporting periglacial research, especially for the observation and analysis of thermokarst-related structures, has already been demonstrated for the Bykovsky Peninsula in the eastern Laptev Sea coastal lowlands (Grosse et al., 2005). For the analysis and evaluation of the classification result, additional data was collected for each class with the CORONA images to supplement the field data. Individual geomorphological structures (thermokarst depressions, river valleys, pingos) were manually mapped for the whole investigation area with a simple image combination technique of high-resolution CORONA images and multispectral Landsat-7 data, based on the overlay of both image types in the form of semi-transparent GIS-layers. This technique allowed for the beneficial use of both high-resolution and multispectral information in one image. Thermo-erosional valleys and Edoma uplands were mapped with the same technique at two sites (Figure 3-2, sites A+B).

3.7.2 Classification approach

Before data processing, the few cloudy areas in the image were manually masked. The classification approach adopted was based on a combination of image stratification and maximum likelihood classification (Figure 3-4). Thermokarst terrain is situated only in the coastal plain, thus we separated the coastal plain from other regions.In the first step, a decision tree was used to stratify the image into three regions ('Water', 'Plain', 'Hill range'). We separated water from land using a threshold of 15 % reflectance in the short wave infrared wavelength (band 5). Pixels with lower reflectance were assigned to water. We applied a DEM-derived altitude threshold of 55 m to separate the remaining non-water pixels into a 'Hill range' and a 'Plain' region. The altitude of 55 m was empirically defined, as outcropping bedrock and rock debris was detected by visual inspection only in pixels >55 m in the investigated region. When pixels with outcropping bedrock or rock debris occurred in the resulting mask polygon, all pixels in this particular polygon were associated with the 'Hill range' region, otherwise these pixels were reintegrated in the 'Plain' region. The region 'Water' was further divided into a marine part (Laptev Sea and bays) and an inland part (thermokarst lakes and rivers) by an image segmentation algorithm. For further classification with the maximum likelihood algorithm only pixels from the region 'Plain' and the sub-region 'Inland water bodies' were used, as only these regions covered the features of interest (Figure 3-2).

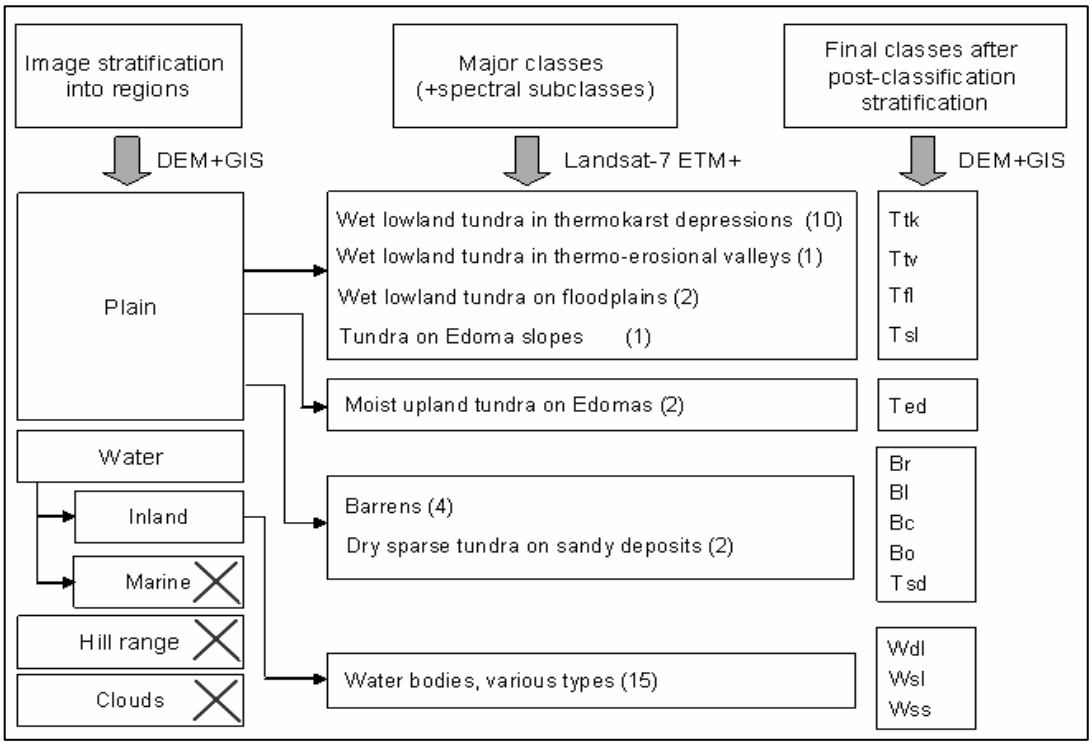

Figure 3-4: Image classification scheme for the investigation area.

Training data acquired from visual interpretation of the Landsat-7 ETM+ images was used for the maximum likelihood classification. Data selection was guided by field knowledge and a geological map. The whole set of training data consisted of 8 major classes (7 land, 1 water), divided into 37 spectral subclasses (22 land, 15 water) (Figure 3-4).

The spectral separability of the individual training data was evaluated and improved with the n-dimensional visualiser tool in the ENVI™ image processing software for each region. With this tool it is possible to rotate a scatterplot with pixel clusters of training classes interactively in n dimensions. The coordinates of a pixel in the scatterplot are determined by its spectral properties, or by its reflectance values in different wavelengths. For the region 'Plain' we used the six optical Landsat-7 ETM+ bands, the Normalised Difference Vegetation Index (NDVI) derived from bands 3 and 4, the DEM (scaled to 0-1) and a derived slope map (scaled to 0-1). Hence, the scatterplot had n=9 dimensions. The pixel clusters of the training classes were compared to each other with respect to how well they were separated from each other in all 9 dimensions and how compact the pixel clusters were. Scattered clusters were condensed by omitting obviously outlying pixels. Means and standard deviations from each cluster were enhanced in this way, resulting in an improved classification using the maximum likelihood method. The standard parameters of the Jeffries-Matusita Distance and Transformed Divergence were computed to measure the spectral separability for all classes. Both values, based on covariance-weighted distance between the class means, were scaled between 0 to 2 and indicate how each class is statistically separate from another class. During the iterative evaluation process, classes with separability values less than 1.9 were re-examined in the n-dimensional visualiser and further refined by condensing the clusters and omitting outlying pixels. Finally, the maximum likelihood classification was applied separately for the region 'Plain'. For the sub-region 'Inland water bodies' the maximum likelihood classification was conducted in the same manner, but with the 6 Landsat-7 bands only (i.e. omitting the DEM, slope and NDVI data layers).

For further improvements in classification accuracy, several rule-based algorithms for post-classification stratification were applied for some of the classes within a GIS. The rules were based on altitude and distance to coast, rivers or lakes. In this way the classes 'Barrens' and 'Inland water bodies' were refined and further separated.

3.8 Results and analyses

3.8.1 Classification results

Of the 3403 km^2 for the total investigation area, the cloud mask accounted for 14 km^2. The first image stratification of the remaining area resulted in 870 km^2 for the 'Marine water' class, 202 km^2 for 'Hill range', 2111 km^2 as 'Plain' and 206 km^2 as 'Inland water bodies'. In the regions of interest, 'Plain' and 'Inland water bodies', 13 final classes were obtained using spectral classification with the supervised maximum likelihood classification and a second stratification (Table 3-1). The total spatial coverage of each class is given in Table 3-2.

3.8.2 Evaluation and accuracy assessment of the classification

No previous maps with similar information on thermokarst or other thaw-induced landscape features were available for the generation of an independent data set for accuracy evaluation. Thus, the accuracy of the classification result was evaluated initially through visual inspection of the Landsat-7 ETM+ image. A second independent dataset was compiled with a stratified random selection using 10 % of each class from a pixel pool, derived from the field data and interpretation of the 10 m CORONA image. This dataset was used for the calculation of a confusion matrix (Table 3-3). The 4 barren classes and 3 water classes were condensed for the accuracy assessment to the classes B and W. The overall classification accuracy for our approach with the Landsat-7 ETM+ image was 78.92 %. The Kappa value, a measure of aggreement with the training data, was calculated as 0.76.

Thermokarst-affected tundra landscapes are spatially complex in terms of geomorphology and vegetation cover. Therefore some mis-classification with remote sensing data will arise. One of the most important factors is, that geomorphological features, hydrological conditions and vegetation communities can change dramatically over small distances even at scales smaller than those of a Landsat pixel. This makes the referencing process of the various data layers for the classification, including the field data, a crucial step and a prominent source of misclassification. Another source of classification error is the lack of correspondence between the map-derived DEM and real geomorphological features, when they are below recognition at the 1:100,000 map scale. Field data was relatively sparse and spatially limited due to restricted field time, but supplementary mapping with the high-resolution CORONA images proved very useful for the generation of additional information and complemented the classification evaluation process.

Table 3-1: Characterisation of the final classes and their relevance to thermokarst and degradation of permafrost deposits

Name of final subclass	Description	Interpretation of thermokarst and degradation of the ice-rich Ice Complex deposits
Bc	Barrens, coastal: Marine terraces with mainly sandy deposits, elevated about 1 m a.s.l., barren or sparsely vegetated; driftwood accumulations; several 100 m in width; active layer >1 m deep; tidal flats with clayey to sandy deposits, >100 m width during low tide	Ice-rich Ice Complex deposits already completely degraded
Br	Barrens, riverine: Fluvial terraces with silty-sandy deposits, point bars with spotty vegetation or sandbanks; active layer >1 m deep; width of these terraces mostly <50 m	Ice-rich Ice Complex deposits already completely degraded
Bl	Barrens, lacustrine: Beaches or barren terraces of some large lakes; mostly in areas, where the sandy deposits underlaying the Ice Complex outcrop	Ice-rich Ice Complex deposits already completely degraded
Bo	Barrens, other types: Includes nival niches, snow patches, and barrens in front of them, which were identified mainly in thermo-erosional valleys close to the hill range for this Landsat-7 image; other pixels, which probably indicate patches of non-vegetated sandy deposits, were observed in the SE of the investigation area	No common interpretation possible; snow patches accumulate mostly in nival niches of thermo-erosional valleys; they are important factors of erosion in the lowland
Ttk	Wet tundra with indications of thermokarst: Areas with many small ponds and low centre polygons dominated by wetness-adapted plants, like sedges and moss; this class occurs mainly on the bottoms of the extensive subsidence areas in thermokarst depressions; Ttk is also detected in other regions closer to the hill range, where so-called ‘dellies’ occur (these are initial thermokarst features indicating subsurface drainage from elevated areas)	Ice-rich Ice Complex deposits already partially to completely degraded; existence of taliks possible; refreezing taliks are indicated by the presence of pingos especially in the north-eastern part of the study area
Tfl	Wet lowland tundra in floodplain-like areas: Riverine, lacustrine and coastal lowlands with very poor drainage, large amount of ponds in low-centre ice- wedge polygons and relatively sparse vegetation (mostly sedges); high ratio of water sufaces compared to land surface	Ice-rich Ice Complex deposits already strongly to completely degraded
Ttv	Wet tundra mainly in thermo-erosional valleys: Wet and flat floors of wide U-shaped thermo-erosional valleys with shallow running water or small ponds; dominated by dense vegetation of grass, sedges and moss	Ice-rich Ice Complex deposits already partially to strongly degraded; thermokarst valleys are important factors of hydrology due to drainage of uplands and water supply for thermokarst depressions

Table 3-1: Continuation

Name of final subclass	Description	Interpretation of thermokarst and degradation of the ice-rich Ice Complex deposits
Ted	Moist to wet tundra on Edomas uplands: Areas with moist and moderate moist upland tundra (grass, moss, lichen); these upland areas represent remnants of the Late Pleistocene accumulation surface; the deposits below consist of syn-sedimentary frozen, ice-rich sediments	Ice-rich Ice Complex deposits largely not degraded; in places occurrence of small ponds with initial thermokarst development and active layer deepening
Tsl	Tundra on Edoma slopes: Relatively well drained slope areas surrounding the Edoma uplands towards depressions or valleys; dominated by tussocky grass tundra and often covered with thermokarst mounds	Ice-rich Ice Complex deposits already weakly to partially degraded
Tsd	Tundra above sandy, relatively well drained deposits: Occurs mainly in the eastern part of the investigation area, where sandy deposits outcrop at the surface, which in other regions are covered by the Ice Complex, and in large river valleys, where sand was deposited due to fluvial processes	Ice-rich Ice Complex deposits already completely degraded; occurence of small basins or basin remnants indicates thermokarst also in sandy deposits
Wdl	Water, deep large lakes: Extensive deep thermokarst lakes, often with shallow littoral terraces, and situated in thermokarst depressions; known lake depths up to 29 m below lake level, diameter of the lakes is up to several km	Ice-rich Ice Complex deposits already completely degraded; existence of deep basins indicates thawing also of underlaying sandy deposits; extensive taliks very likely
Wsl	Water, shallow large lakes: Extensive lakes with general shallow bathymetry, situated within a depression or river valley; lake area in this class was empirically defined with >0.15 km^2	Ice-rich Ice Complex deposits already partially to completely degraded; existence of taliks possible
Wss	Water, small shallow lakes, rivers and mixels: small lakes or lake remnants in lowlands and small ponds on Edoma uplands, lake area in this class was empirically defined with <0.15 km^2; Active and dead river channels, maximal river widths are 60 m, maximal lengths 100 km; Mixels, consisting of vegetated or barren shores of lakes and rivers and overgrown ponds	On Edoma uplands: ice-rich Ice Complex deposits not or weakly degraded; depending on drainage high potential of lake-growing, initial thermokarst and permafrost degradation; In lowlands and river valleys: ice-rich Ice Complex deposits already strongly to completely degraded

Table 3-2: Spatial extent of each class in the study area. The number in brackets behind the water classes indicates the number of individual lakes.

Class name	Area	
	km^2	%*
Bc	51.6	2.2
Br	11.2	0.5
Bl	3.9	0.2
Bo	0.5	0.0
Ttk	260.0	11.2
Tfl	99.8	4.3
Ttv	340.0	14.7
Ted	514.8	22.2
Tsl	674.1	29.1
Tsd	155.1	6.7
Total land surface	2111.0	91.1
Wdl (121)	129.0	5.6
Wsl (58)	30.9	1.3
Wss (8928)	46.6	2.0
Total water bodies (9107)	206.5	8.9
Total classified area	2317.5	100

Table 3-3: Confusion matrix of classification and ground truth data.

	Ground truth (pixel)								
Class	B	Tsd	Tsl	Ttv	Ttk	Tfl	Ted	W	Total
B	95	0	0	0	0	3	0	0	98
Tsd	1	57	0	1	1	0	0	1	61
Tsl	1	1	90	17	12	1	9	0	131
Ttv	0	0	11	44	28	1	1	0	85
Ttk	0	0	3	11	36	8	5	0	63
Tfl	0	0	0	0	5	33	0	0	38
Ted	0	0	0	3	4	0	108	0	115
W	0	0	0	0	0	16	0	76	92
Total	97	58	104	76	86	62	123	77	683

3.8.3 Analysis of the classification result

For each of the classes the mean elevation above sea level and spectral characteristics for the whole investigation area were calculated (Figure 3-5). The class Ted has the highest mean elevation of about 40 m. The mean elevations of Ttk, Ttv and Tsl are between 20-25 m. All other classes have mean elevation of less than 15 m. As expected, the barren (B) and water (W) classes are well separated from vegetated classes by their spectral properties. Obviously, the class Wdl has the lowest reflectance and NDVI values, whereas Wss has a relatively high

NDVI, indicating the membership of mixed water/vegetation pixels along shorelines and pixels where vegetation grows in shallow ponds. The classes Ted, Ttk, Ttv and Tsl have rather similar reflectance curves, although Tsl has a slightly lower NDVI and the reflectances of Ttk and Ttv are slightly lower, probably indicating the higher soil water content in both classes. Tfl has the lowest reflectances and NDVI due to the high amount of ponds less than the nominal pixel size (predominantly low-centre ice wedge polygons) or generally strong water saturated ground. Tsd has a similar low NDVI and a relatively high reflectance in band 5, indicating sparse vegetation and a high soil signal. The final thematic map derived from the classification is shown in Figure 3-6.

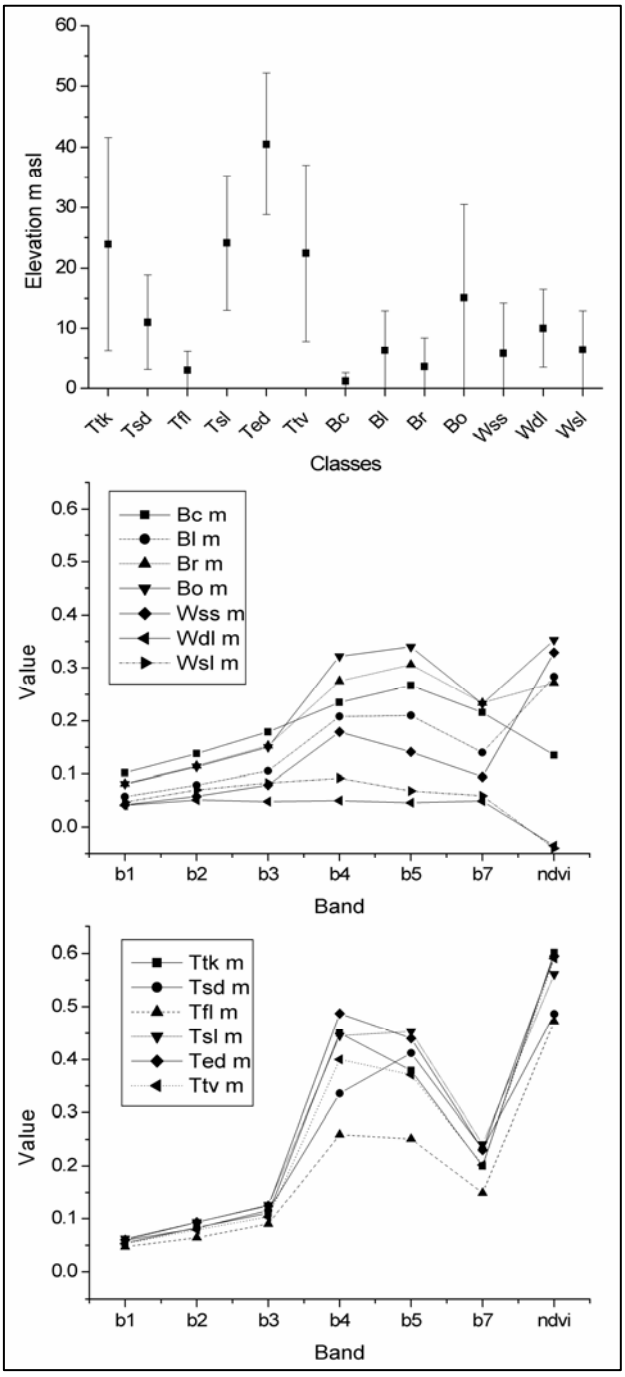

Figure 3-5: Mean elevation and spectral characteristics for each class (Top – mean elevation and standard deviation for each class; Middle – mean reflectance and NDVI for barren and water classes; Bottom – mean reflectance and NDVI for vegetated tundra classes).

Most difficulties were encountered for the discrimination between the classes Ttk, Ttv and Tfl, which frequently led to misclassification between them (Table 3-3). These classes cover similar thermo-denudation terrain types, often with similar vegetation communities (sedges, grasses and mosses) and soil moisture conditions or presence of sub-pixel water bodies. Thus, their spectral characteristics were also similar (Figure 3-5). The generally low mean elevation of the class Tfl was partially useful for the separation from Ttk and Ttv.
For further evaluation of the classification, the class composition of several manually mapped geomorphological structures were analysed (Table 3-4).

Table 3-4: Class composition for some geomorphological structures.

Mapped structures	4 most common classes (%)			
156 thermokarst depressions, inclusive surrounding slopes	W (34)	Tsl (18.5)	Ttv (16)	Ttk (12)
16 pingos	Tsl (59.5)	Tsd (18)	Ttv (10)	Ttk (4.5)
7 river valleys, inclusive surrounding slopes	Tsd (23.5)	Ttv (22)	Tsl (20)	Ttk (12.5)
68 thermo-erosional valleys as 30m buffer around the central valley axis	Ttv (51)	Tsl (35)	Tsd (5.5)	Ttk (5)
68 thermo-erosional valleys as 60m buffer around the central valley axis	Tsl (45.5)	Ttv (41.5)	Tsd (5)	Ttk (4.5)
12 Edoma uplands	Ted (80)	Tsl (10.5)	Ttk (5.5)	Ttv (3.5)

Thermokarst depressions and river valleys were mapped along the upper boundary of the slopes surrounding them. The main class in thermokarst depressions clearly is water (W). Tsl and Ttv are next, indicating mainly the included slopes, followed by Ttk. River valleys were mapped including the surrounding slopes. These valleys are very heterogeneous in their class composition, consisting of similar proportions of Tsd, Ttv and Tsl, and to a smaller extent of Ttk. Tsd in the river valleys represents fluvial transported sands and sandy deposits, which usually underlie the Ice Complex in the region and outcrop in the deep valleys. As most of the rivers in this area are not very wide, the class W occurs only at 7.5 %. Pingos are mainly characterised by Tsl and to a lesser amount by Tsd, indicating a relatively dry surface due to upheaval and subsequent good drainage. Edoma uplands are mainly composed of Ted, and to a much lesser extent of Tsl, Ttk and Ttv. The class Ttk also occurs in uplands close to the Pronchishchev Range. Analyses with 3 m CORONA images proved that these Ttk-classified areas in uplands are so-called delly structures, which are subsurface drainage features on

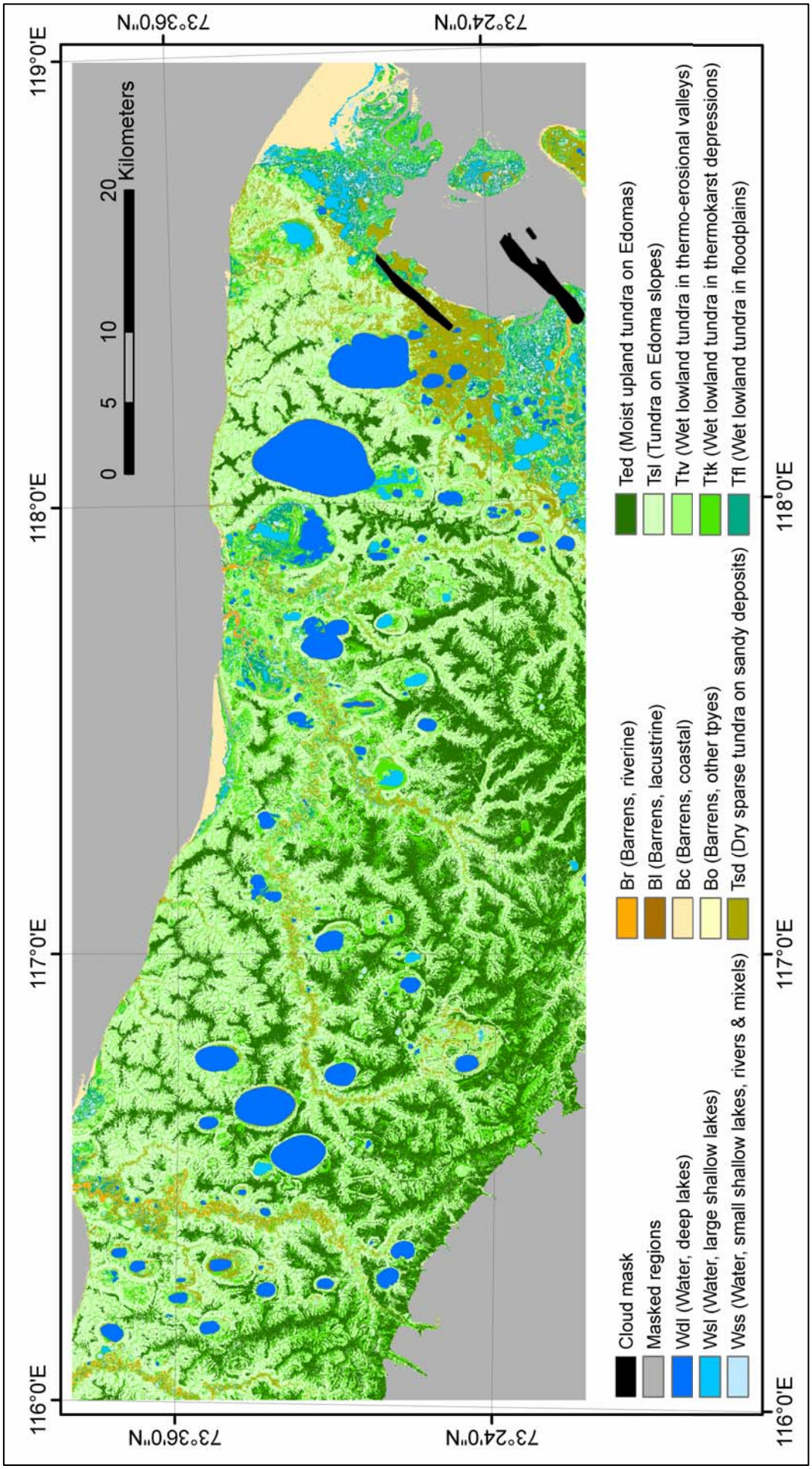

Figure 3-6: Final classification map of terrain surfaces the investigation area.

slopes containing ice-rich deposits. They are considered to be an early form of thermokarst. The same images indicate that the class Ttv on Edoma uplands is characterised by many water-filled low-centre ice wedge polygons especially in regions with poor drainage. The central axes of the thermo-erosional valleys were mapped, and a buffer around these features was formed. Within the 30 m buffer, the class Ttv dominates, followed by Tsl and other tundra types. Within the 60 m buffer, the class Tsl dominates over the other classes. This pattern indicates that the class Ttv in thermo-erosional valleys is bound to the narrow valley floor, which is often less than 50 m wide.

Other classification approaches, i.e. for vegetation classification in tundra environments, reported comparable classification accuracies mostly in the range from 60-85 % overall accuracy (e.g. Joria & Jorgenson, 1996; Virtanen et al., 2004). In our approach the most obvious misclassification was identified for classes which are spectrally and genetically very similar (Table 3-3: Ttk and Ttv). These classes are also similarly interpreted in terms of relevance for thermokarst, thus the misclassification is not so severe.

3.9 Discussion

An interpretation of the relevance of each class for thermokarst and the degradation of the ice-rich deposits of the Ice Complex in the investigation area is given in Table 3-1.

Following this interpretation, thermokarst formation and subsidence processes were major factors in the development of the coastal plain around Cape Mamontov Klyk in the western Laptev Sea area during the Holocene. When considering only the Edoma terrain surfaces (Ted) as not affected by permafrost degradation, 78 % of the investigated area is affected by thermokarst, thermo-erosion or slope denudation (Table 3-2, Figure 3-6). The spatial distribution and morphology of thermokarst and thermo-erosion features in the investigation area indicate the self-reinforcing effect of thermokarst formation in ice-rich permafrost and accompanied drainage change. Persistent thermal denudation and slope processes like solifluction or slope wash lead to spatial expansion and coalescence of negative relief structures. The significance of these still active processes is suggested by the extensive areas classified as slopes (Tsl: 29 %). Surfaces in the southern upland part of the investigation area near the Pronchishchev Ridge are clearly less affected by permafrost degradation than in the northern region, which has lower elevations and is closer to the modern coast. Deep thermokarst depressions with lakes mostly occur in the northern region, whereas the southern area is dominated by Edomas with thermo-erosional valleys and extensive slopes. In southern uplands close to the hill range the discharge is more directional and the terrain is better

drained than in the coastal lowlands. Large subsidence areas have formed near the mouths of large rivers at the coast. Here, the thermal and erosive effect of rivers is combined with subsidence in thermokarst depressions and the fluvial truncation of thermokarst lakes. These observations suggest that thermokarst in the region did not develop evenly in both space and time during the Holocene, but was strongly dependent on the development of the hydrology of the region. The occurrence of several lake terraces in many thermokarst depressions also supports the idea of changing hydrological conditions and for variable thermokarst development in the region.

The spatial distribution of thermokarst depressions and thermo-erosional valleys strongly influences the pattern of coastal retreat. The existence of deep thermokarst depressions close to the coast is the first step towards the development of a lagoon formed by sea ingression. In such thermokarst lagoons the thermokarst activity and destruction of ice-rich permafrost is increased due to changes in hydrology and hydro-chemistry. This process probably has accelerated the coastal retreat in areas with intense thermokarst subsidence during the Holocene marine transgression (Romanovskii et al., 2000).

The Edoma surfaces are considered to be the remnants of the Late Pleistocene palaeo-surface that was part of an extended accumulation plain in front of the Pronchishchev Ridge. Their distribution and morphology changes from the foothills of the Pronchishchev Ridge to the coast. Near the hills these surfaces are much less dissected by thermo-erosional valleys, depressions and slopes. Close to the coast only a few Edoma upland surfaces remained unaffected by permafrost degradation, as the classes Tsl and Ttv indicate. A high concentration of thermokarst occurs in the form of extensive thermokarst depressions, which often contain large lakes. Two types are obvious: distinct and predominantly N-S oriented depressions on interfluve areas, and extensive lowlands at the coast, especially at river mouths. The first type often contains large oriented lakes. Probably depending on the maturity of the depression and the supply of water from snowmelt and permafrost thawing, basins can contain large deep lakes, large shallow lakes, or even no lakes. The deep lakes are an indicator for very deep permafrost degradation and probably deep talik formation. The bathymetries of three deep lakes in the study region, one situated 14.5 km and the other two 22 km away from the coast, were measured by Bolshiyanov & Makarov (2004). The observed maximum water depths for the central lake basins were 20.5 m, 27.0 m and 29.0 m. When compared to modern lake levels (19.6 m, 19.9 m, and 18.7 m a.s.l., respectively), it is clear that the bottoms of all three lakes are situated well below the modern sea level. Two of the lakes are situated only 1.5 to 2 km north of the Pronchishchev Range, indicating the presence of thick ice-rich

sediments close to the mountain range. In basins with only shallow or no lakes, ice-rich permafrost is at least partially destroyed. A few basins in the eastern study area show signs of refreezing taliks, indicated by the formation of pingos. The reason for the specific orientation of the lakes and basins in the study area has not been investigated in detail, but there is agreement in the literature that wind plays an important role for lake orientation in the North American Arctic (e.g. Carson & Hussey, 1962; Coté & Burn, 2002). In addition, in the study area a northward migration of lakes following the general inclination of the coastal plain, seems to be a factor in determining lake orientation. Indicators for this hypothesis are sequential lake terraces in many depressions, which are wider in the south and narrower in the north.

The other type of thermokarst is formed by extensive lowlands on the coast, which have formed especially at the wide mouths of large rivers. In these regions various features occur, like active and inactive river channels, truncated and coalesced thermokarst depressions, lakes, lagoons, and floodplain-like areas. The lakes are generally shallow and smaller lakes are often overgrown with vegetation. Strong permafrost degradation is also observed along the river valleys. Generally, thermo-erosional valleys are widespread in the interfluve areas. The ramification of these valleys increases from south to north, or from higher elevations to lower elevations of the plain. The valleys drain the upland areas and generally have wide slopes.

3.10 Conclusion

Landsat-7 ETM+ imagery, in combination with elevation data, was used as an efficient tool for classification and mapping of thermokarst-affected terrain in a periglacial tundra landscape in northern Siberia and provided the spatial coverage which was necessary for observations over a large study area. Tools for the combination of different data types from various sources (remote sensing images, DEM, field data) provided by GIS software were very beneficial for the classification approach and for analysing the complex periglacial terrain of the study area. It is possible to further refine the results by applying additional GIS-based stratifications, i.e. when other thematic data, like vegetation or soil maps, become available. A more detailed characterisation of vegetation, soils and their spectral properties in the field will also enhance the classification result. An improvement would also be made by using a better resolution DEM for the classification approach. This would particularly increase the classification accuracy for the slopes (Tsl).

The quality, quantity and spatial distribution of thermokarst-affected terrain were investigated

at the key site around Cape Mamontov Klyk in the Laptev Sea coastal lowland. Thermokarst was identified to be the dominating process in relief formation in the study area during the Holocene. Only 22 % of the investigated coastal lowland is not influenced by thermokarst.

The proposed method, with modifications for local peculiarities, can be applied for the characterisation and mapping of terrain features at large regional scales, e.g. for the whole Laptev Sea coast or other Arctic regions. The results of this study are of particular interest for the palaeo-environmental reconstruction and assessment of coastal dynamics at ice-rich permafrost coasts. Furthermore, the results can be used for the development of GIS- and DEM-based volumetric modelling of thermokarst and connected matter fluxes (i.e. freshwater, sediment, organic carbon) in periglacial landscapes under global climate change scenarios.

4. Geological and geomorphological evolution of a periglacial landscape complex in Northeast Siberia during the Late Quaternary

Guido Grosse[a], Lutz Schirrmeister[a], Christine Siegert[a], Viktor V. Kunitsky[b], Elena A. Slagoda[c], Andrei A. Andreev[a], Alexander Y. Dereviagyn[d]

[a] Alfred Wegener Institute for Polar and Marine Research, Research Unit Potsdam,
[b] Permafrost Institute, Siberian Branch of Russian Academy of Science, Yakutsk
[c] Tyumen State Oil and Gas University, Russia
[d] MGU Moscow State University, Faculty of Geology, Russia

4.1 Abstract

The development of a permafrost-dominated landscape during the Late Quaternary was studied in detail with a combination of sediment studies, remote sensing and terrain modelling, all combined with a geographical information system. The investigation area of the Bykovsky Peninsula and the adjacent Khorogor Valley in the Kharaulakh Ridge is situated in NE Siberia, a few kilometre southeast of the Lena Delta. For the investigation a comprehensive cryolithological database was compiled, which is based on the review of previously published boreholes, outcrop profiles, and surface samples from a variety of sources, and on own field data. The main sediment sequences on the Bykovsky Peninsula consist of up to 50 m thick ice-rich Ice Complex (IC) deposits that accumulated during the Late Pleistocene. The main processes during the time of IC formation were niveo-aeolian processes around extensive snowfields in the Kharaulakh Ridge, slope processes in valleys (Khorogor Valley) and alluvial/proluvial sedimentation in the mountain foreland (Bykovsky Peninsula). A general metamorphosis of the landscape from an extensive Late Pleistocene accumulation plain to a strongly dissected thermokarst-dominated relief occurred during the Early-Middle Holocene. Thermokarst subsidence had an enormous influence on the hydrology, the sediment deposition, and the composition of biocoenoses. The Middle-Late Holocene is characterised by lake shrinking and talik refreezing, indicating the general climate deterioration in the region. Finally, the region was reached by the global marine transgression, resulting in thermo-abrasion of ice-rich coasts, and the truncation and marine inundation of thermokarst depressions.

4.2 Introduction

The palaeo-environmental conditions of permafrost-dominated landscapes in northeastern Siberia during the Late Quaternary have been a major research topic for many years. During the Late Pleistocene, the global sea level was lowered about 120 m (Fairbanks, 1989) and the

several 100 km wide and shallow subaerial shelfs of the Laptev, East Siberian and Chukchi Seas in NE Siberia were part of the so-called Beringia, which has no analogue in the present landscapes of the northern hemisphere (e.g. Sher et al., 2005). Furthermore, due to a strongly continental climate, the northeast Siberian shelf regions were not covered by an ice sheet at least since the Late Saalian (Hubberten et al., 2004; Svendsen et al., 2004). Instead, the flat shelf regions were characterised by an extensive deposition of thick fine-grained and ice-rich sediments of the Ice Complex (IC) and periglacial-fluvial sediment accumulations in major river valleys during the Late Pleistocene. With the post-glacial marine transgression and the beginning of the Holocene warming, shelf submerging and thermokarst development destroyed most parts of the depositional environment and the IC (Romanovskii et al., 2004). Today, only erosional remnants of the IC are preserved along the coastline and some islands in the Laptev Sea, which both are subject to continuing coastal erosion (Gavrilov et al., 2003).

The IC in the Laptev Sea region contains high amounts of frozen fossil remains, which have been used for the reconstruction of a variety of environmental parameters, like floristic and faunistic assemblages, pedogenesis, soil moisture, summer temperature and summer precipitation (e.g. Andreev et al., 2002; Schirrmeister et al., 2002b; Bobrov et al., 2004; Kienast et al., 2005; Sher et al., 2005). Additionally, the high content of ground ice in the IC in the form of segregated ice and large ice wedges was used for the reconstruction of winter temperature and general precipitation sources by the analysis of the isotopic composition of ground ice (Meyer et al., 2002a, b). But although the IC deposits are excellent palaeo-environmental archives for the Late Pleistocene, many hypotheses have been debated in the last decades on the origin of the IC sediments and the general processes which led to their deposition in the Laptev Sea region (Table 4-1). Various IC key sites have been investigated by Russian and other researchers, and local palaeo-environmental conditions were reconstructed for these sites. However, often only assumptions based on sparse local data were made about the origin and regional genesis of the IC, and the context of environmental dynamics in an entire landscape was rarely considered.

One of the best-investigated locations for Siberian IC deposits is the outcrop section of Mamontovy Khayata at the eastern coast of the Bykovsky Peninsula, several 10 km southeast of the Lena Delta (Figure 4-1). The Bykovsky Peninsula has been in the focus of palaeo-environmental research since more than 200 years, when in 1799 the remains of a mammoth carcass were discovered there (Adams, 1807). Since that time, the peninsula was recurrently visited by researchers, arguing about the palaeo-environmental and geological conditions during the time of deposition of the IC (Table 4-1).

Table 4-1: Hypotheses of Ice Complex genesis in various North Siberian regions.

Citation	Origin	Period of formation	Investigated region
Toll (1895) Vollossovitch (1914)	Buried remnants of glaciers	Quaternary	- Bol'shoy Lyakhovsky Island - Coastal lowlands
Popov (1953, 1969)	River floodplain sediments	Upper Middle Pleistocene	- Lower Yana river
Gusev (1958)	Extensive frozen mud flows	Late Pleistocene	- Bykovsky Peninsula - Coastal lowlands
Romanovskii (1958a, b) Katasonov (1954) Vtyurin et al. (1957)	Fluvial deposits of meandering rivers	(Middle-) Late Pleistocene	- Coastal lowlands - Lower Yana river - Bol'shoy Lyakhovsky Island
Strelkov (1959)	Sediments of a fluvial-lacustrine plain	Kargin "Interglacial"	- Coastal Lowlands
Lavrushin (1962)	Fluvial (shallow channel facies)	Vorontsov Formation - Middle Pleistocene (Tazov)	- Lower Indigirka river
Kayalaynen & Kulakov (1966)	Lacustrine-palustrine sediments	Oyagoss Formation - (Middle)-Late Pleistocene	- Coastal lowlands
Ivanov (1972)	Fluvial and fluvial-lacustrine sediments	Oyagoss Formation (Zyryan)	- Coastal lowlands
Tomirdiaro et al. (1970, 1984)	Cryogenic-aeolian (loess-ice) formation	Late Pleistocene (Zyryan and Sartan ice complexes separated by Kargin peat)	- Bykovsky Peninsula - Oyagoss Yar
Grosswald (1983, 1998)	Deposits of basins dammed by an assumed shelf glacier, pro-glacial stream sediments	Late Pleistocene	- Bykovsky Peninsula - Coastal lowlands
Sher et al. (1987, 2005)	Polygenetic origin (lacustrine, fluvial, slope downwash, aeolian)	Late Pleistocene Edoma Superhorizon, subdivided into Oyagoss (=Zyryan), Molotkov (=Kargin) and Sartan Horizons	- Coastal lowlands
Kunitsky (1989, 2002)	"Extranivites" (accumulations on cryoplanation terraces, that origin from nival processes related to extensive snowfields)	Late Pleistocene	- Bykovsky Peninsula - Bol'shoy Lyakhovsky Island
Slagoda (1991, 1993)	Floodplain sediments, proluvial slope sediments	Lower Ice complex (Middle-Late Pleistocene) and Upper Ice Complex (Sartan)	- Bykovsky Peninsula
Nagaoka (1994) Nagaoka et al. (1995)	Sediments of the Lena river delta and "swamp deposits", dammed by the shelf ice-sheet	Kargin "Interglacial"	- Bykovsky Peninsula - Bol'shoy Lyakhovsky Island - Oyagoss Yar
Siegert et al. (2002)	Transport of slope sediments from mountains by seasonally active rivers forming proluvial fans	Late Pleistocene	- Bykovsky Peninsula
Schirrmeister et al. (2001, 2002a, 2003a, 2004)	Accumulation from seasonal runoff of periglacial rivers, additional influence of aeolian, nival and soil erosion processes	Late Pleistocene	- Bykovsky Peninsula - New Siberian Islands - Anabar-Olenek lowland - Oyagoss Yar coast

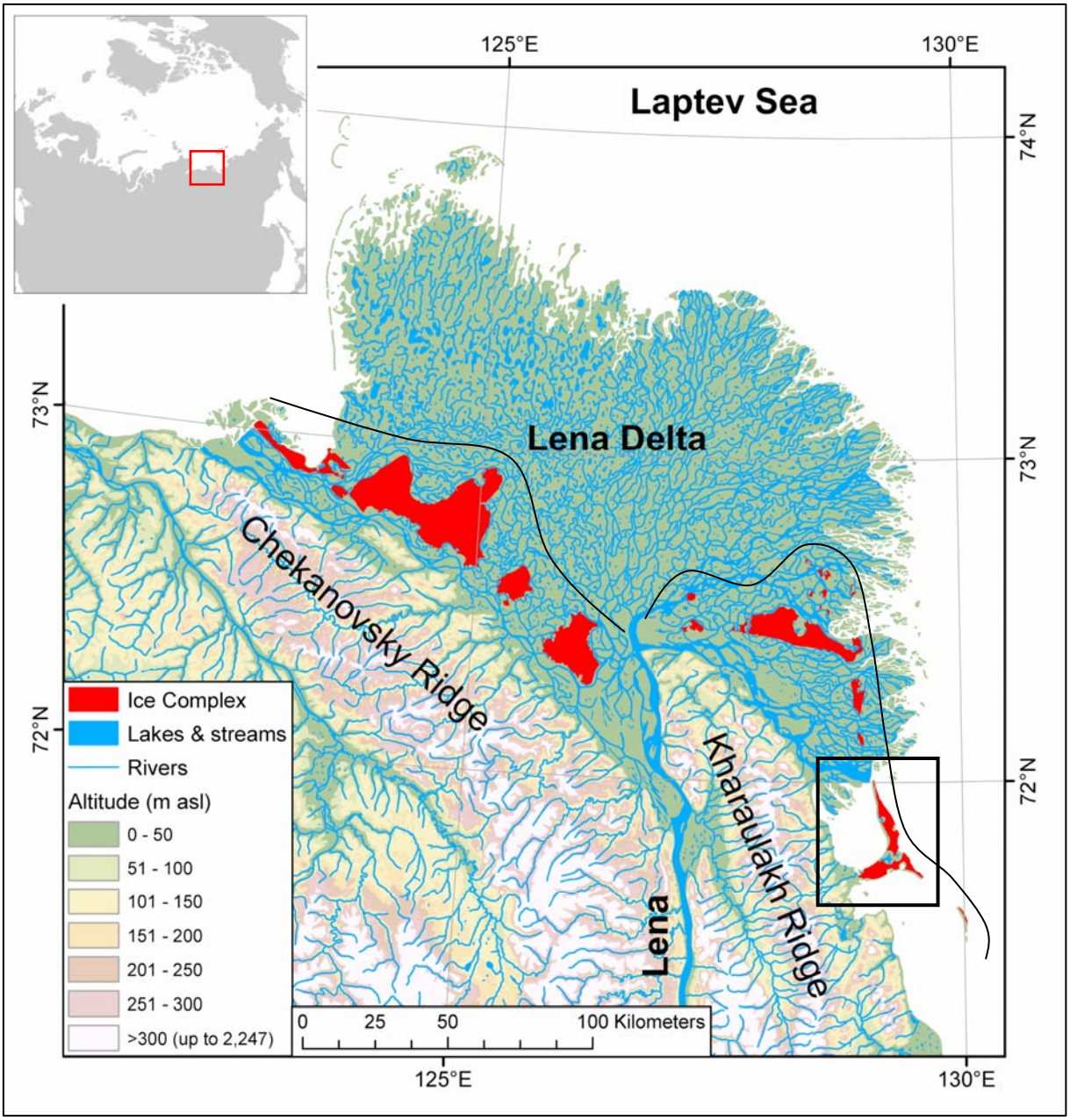

Figure 4-1: Location of the study area in NE Siberia (red rectangle in the small map). The Bykovsky Peninsula and the Khorogor Valley are siutated in the SE of the Lena Delta (black rectangle). The modern distribution of erosional remnants of Ice Complex deposits in the Lena Delta region is almost parallel to the coastal mountain ranges (black line). The Ice Complex distribution was mapped from Landsat-7 ETM+ images. The DEM was produced using digitised topographic maps 1:500,000.

The large amount of radiocarbon datings, which recently became available for the IC and Holocene deposits on the Bykovsky Peninsula (Schirrmeister et al., 2002a), provides new detailed insights not only for the key site Mamontovy Khayata, but also for the depositional history, the regional landscape evolution, and the IC origin. Our goal was, to combine and to use these and all other available data sources for answering the questions concerning the general evolution of the periglacial landscape complex on the Bykovsky Peninsula and in the

adjacent mountainous hinterland of the Khorogor Valley. In particular these are the origin of the IC and the history of its degradation due to thermokarst and erosion. For the first time, the relationship between both the Bykovsky Peninsula and the Khorogor Valley were investigated. For our reconstruction we analysed the available data from different sources within a geographical information system (GIS) of the region. The data included already published data from peer-reviewed literature, published data from Russian and German-Russian field reports, unpublished data acquired from Russian archive sources, and results from own field work, remote sensing and terrain modelling. Additionally, new sedimentological, geocryological and palaeo-ecological data of outcrops in the Khorogor Valley, which were studied during the Russian-German expedition "Lena Delta – New Siberian Islands 2002" by some of the authors (Grosse et al., 2003), are presented in this paper.

Generally, the available field data consists of sedimentological and cryolithological descriptions from boreholes, outcrop sections, subsurface and surface samples, a large amount of radiocarbon datings and field knowledge in terms of geological and geomorphological observations. Although parts of the data were already used for detailed cryolithological studies (Kunitsky, 1989; Slagoda, 1993, 2004; Schirrmeister et al., 2002a; Siegert et al., 2002; Grigoriev, 1993), only few assumptions were made about the general context of landscape evolution in the region including both the Kharaulakh Ridge and the accumulation plain in front of it. In contrary to palaeo-environmental reconstructions on individual outcrop sections or boreholes, our landscape approach promises a more comprehensive understanding of the palaeo-environmental conditions, especially when considering their spatial dimension and variability over the investigated period.

The derived concept has implications for the genesis of many other sites with IC occurrence in the Laptev Sea region, as the general geomorphological setting including relatively low mountain ranges and adjacent IC accumulation plains in these regions is similar to the setting in our investigation area.

4.3 Study area

The study area, the Bykovsky Peninsula and the adjacent Khorogor Valley, is part of the Republic of Sakha (Yakutia) within the Russian Federation and is located on the northern margin of the Siberian mainland at the Laptev Sea coast (Figure 4-1). The region is dominated by arctic tundra, periglacial conditions, and a continental climate with severe winters, cool summers, and low precipitation rates (Treshnikov, 1985). The terrestrial continuous

permafrost in the region has temperatures of –9 to –11 °C and reaches down to 300-500 m depth below the surface (Yershov, 1998). The region consists of two geological main parts (Figure 4-2). In the west, the Kharaulakh Ridge with heights up to 500 m a.s.l. represents the northern foothills of the Verkhoyansk Mountains. In the east, the Bykovsky Peninsula represents the remains of a former accumulation plain with maximum elevations of 45 m a.s.l..

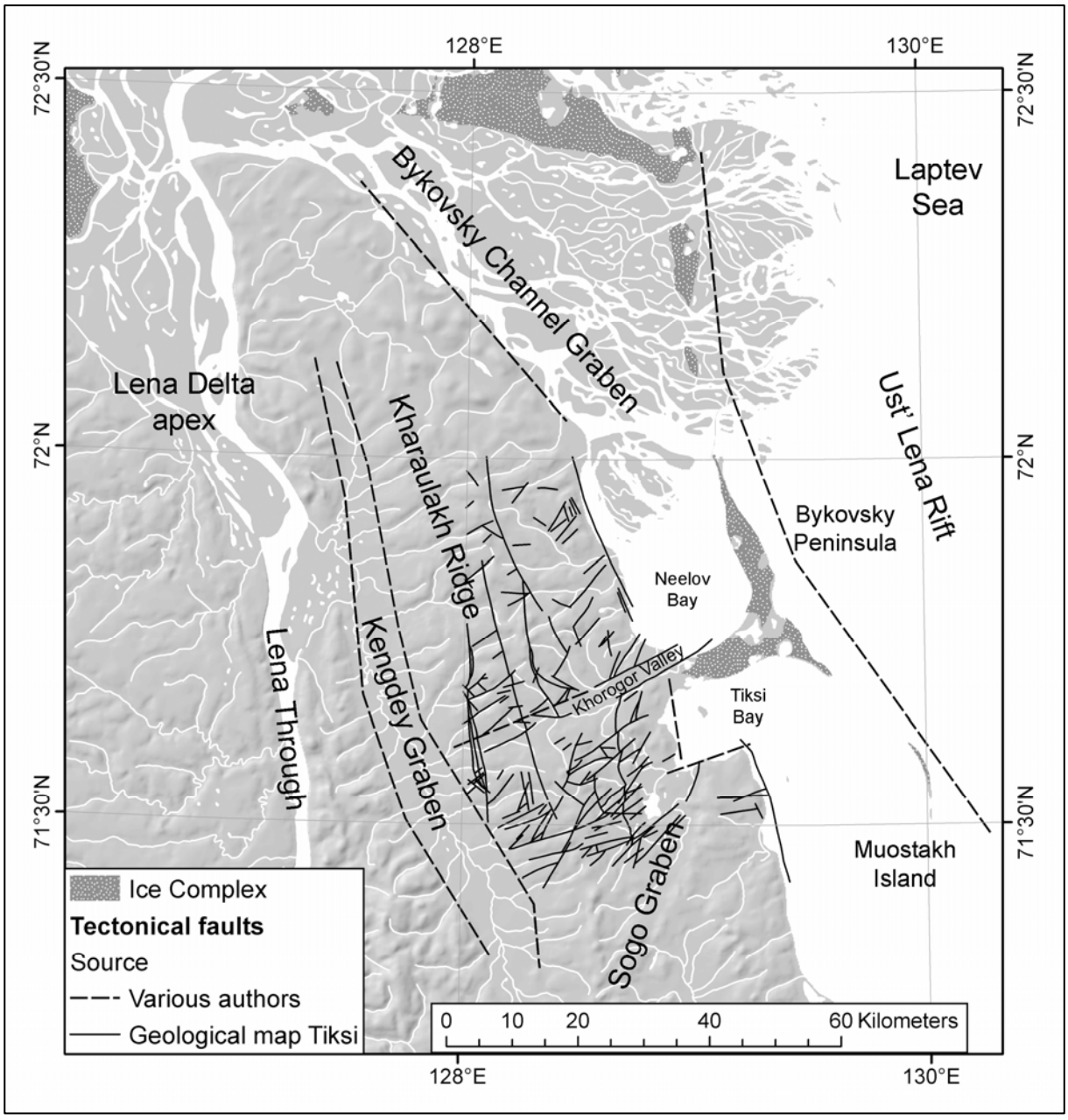

Figure 4-2: Shaded relief map of the region around the investigation area showing the location of IC deposits, and of tectonical faults and structures according to various authors (Geological Map Tiksi, 1986; Imaev et al., 2000; Drachev et al., 1998).

The Kharaulakh Ridge consists mainly of intensely folded and imbricated permo-carboniferous sandstones and slates. The relief of the northern Verkhoyansk Mountains is characterised by strong dissection due to tectonic activity during the Cenozoic. According to Imaev et al. (2000) the major landscape shaping occurred with linear uplifts during the late Oligocene to the Early Pleistocene. A new uplift occurred during the Middle Pleistocene-Holocene. The Laptev Rift System is situated close in the eastern Laptev Sea and neotectonic activity in the whole region is proven by seismic studies (Grigoriev et al., 1996; Drachev et al., 1998; Franke et al., 2001). Many SW-NE orientated valleys of up to several 10 km length are situated within dislocation zones in the northern Verkhoyansk Mountains. The largest is the Khorogor Valley, which in most parts is gently inclined (< 2.5°), and about 30 km long and 10 km wide at the mouth. The valley shape is probably strongly influenced by tectonics. Two WSW-ENE striking major faults were supposed, which are flanking the valley (Geological Map Tiksi, 1986; Imaev et al., 2000) (Figure 4-2). Along these supposed faults two small rivers discharge the valley in the NW (Khatys-Yuryakh River) and SE (Khorogor River) towards the Neelov Bay, which is situated in the NE. The western Neelov Bay shore is formed by a major SSE-NNW striking fault, bordering the Bykovsky Channel Graben (Grinenko & Imaev, 1989). In the higher Verkhoyansk Mountains small glaciers occurred during the Late Pleistocene, but no traces of extensive glaciation was found in the lower Kharaulakh region. Periglacial and nival processes played the most important role for weathering, erosion, transport, and accumulation in these lower mountains. Imaev et al. (2000) reports the presence of pediment terraces of 2-15 m thickness on the slopes and floors of the valleys in the northern Verkhoyansk Mountains.

The relief of the Bykovsky Peninsula is formed by Edoma uplands, and deep depressions and valleys formed by permafrost degradation due to thermokarst and thermo-erosion. The Edomas consist mostly of ice-rich, fine- to medium-grained sandy permafrost deposits of the Late Pleistocene IC. The ground ice occurs in the form of large ice wedge of several metres in width and up to 40-50 m in depth, subhorizontal ice bands, and segregated ice mainly in the form of small ice lenses. The deposits are partially very organic-rich and contain palaeosols and peat horizons. The depressions and valleys contain a variety of reworked IC sediments (slope deposits) or newly formed deposits (i.e. peat and lacustrine sediments).

The post-LGM (Last Glacial Maximum) transgression of the Laptev Sea reached the area of the Bykovsky region in the Middle-Late Holocene (Bauch et al., 2001). The Bykovsky Peninsula and a few other similar, but smaller erosional remnants in the south (Muostakh Island) and north (several islands in the eastern Lena Delta) (Figure 4-1) were part of an

extended accumulation plain covering probably large parts of the shallow subaerial Laptev shelf during the Late Pleistocene. The modern shore of the peninsula is continuously shaped by interactions of thermo-abrasion and coastal processes. The location of the eastern Bykovsky shore is close to the rim of the Ust' Lena Rift, which is part of the Laptev Rift System. A major fault is suggested along the relatively straight eastern coast of the Bykovsky Peninsula, which is in a line with Muostakh Island in the south and some IC islands in the Lena Delta in the north (Grigoriev, 1996; Drachev et al., 1998) (Figure 4-2).

4.4 Methods and Materials

We used various data sources for our approach of an extensive analysis and reconstruction of the regional landscape development during the Late Quaternary (Figure 4-3). To combine the different data types, we employed a GIS (ArcGIS^{TM}), as such a system can effectively handle vector and raster data sets and makes the exchange between them uncomplicated. Furthermore, the GIS environment provides tools for easy interaction with all data sets and for spatial modelling, both which is useful for our reconstruction. The basic input consisted of all available geocryological field data from the investigation area, which was compiled in a comprehensive database (chapter 4.4.1). Another major input were remotely sensed satellite images in the form of base raster images, and detailed maps of various terrain units mapped from these images (chapter 4.4.2).

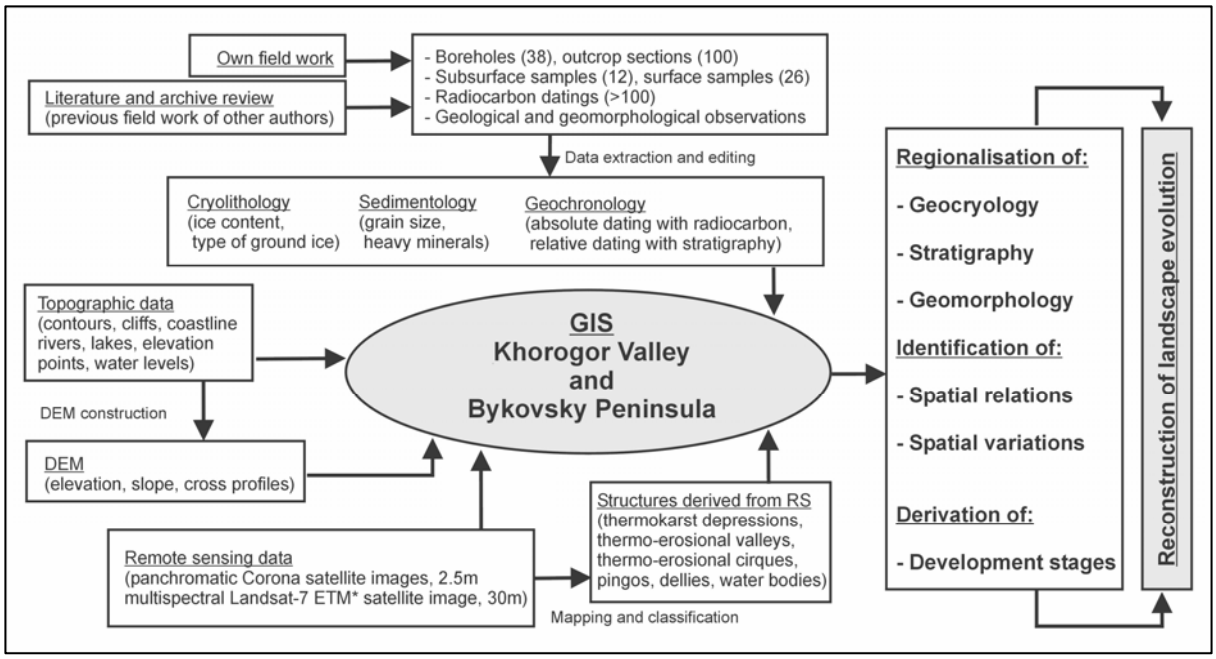

Figure 4-3: A wide variety of data sources and types were combined and used for an extensive analysis and reconstruction of the regional periglacial landscape and its development during the Late Quaternary. For the handling and combination of the data a geographical information system (GIS) was generated for the investigation area at the Bykovsky Peninsula and in the adjacent Khorogor Valley.

Finally, a medium-resolution digital elevation model (DEM) was incorporated in the GIS to provide further options of data exploitation in terms of geomorphological analyses and spatial modelling (chapter 4.4.3). As base projection for the GIS we chose the Russian 3° Gauss-Krueger system Pulkovo 1942 and the geodetic ellipsoid Krassovsky 1940, as the available topographic maps 1:100,000 were provided in this projection. For the investigation area, the Gauss-Krueger zone 22 applied.

4.4.1 Compilation of a cryolithological field data base

The database contains all the information on sedimentology and cryolithology from previously achieved fieldwork, acquired from boreholes, outcrop sections, subsurface samples and surface samples. Most fieldwork of previous investigators focussed on the Bykovsky Peninsula, thus we additionally investigated several new sites in the adjacent Khorogor Valley. The data compilation originated from own field work and the intensive review of different sources ranging from peer-reviewed articles to personal communications with scientist, which have worked in the investigation area (Kunitsky, 1989; Slagoda, 1993; Grigoriev, 1993, 1996; Siegert et al., 1999; Sher et al., 2000; Schirrmeister et al., 2002a, b; Siegert et al., 2002; Grosse et al., 2003; Kholodov et al., 2003; Kholodov, pers.comm.; Sher et al., 2005). Thus, the data are of different quality. Especially for older data, where sometimes no original descriptive material was available, the information was extracted from schematically drawn drill logs or outcrop profiles. For some sites, only rough descriptions of location and/or geocryology were available.

For our approach, we used only the data, which were reliable in terms of relatively precise descriptions of the recorded geocryological conditions and proper information on the three-dimensional location for the described site. Altogether, 176 sites of acceptable quality were compiled in the database and geolocated in a GIS (Figure 4-4). For each of these sites, the database contains information on the xyz-location, type of data acquisition, date of field work, primary investigator, source of data (or reference), and for each identified layer also the lithology, geocryology, fossil remains, facial and stratigraphical interpretations and potentially existing datings. Additionally, to aid the upscaling of data from local sites, general geological and geomorphological field observations were recorded.

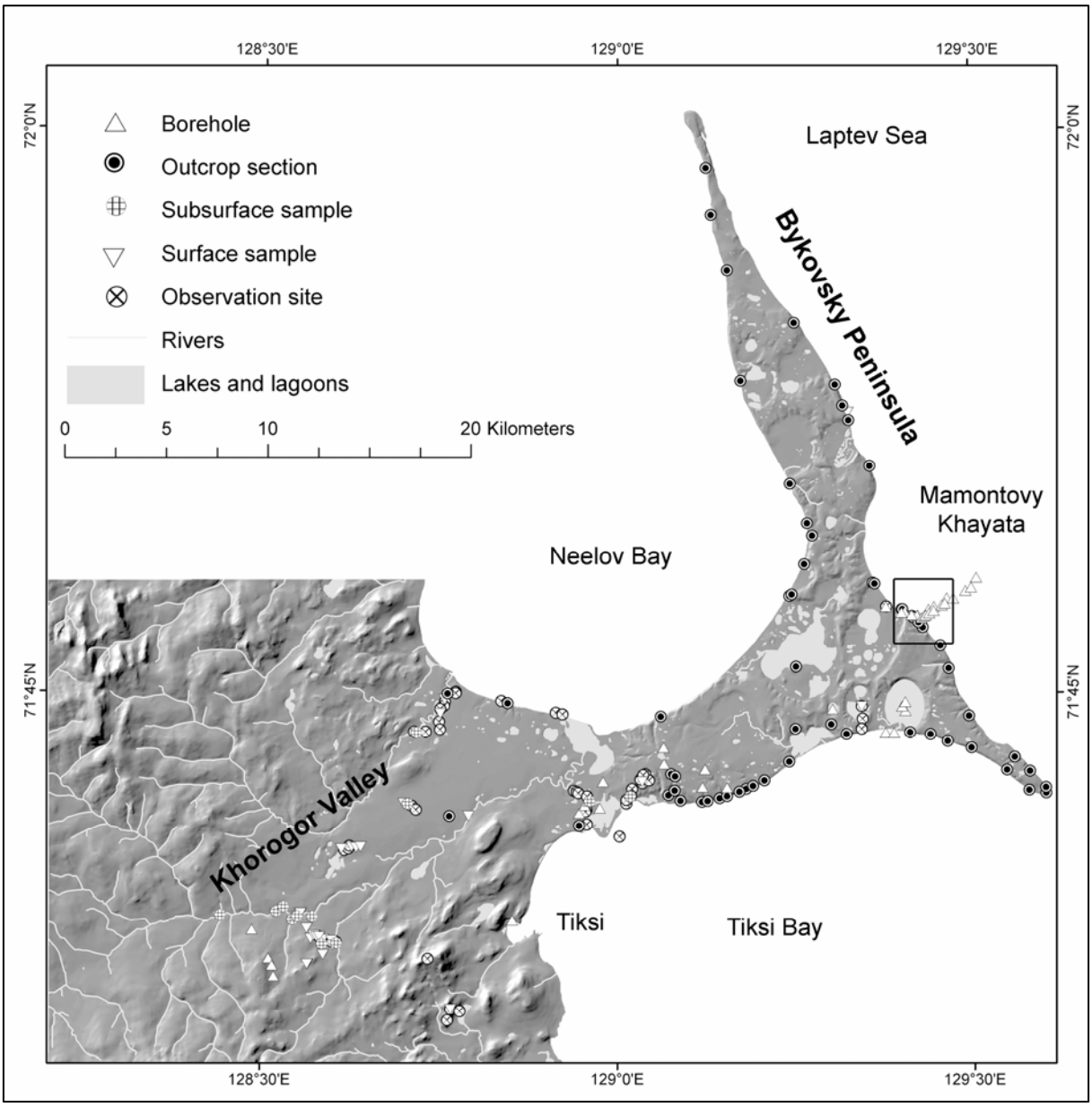

Figure 4-4: The shaded relief map shows the location of different types of field data, that were available for compilation of a sedimentary database for the Bykovsky Peninsula and the Khorogor Valley from various sources (Kunitsky, 1989; Slagoda, 1993; Grigoriev, 1993, 1996; Siegert et al., 1999; Sher et al., 2000; Schirrmeister et al., 2001, 2002; Grosse et al., 2003; Kholodov et al., 2003; Kholodov, pers.comm.; Sher et al., 2005).

The geochronology of the investigation area is mainly based on more than 100 radiocarbon dates, though the dates are distributed inhomogeneously in the region (Figure 4-5). The most radiocarbon dates were acquired by several Russian, Japanese and German researchers for the analysis of the Mamontovy Khayata outcrop section (Tomirdiaro, 1984; Kunitsky, 1989; Slagoda, 1993; Nagaoka, 1994; Nagaoka et al. 1995; Schirrmeister et al., 2002a).

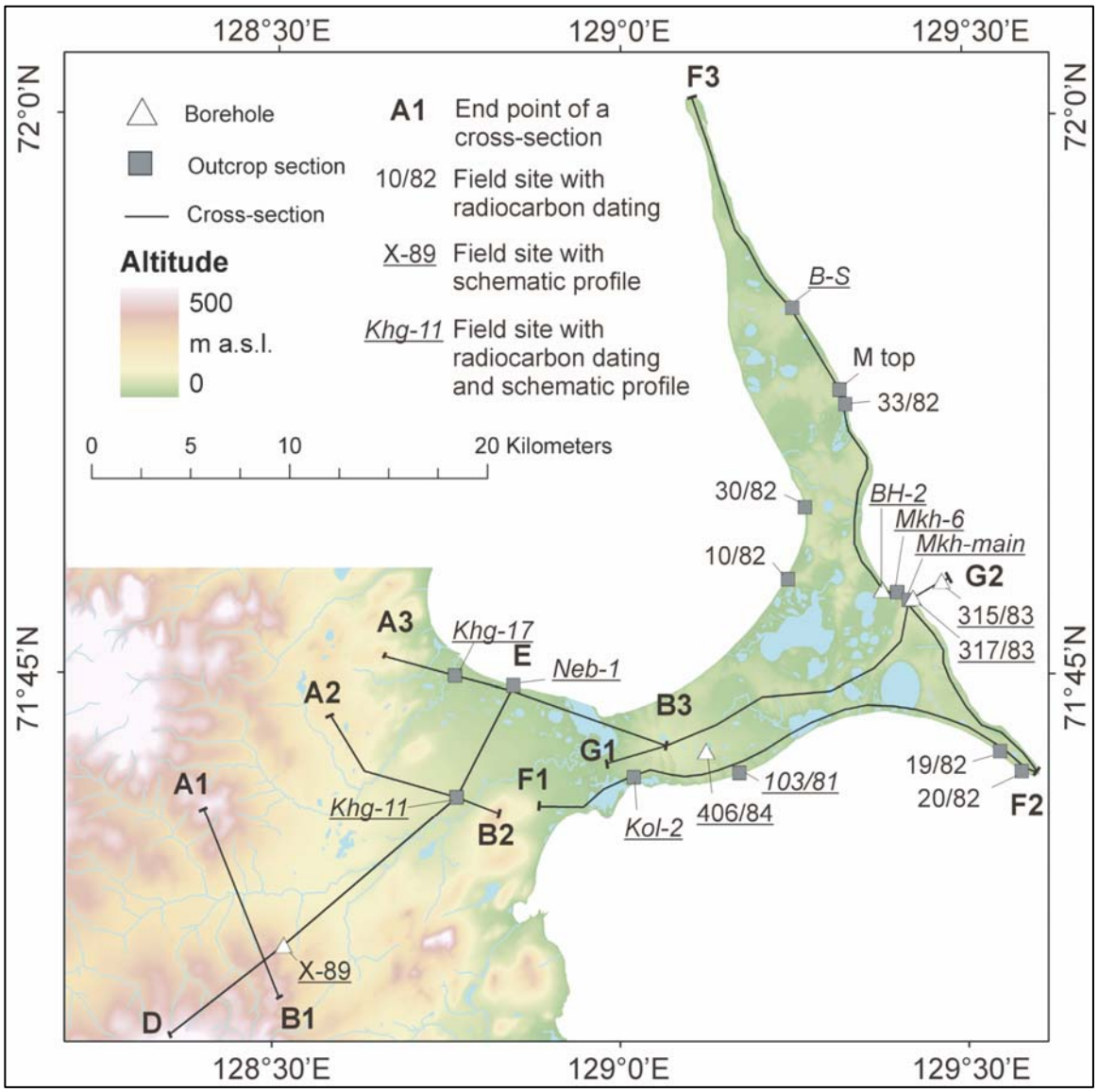

Figure 4-5: DEM with location of field sites, for which radiocarbon datings exist (Table 4-2), or which are shown as schematic profiles in figures 4-6 to 4-8. Furthermore, the location of several geomorphological cross-sections is indicated, which are presented in figures 4-9 and 4-10.

To accomplish the goal of qualifying the Mamontovy Khayata outcrop section as a chronological high-resolution palaeo-environmental permafrost archive for the Late Quaternary, 76 radiocarbon ages ranging from about 55 ky BP to recent were dated within a joint Russian-German research effort for this site and some adjacent thermo-denudation structures (Schirrmeister et al., 2002a). Other sites on the Bykovsky Peninsula were dated by Slagoda (1993) and within this work (Table 4-2). Furthermore, we present first radiocarbon datings (Table 4-2) and preliminary results from pollen analysis from several profiles in the Khorogor Valley. Additionally, about a dozen sedimentation ages dated with thermo-luminescence (Kunitsky, 1996) and infrared-optical stimulated luminescence (Grosse et al., in prep.) were available for the Bykovsky Peninsula, again most of them for the Mamontovy Khayata site.

Table 4-2: Radiocarbon dates from various sites in the Khorogor valley and the Bykovsky Peninsula. The location of the sites is shown in figure 4-5.

Outcrop or sample no.	Lab code*	Deposit type	Dated material	Altitude m a.s.l.	Radiocarbon age y BP	Calendar age** y cal BP (2 sigma)	Source
Khorogor Valley, Late Sartan-Early Holocene deposits							
Khg-11/2	KIA 20692	Alas deposit	Peat	35.4	11,710 ± 50	13,892 – 13,456	this work
Khg-11/3	KIA 20693	Alas deposit	Peat	35	12,145 ± 55	14,371 – 13,835	this work
Neb 1/11	KIA 20699	Alluvial	Peat	4.5	945 ± 25	879 – 822	this work
Neb 1/6	KIA 20698	Alluvial	Peat	3.45	10,690 ± 55	12,970 –12,623	this work
Neb 1/2	KIA 20697	Alluvial	Peat	2.6	11,260 ± 40	13,461 – 13022	this work
Neb-1/1	KIA 20696	Alluvial	Plant remains	2.1	11,400 ± 100	13,519 – 13,145	this work
Khg-17/12	KIA 20695	Alas deposit	Peat	7	10,120 ± 50	12,121 – 11,552	this work
Khg 17/1	KIA 20694	Alas deposit	Peat	4.8	10,190 ± 70	12,336 – 11,559	this work
Bykovsky Peninsula, Pre-Holocene deposits							
B-S-2b	KIA 8167	Fluvial sand	Wood	22.0	13,410 ± 55	16,591 – 15,666	this work
B-S-5	KIA 8166	Ice Complex (IC)	Wood	20.0	19,330 ± 100	23,321 – 22,555	this work
B-S-7	KIA 8165	IC	Peat	10.0	53,020 +2670/-2000		this work
Byk-BH2-21	KIA 11443	Fluvial sands in a pingo	Twigs, l.r h.a.	22,3	>53,000 30,950 +690/-640		this work
MKh-6.3-1	KIA 6737	IC, taberite	Grass roots	2.0	47,400 +2730/-2030		this work
M-1.2	KIA 8164	IC	Twigs	24	35,050 +340/-330		this work
30/82	IM-767	IC	Peat	20.0	28,180 ± 300		Slagoda (1993)
19/82	IM-766	IC	Peat	11.0	23,700 ± 500		Slagoda (1993)
103/81	LU-1328	IC	Peat	7.0	21,630 ± 240		Slagoda (1993)
103/81	LU-1130	IC	Peat	6.0	33,040 ± 810		Slagoda (1993)
103/81	GIN-4597	IC	Plant material	5.0	40,200 ± 1200		Slagoda (1993)
103/81	GIN-4593	IC	Plant material	4.0	40,400 ± 1200		Slagoda (1993)
103/81	GIN-4391	IC	Plant material	2.5	40,800 ± 1600		Slagoda (1993)

* Laboratory code KIA indicates AMS radiocarbon datings carried out at the Leibniz Laboratory for Radiometric Dating and Stable Isotope Research, Kiel University (Germany); All others are conventional radiocarbon dates from various Russian facilities.

** Calibration was done using CALIB 4.3; 5.0 (Stuiver et al., 1998).

Table 4-2: Continuation

Outcrop or sample no.	Lab code*	Deposit type	Dated material	Altitude m a.s.l.	Radiocarbon age y BP	Calendar age** cal y BP (2 sigma)	Source
Bykovsky Peninsula, Holocene deposits							
Kol 2/2	KIA 20701	Holocene cover on IC	Peat	14.0	4555 ± 30	5326 – 5262	this work
Kol 2/1	KIA 20700	Holocene cover on IC	Peat	13.8	4720 ± 35	5417 – 5332	this work
19/82	IM-764	Holocene cover on IC	Peat	22.0	4430 ± 300	5755 – 4241	Slagoda (1993)
20/82	IM-765	Holocene cover on IC	Peat	21,5	5450 ± 150	6564 – 5918	Slagoda (1993)
10/82	IM-763	Alas deposit	Wood	11.0	9450 ± 100	11,116 – 10,488	Slagoda (1993)
33/82	IM-762	Alas deposit	Wood	8	9250 ± 500	12,059 – 9248	Slagoda (1993)

* Laboratory code KIA indicates AMS radiocarbon datings carried out at the Leibniz Laboratory for Radiometric Dating and Stable Isotope Research, Kiel University (Germany); All others are conventional radiocarbon dates from various Russian facilities.

** Calibration was done using CALIB 4.3; 5.0 (Stuiver et al., 1998).

4.4.2 Satellite remote sensing data

Aerial imagery is used for decades for local investigations of periglacial landscapes. However, the extensive use of satellite remote sensing in periglacial geomorphology and for the observation of periglacial processes is still in the beginning. The application of satellite imagery for regional investigations was hampered mainly by coarse image resolution and lacking coverage over remote Arctic regions until recent years. With the advent of higher-resolution multispectral satellite data with global coverage and the release of formerly classified archives with very high-resolution space photography, satellite remote sensing of Arctic periglacial landscapes is possible on a new scale. Some applications for high-resolution satellite remote sensing in periglacial geomorphology include the detailed mapping of permafrost degradation structures in extensive remote Arctic regions (e.g. Grosse et al., 2005). Other especially prospective approaches combine remote sensing and digital terrain modelling for the identification of geomorphic periglacial process units (Etzelmüller et al., 2001; Bartsch et al., 2004; Grosse et al., submitted, chapter 3).

In this paper we applied optical satellite remote sensing for the detection and analysis of periglacial surface structures and for the investigation of their spatial distribution and possible interactions between different features. The remote sensing was used as a tool for identifying processes on landscape scales and for the upscaling of cryolithological information from our database. For the high spatial resolution mapping of periglacial surface features we used panchromatic CORONA satellite photography with calculated 2.5 m ground resolution (Grosse et al., 2005). Two images of the CORONA KH-4B camera system from 24th July 1969 covering most parts of the investigation area were digitised, digitally enhanced, geo-referenced, and mosaicked. Using this mosaic, surface features in the study area were investigated or mapped in detail, including thermokarst depressions, thermo-erosional valleys, thermo-erosional cirques, thermokarst lakes, thermokarst lagoons, thermokarst mounds, pingos, and different types of ice wedge polygonal surfaces. Other features that were investigated especially in the Khorogor Valley include cryoplanation terraces, slope wash areas, small rivers, small thermokarst lakes, thermokarst mounds, and polygonal ice wedge nets.

For a better identification of individual geomorphological structures we employed a simple GIS-based technique by combining either high-resolution CORONA images with DEM data (see next chapter) or with multispectral Landsat-7 ETM+ data. The combination is based on overlay of both image types in the form of semi-transparent GIS-layers. This technique was very straightforward and beneficial for the use of both high spatial resolution and elevation

information or high spatial resolution and multispectral information in the GIS mapping environment. The multispectral Landsat-7 data with 30 m ground resolution (e.g. Goward et al., 2001) was especially helpful for the discrimination between geomorphological structures with different vegetation complexes and the discrimination of slope areas with or without vegetation and sediment cover. For this approach the Landsat-7 band combinations 3-2-1 (red - green - blue or true colour) and 5-4-3 (short-wave infrared 1 - near infrared - red) were used for the mapping, as these band combinations were identified as those with the best visual separation of the structures.

4.4.3 Digital elevation data

Digital elevation models are important tools for the three-dimensional investigation and analysis of landscapes. We produced a DEM from digitised topographic maps in the scale 1:100,000 for the investigation area (Figure 4-5). The governmental maps, produced with field data and aerial surveys from 1971-1983, were scanned, geo-referenced and manually digitised for the entire investigation area. All available height information (contours, elevation points, streams, and lakes) were then used for the calculation of a DEM with 15 m grid cell size by applying the TOPOGRID tool of ArcInfo^{TM}. This tool is based on an enhanced ANUDEM algorithm (Hutchinson, 1989) and calculates a hydrologically correct DEM by using drainage enforcement and removal of spurious sinks. A test of the vertical accuracy of the interpolation algorithm with 52 original elevation points from the map and their accordant grid cells suggested a mean vertical error of +0.49 m in the DEM, although some elevations at extreme terrain positions like cliffs or peaks had larger errors. Lake bathymetry was not provided with the topographic maps, thus the lake levels are treated as relief surface. The accuracy of the elevation model is considered sufficient for our geomorphological/geological approach, although base topographic maps of a smaller scale (e.g. 1:25.000 or better) and a much higher DEM grid cell resolution would be preferable for more detailed volumetric analyses and precise modelling of periglacial hydrology. Finally, various derivates were produced from the DEM, including maps on slope, aspect, shaded relief, and several cross-sections for the Khorogor Valley (Figure 4-6) and the Bykovsky Peninsula (Figure 4-7).

4.5 Results

4.5.1 Sediment studies

In this paper some schematic profiles from the investigation area are presented, which are considered key sites for the development of our landscape evolution scheme. In the Khorogor

Valley these are the borehole X-89 from the upper valley (Slagoda, 1993), and the new outcrop sections Khg-11, Khg-17 and Neb-1 from the central and lower valley regions (Figure 4-8, 4-5). On the western Bykovsky Peninsula these are the borehole 406/84 (Kunitsky, 1989), the combined outcrop profiles 103/81 and 203/82 (Slagoda, 1993) and the new profile Kol-2 (Figure 4-9, 4-5). Finally, from the eastern Bykovsky Peninsula we combined the previously published profiles of the Mamontovy Khayata main section (Schirrmeister et al., 2002a), the boreholes 317/83 and 315/83 (Kunitsky, 1989), and the outcrops MKh-6 in an adjacent thermokarst depression (Alas) (Schirrmeister et al., 2002a) in one profile. The terminus 'Alas' is used as synonym for thermokarst depression in the Russian literature. Further new profiles include the pingo-borehole BH-2 in a thermokarst depression close to the Mamontovy Khayata section and the outcrop section B-S in the north-eastern peninsula (Figure 4-10, 4-5).

The Late Pleistocene sedimentary sequences in the investigation area include the Zyryan Stadial, the Kargin Interstadial, the Sartan Stadial and the Holocene Interglacial according to the East Siberian Quaternary Stratigraphy (Stratigraphy of the USSR, 1982, 1984; Velichko, 1999). These periods correspond to the MIS 4 to 1, respectively.

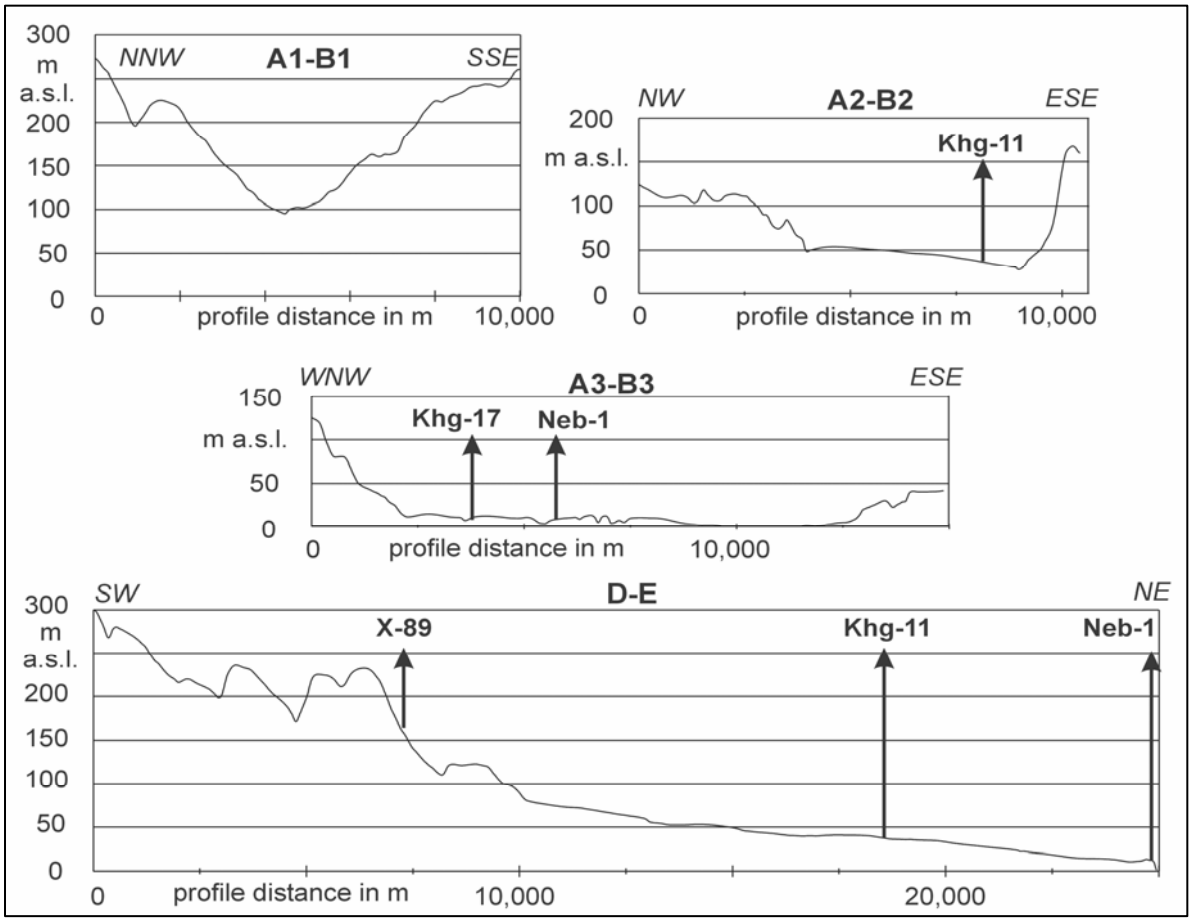

Figure 4-6: Geomorphological cross-sections from the Khorogor Valley. Arrows indicate the location of the profiles shown in figure 4-8.

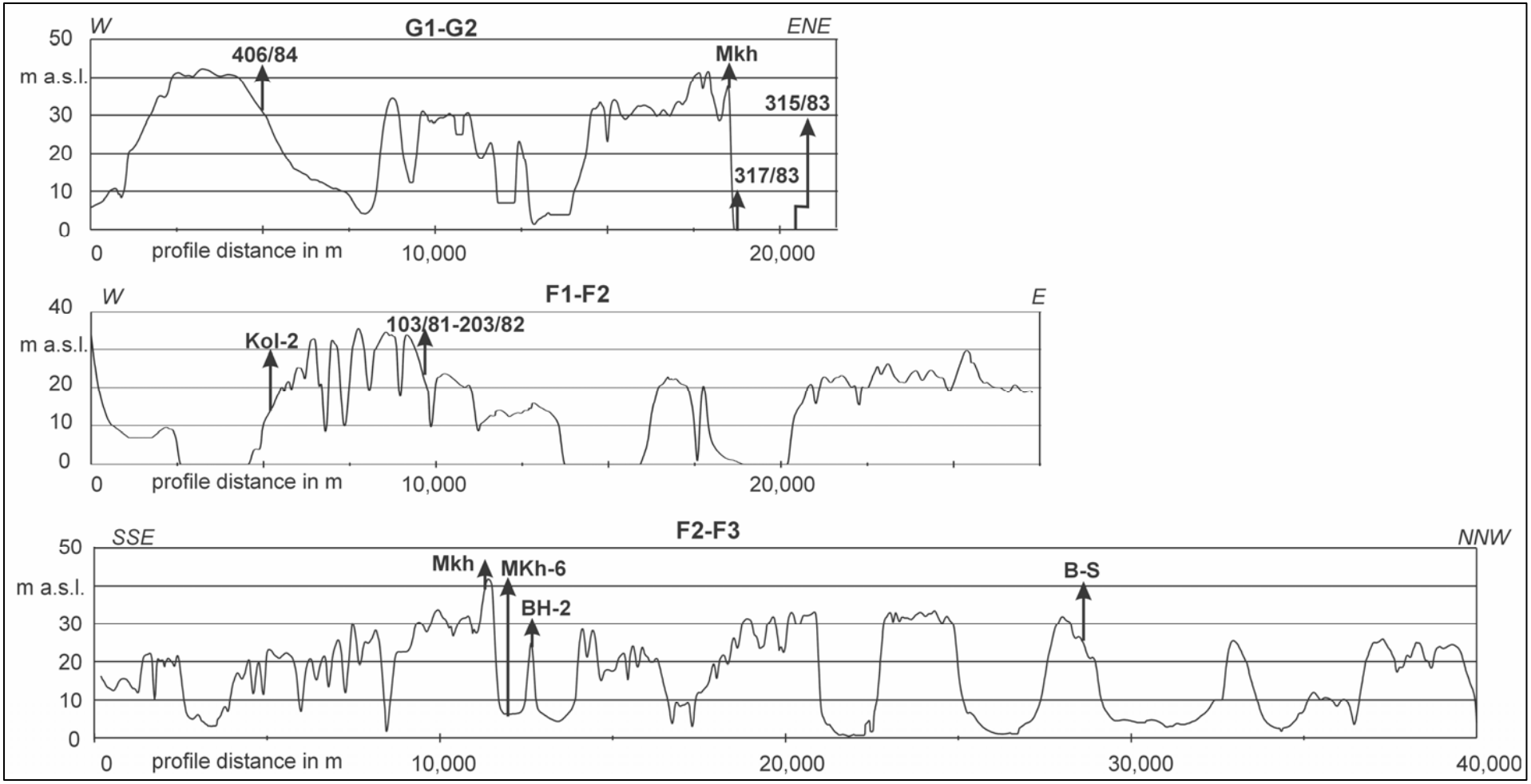

Figure 4-7: Geomorphological cross-sections from the Bykovsky Peninsula. Arrows indicate the location of profiles shown in the figures 4-9 and 4-10.

4.5.1.1 Khorogor Valley (Figure 4-8, 4-9)

The borehole X-89, located at 160 m a.s.l., proved that at least 30 m thick sediments are present on slopes in the upper valley regions (Figure 4-8). Above the bedrock, a thin layer of cryogenic eluvium was detected, which is interpreted as Pliocene to Early Pleistocene by Slagoda (1993). Following is a 15 m sequence of pebbles in silty-sandy matrix, interpreted as Early Pleistocene alluvial deposits. The next 12 m above consist of interbeddings with fine-grained silty-sandy sediments with some gravels. This horizon has high ice contents and contains plant remains, which are partially in situ (grass roots), and is interpreted as Late Pleistocene proluvial IC deposit. The upper 2 m consist of peat with silty-sandy interlayers.

The outcrop Khg-11 was a thermokarst mound, which has formed in c. 35 m a.s.l. close to a road (Figure 4-8). Above weathered slate in the base, two 10 cm alluvial layers of gravel and silty-sand were interpreted as Sartan. These are followed by a 1.1 m thick peat horizon, which is radiocarbon-dated with two ages in the Bølling-Allerød period (Late Sartan) (Table 4-2). The peat is finally covered by a 10 cm alluvial layer of silty sand. The lower 2.2 m of the outcrop Neb-1 on the shallow cliff of the Neelov Bay shore consist of fine-grained sandy alluvial deposits with small gravels (Figure 4-8). The deposits have a massive cryostructure with large ice wedges and some ice bands. Three peat inclusions were dated to the Bølling-Allerød period (Late Sartan) (Table 4-2).

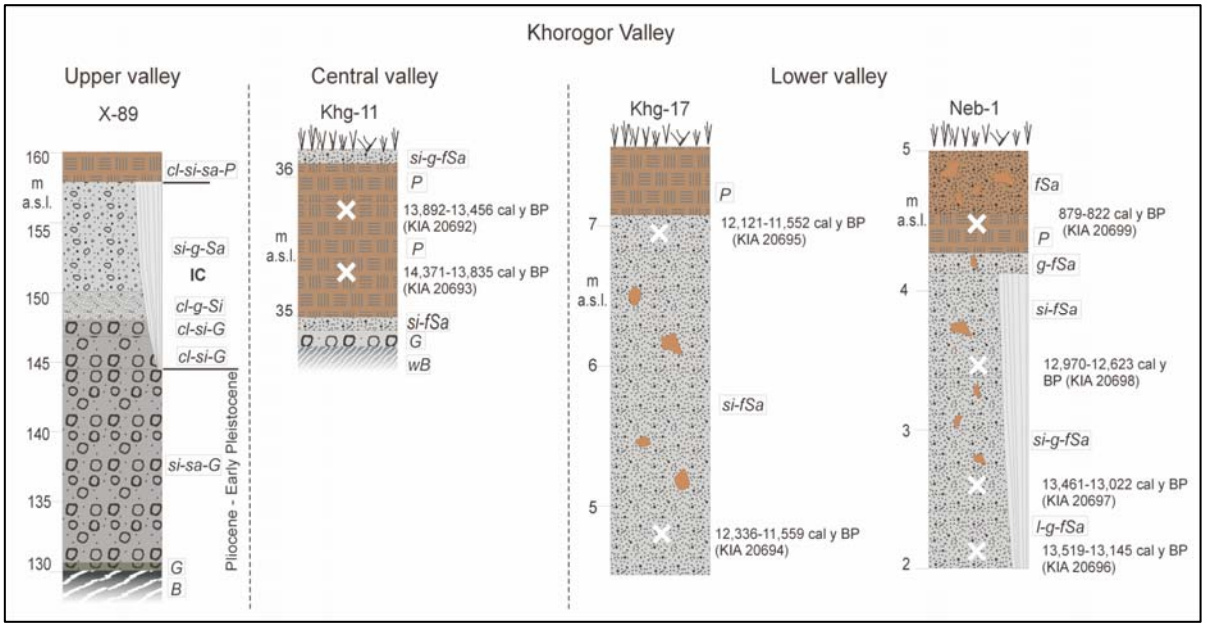

Figure 4-8: Schematic sedimentological profiles for outcrops in the Khorogor Valley: borehole X-89 from a slope in the upper valley (Slagoda, 1993), section Khg-11 from a thermokarst mound in the central valley, section Khg-17 from a river bank in the lower valley and section Neb-1 from a cliff on the Neelov Bay shore. For the location of the profiles see figure 4-5. The legend is shown in figure 4-10.

Above the alluvial deposits a 0.7 m thick peat horizon is situated, dated with a subrecent age.
The outcrop Khg-17 is situated on the eastern bank of the Khatys-Yuryakh River, close to the river mouth. The lower 2.5 m consist of alluvial silty-sandy sediments with peat inclusions and a massive cryostructure (Figure 4-8). Two radiocarbon dates from the lower and the upper part of this horizon have Younger Dryas ages (Late Sartan) (Table 4-2). A 0.5 m peat layer is following on top, which probably is of subrecent age like the peat cover in Neb-1.

4.5.1.2 Western Bykovsky Peninsula (Figure 4-9, 4-7)

The borehole 406/84 covers sediment sequences from 32.5 m a.s.l. to 25 m b.s.l. (Figure 4-9). The lowest 25 m of sediments are fluvial coarse-grained sandy and gravelly deposits with plant remains and a massive cryostructure. The deposits are interpreted as cryotaberal Early Quaternary sediments, which means that they are refrozen sediments of a talik (Grigoriev, 1996). They are followed by 5 m of alluvial interbeddings of silty-sands, gravels, and silts with banded cryostructure, interpreted as Zyryan IC. Above, 27 m of proluvial, silty-sandy IC deposits are following, interpreted as Kargin and Sartan. They are ice-rich, ice-banded and contain ice wedges and peat inclusions. The upper 0.5 m consists of the unfrozen Holocene soil.
The combined profile 103/81-203/82 is located not far from this borehole, thus the lithological composition is very similar (Figure 4-9). For this outcrop sections 5 datings exist for elevations between 2.5-7 m a.s.l., ranging from Kargin to Early Sartan (Slagoda, 1993; table 4-2).
The outcrop Kol-2 was situated in 14-15 m a.s.l. in a small erosive brook that followed the ice wedge net on an Edoma slope. The deposits consisted largely of peat, which was dated with two samples to Middle Holocene age (Figure 4-9).

4.5.1.3 Eastern Bykovsky Peninsula (Figure 4-10, 4-7)

The Mamontovy Khayata section was intensively studied and described in several publications (e.g. Schirrmeister et al., 2002a, b; Sher et al., 2005). Thus we give only a short description of the profile combined with the adjacent alas profiles and two offshore boreholes. The covered sequence is 89 m thick, ranging from 51 m b.s.l. to 38 m a.s.l. (Figure 4-10). From 51 m b.s.l. to 9 m b.s.l. sandy-gravelly fluvial deposits occur, interpreted as Pliocene-Early Pleistocene (Kunitsky, 1989). They are followed discordant by shallow fluvial or more general alluvial fine-grained sandy deposits (9 m b.s.l. - 8 m a.s.l.), which are already considered as Zyryan IC containing typical lens-like reticulated cryostructures, ice bands, and ice wedges. In situ grass roots, small twigs and peat inclusions occur.

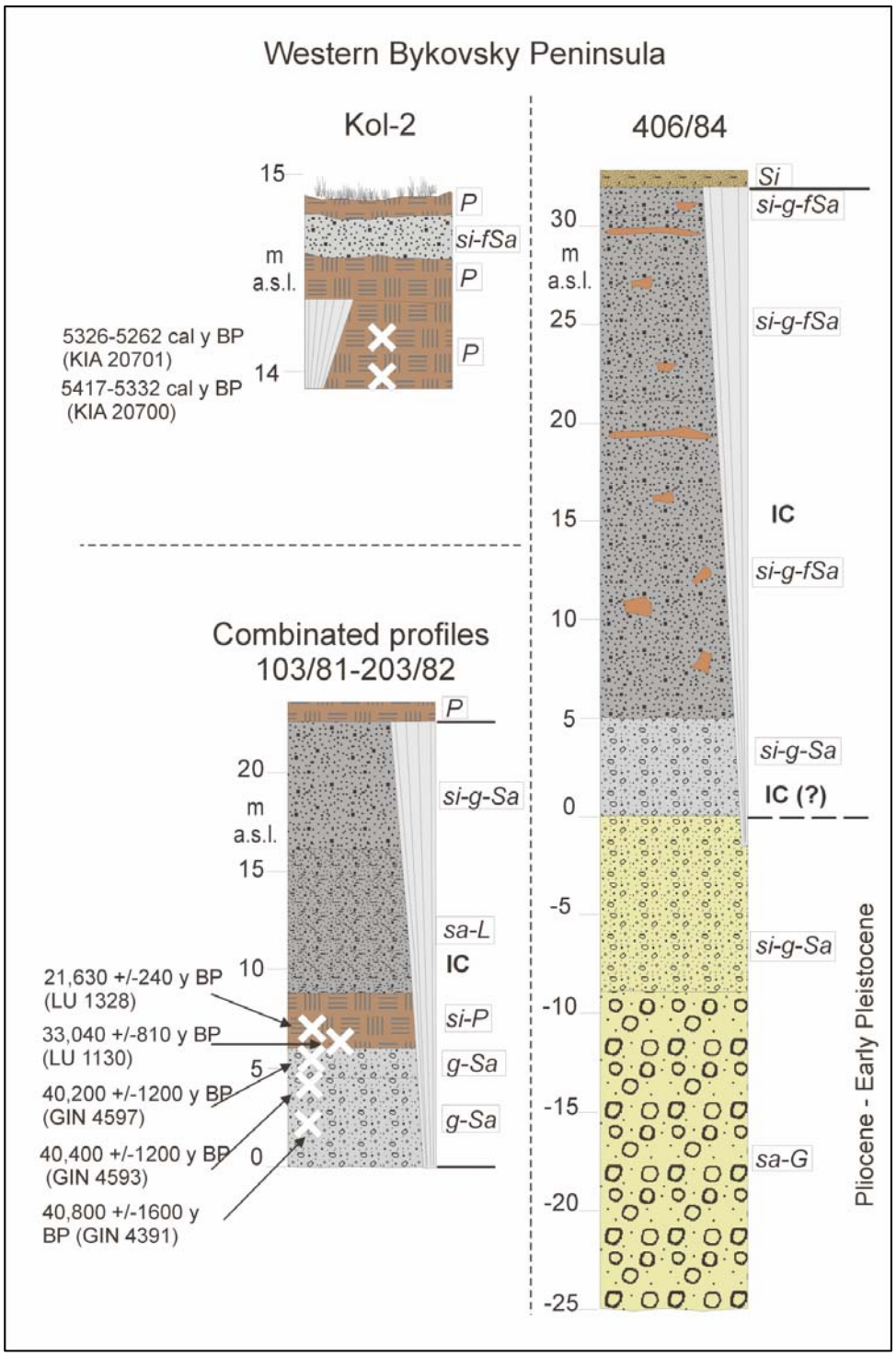

Figure 4-9: Schematic sedimentological profiles for outcrops in the western part of the Bykovsky Peninsula: section Kol-2 from a gentle slope on the flank of an Ice Complex elevation, a combined profile from sections 103/81-203/82 from the southern coast at Cape Razhdelny (Slagoda, 1993) and borehole 406/84 from an IC Complex elevation in the hinterland of Cape Razhdelny (Kunitsky, 1989). For the location of the profiles see figure 4-5. The legend is shown in figure 4-10.

The age interpretation of this lowermost IC is guided by few datings of the upper parts, which are hard on the radiocarbon dating limit. Extrapolated age estimations for the IC derived from an age-height relation, which was based on uncalibrated radiocarbon ages and mean accumulation rates, suggest the start of IC sedimentation at around 80 ky BP (Meyer et al., 2002a). The next IC horizon with silt, clayey silt and silty sand between 8-23 m a.s.l. is interpreted as Kargin. This ice-rich horizon contains many palaeosols and peat inclusions. From 23-36 m a.s.l. the IC consists of ice-rich silty sand to fine-grained sand. The following uppermost 2 m of peat-rich silts are dated with Holocene ages. According to Sher et al. (2005), a sedimentary gap exists on top of the IC of the Mamontovy Khayata main section between *c.* 8-12.5 ^{14}C ky BP at the transition from the Sartan to the Holocene. The sedimentation rate of the IC was relatively stable during the Late Pleistocene, which is suggested by the good age-height relation in the deposits. The ground ice content of the IC rises up to 70 weight-%. Large ice wedges of 5-6 m in width and 40 m in depth are embedded in the sediment and segregated ice, like ice bands or lens-like reticulated cryostructure, is common.

The deposits in the adjacent thermokarst depression consist of silty to coarse-grained sandy sediments. They have formed under various conditions as fluvial-limnic or proluvial deposits. Below the thermokarst deposits cryotaberal IC sediments occur, which have refrozen already. The dating of the thermokarst deposits shows Early-Late Holocene ages (Schirrmeister et al., 2002a; Table 4-2). The thermokarst sediments are far less ice rich (25-38 weight-%) than the IC, but ice wedges of 3-4 m width and several metres in depth occur. The ground ice is distributed mainly in fine pores as massive cryostructure. The formation of some peat horizons indicates alternating stages of thermokarst subsidence and stagnation. Sedimentary structures like graded bedding and ripples were observed in some thermokarst deposits.

The outcrop section B-S consists of 22 m of ice-rich silty IC sediments with plant remains and peat inclusions (Figure 4-10). The cryotexture is lens-like reticulated. The IC was covered discordant by 3 m of sandy sediments with thin organic interlayers, representing an aquatic, probably a shallow fluvial deposit. The IC was dated with two ages indicating Kargin and Sartan ages. The sandy deposits were dated with one age indicating deposition during the Late Sartan.

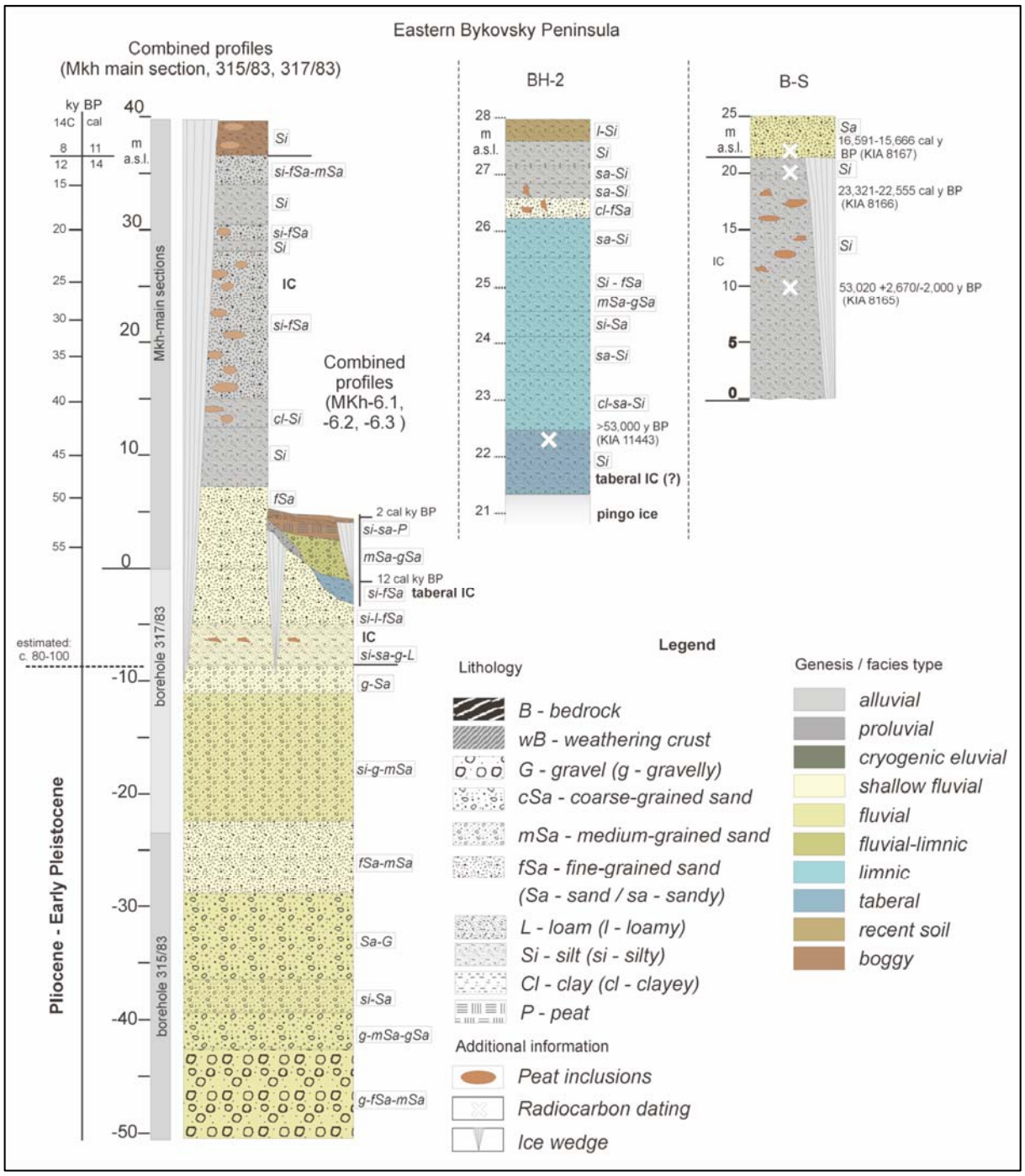

Figure 4-10: Schematic sedimentological profiles for outcrops in the eastern part of the Bykovsky Peninsula: combined profile for the Mamontovy Khayata Ice Complex key site and the adjacent thermokarst depression (MKh main Ice Complex sections, MKh-6 alas sections, boreholes 317/83 and 315/83)(Schirrmeister et al., 2001; Kunitsky, 1989), a sediment core from top of a pingo (BH-2) and a section from the northeastern shore (B-S). For the location of the profiles see figure 4-5.

In the borehole BH-2 6.5 m sediment were recovered (Figure 4-10). Directly above the ice core 1.1 m silty sediments occur. This sediment is probably cryotaberal, which means it is refrozen material from a former talik. The talik sediments were probably Zyryan or Early Kargin IC deposits, what is suggested by a infinite dating >53 ky BP. The taberit has been formed by a thermokarst lake, which has deposited the following silty and sandy sediments. An interlayer of medium grained sand with plant remains and peat inclusions probably indicates the influence of running water and the reworking of material. The uppermost 1.8 m are peaty silty-sandy sediments originating from non-aquatic sedimentation.

4.5.2 Derivation of landscape development stages from surface structures

Periglacial surface structures are indicators of various relief forming processes. The structures and the processes can be related to certain development stages in a periglacial landscape. Usually, structures of various development stages co-exist within small distances in the complex tundra landscapes of the North Siberian coastal lowlands. Such co-existing features of different development stages are for instance the Edomas, which are erosional remnants of the Late Pleistocene accumulation surface, and Holocene thermo-denudation structures like thermokarst depressions. The surface features can be related to permafrost degradation (e.g. thermo-erosional valleys, thermokarst lakes) or permafrost aggradation (e.g. pingos, ice wedge polygonal nets). The nesting of structures indicates several landscape development stages and is common in tundra coastal lowlands like the Bykovsky Peninsula, e.g. a Middle Holocene pingo in an Early Holocene thermokarst depression surrounded by Late Pleistocene Edomas.

Numerous surface structures were identified and mapped in the investigation area with remote sensing. Subsequently, they were related to different landscape development stages by extrapolating the cryolithological and geochronological information from our database to individual surface features or whole feature assemblages. The dominant structures, related processes, and their indications for different landscape development stages in the investigation area are presented in Table 4-3. The Bykovsky Peninsula consists of co-existing landscape elements representing at least 8 different major stages, which are described subsequently.

The oldest observable surface features are the Edoma uplands. They consist of the syncryogene frozen deposits of the IC, which indicate continuous permafrost aggradation during this period (e.g. Figure 4-10: combined MKh-main section).

Table 4-3: Remotely sensed surface structures and their indication for certain processes and periods of landscape development

Observed structures	Process indication and associated landscape stage
Mainly in the Khorogor Valley	
Nival kars	Large perennial snowfields and extensive nivation during the Late Pleistocene
Cryoplanation terraces	Large perennial snowfields and extensive nivation during the Late Pleistocene
(Perennial) snow patches	Recent active nivation
Delly	Holocene sediment transport by slope wash / supra-permafrost drainage; in the upper valley they occur on slopes with thick ice-rich sediment, which are probably remains of the Late Pleistocene valley filling
Braided drainage nets	Late Holocene sediment transport by slope wash
Streams	Holocene sediment transport by fluvial activity
Oxbow lakes, inactive river channels	Late Holocene stream migration and change from fluvial to lacustrine sedimentation
Active Khorogor River delta	Late Holocene sedimentation with marine interaction
Inactive Khorogor River delta	Middle-Late Holocene sedimentation; after major shift in river flowdirection deactivating of the delta
Mainly on the Bykovsky Peninsula	
Edoma uplands	Erosional remants of the Late Pleistocene (Sartan) terrain surface with only minor thermokarst degradation
Thermo-erosional valleys	Holocene thermokarst und thermo-erosion above the ice wedge net
Nival niches	Late Holocene nivation at small nivation hollows in thermo-erosional valleys or thermokarst depressions with recent snow patches
Low-centre ice-wedge polygons	Middle-Late Holocene refreezing of subaerial depression bottoms, formerly occupied by lakes
High-centre ice wedge polygons	Late Holocene initial thermokarst/thermo-erosion on slopes or on uplands
Thermokarst mounds	Late Holocene thermokarst along slopes or cliffs; presence of Late Pleistocene IC with large ice wedges
Thermo-erosional cirques & thermo-terraces	Late Holocene coastal erosion and rapid coastal retreat; presence of Late Pleistocene ice-rich IC
Large deep thermokarst lakes	Holocene thermokarst with deep subsidence
Large shallow thermokarst lakes	Holocene thermokarst
Small shallow lakes	Late Holocene meteoric or meltwater ponds; possibly initial thermokarst lakes
Thermokarst depressions	Early-Middle Holocene thermokarst subsidence; sometime presence of several slope terraces indicating different stages of subsidence
Pingos	Middle-Late Holocene talik refreezing; presence of Pre-Holocene coarse-grained material in the refreezing talik
Collapsing pingos	Late Holocene collapse of the pingo ice core
Thermokarst-lagoons	Late Holocene coastal erosion and marine inundation; Early-Middle Holocene thermokarst subsidence
Marine lagoons and marine sandbars	Late Holocene coastal dynamics
Technogene thermokarst along vehicle tracks, roads, or constructions	Late Holocene anthropogene influence

The next stage was characterised by permafrost degradation in the form of strong dissection of the Edomas by thermokarst depressions. The development of the extensive net of thermo-erosional valleys started during the same time as the thermokarst subsidence. Presently, the thermokarst lakes in the depressions clearly have a smaller extent than the depressions (Grosse et al., 2005). Thus, a stage of maximum lake extent and a subsequent stage of massive lake shrinking can be inferred. This stage was marked by the formation of wide subaerial lake terraces and Alas bogs. The following stage was characterised by permafrost aggradation again, expressed by pingo growth above refreezing lake taliks and the growth of ice wedge polygonal nets in then subaerial thermokarst depressions.

In the next stage, thermokarst depressions were truncated by coastal erosion and thus formed thermokarst lagoons. This process indicates the subrecent and recent coastal dynamics resulting from the marine transgression that reached the area. The occurrence of thermo-erosional cirques along some Edoma coastal cliffs also belongs to this stage.

Two final stages of local importance were observed at the Kolychev Isthmus, where the peninsula is connected to the mainland. Here the Khorogor River first formed a delta in a thermokarst lagoon south of the Kolychev Isthmus (Figure 4-4). A shift in the river course caused by circumstances not investigated until now, truncated this delta from water and sediment supply. This delta is now inactive. Possible causes could be neotectonics in the area of the Kolychev Isthmus or the blocking and redirecting of the river by ice and sediment jams during a major spring melt flood. A second and still active delta formed afterwards in a thermokarst lagoon north of the Kolychev Isthmus.

A few landscape stages were derived from surface structures in the Khorogor Valley, but the general pattern is different from the Bykovsky Peninsula. The surrounding mountains of the Kharaulakh Ridge consist mainly of sedimentary bedrocks, like alternating slate and sandstone sequences. In the upper Khorogor Valley some dolerite dykes occur. This bedrock assemblage and the varying weathering resistance of the bedrocks are strongly influencing the surface structures in the upper valley. Especially cryoplanation terraces, river courses, and the occurrence of a few lakes are affected by the bedrock geology. The lakes are situated in bedrock depressions at the boundary between upper and central valley. Step-like cryoplanation terraces with bedrock outcrops, debris fields, and patches of fine grained-sediment between them were observed in higher elevations.

The dominating features at lower slopes in the upper valley are extensive slope wash areas, were so-called dellies occur (Figure 4-11). ‘Delly’ is a Russian term for directed, subparallel supra-permafrost drainage features on slopes with mostly fine-grained ice-rich permafrost deposits (Katasonova, 1963). Usually dellies are connected to slope wash and initial thermokarst on slopes. Similar features are described as ‘rills’ in the western literature (e.g.

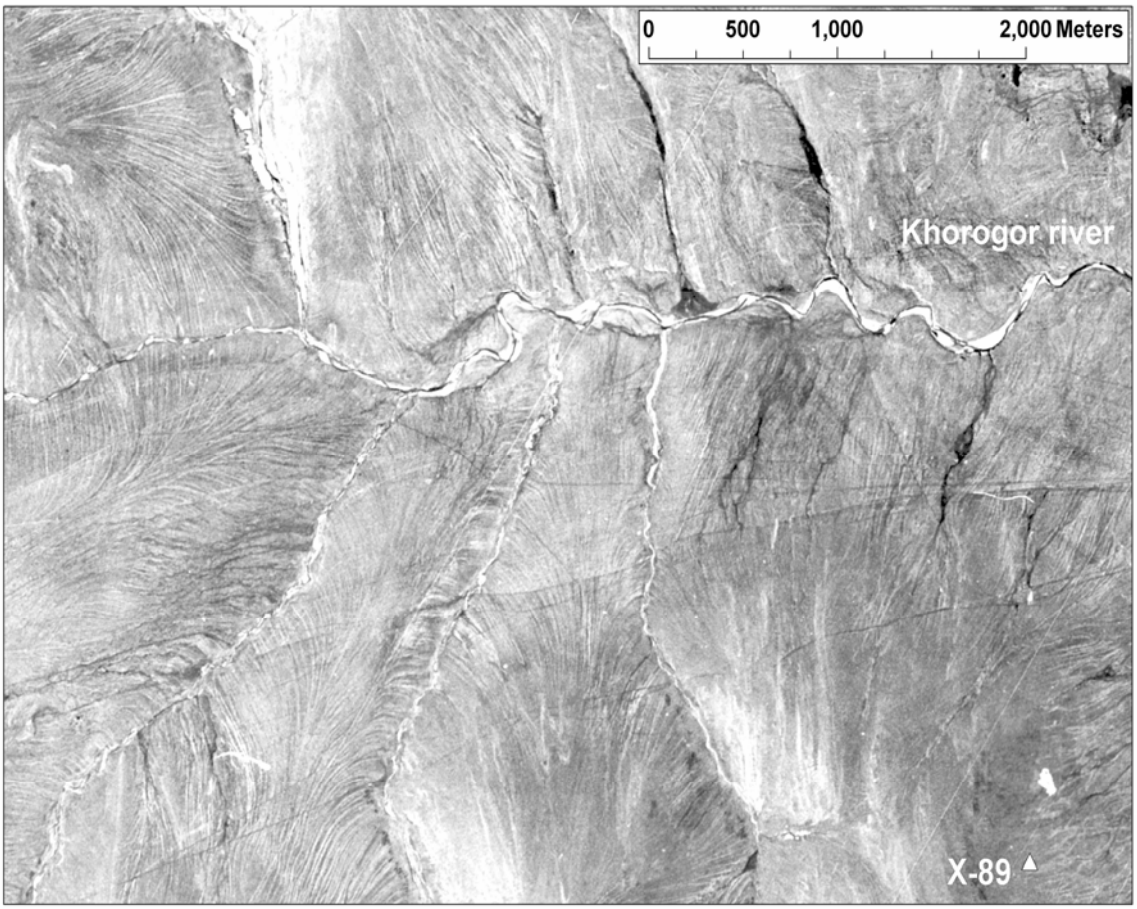

Figure 4-11: Widely distribution subparallel slope structures are visible in the upper and central valley regions. These hydrological features indicate supra-permafrost drainage in direction of the slope inclination towards small valleys or brooks. In the lower right the location of borehole X-89 is indicated. The location of this CORONA image subset is indicated in figure 4-12.

Lewkowicz & Kokelj, 2002). Although these features were observed with remotely sensed images in our investigation area they were hardly visible on the ground, which indicates that in this case the main difference to the surrounding area is not relief but soil moisture.

The sedimentary cover on the valley bottom in the central and lower valley is not very thick. The broad central valley is dominated by a large delly system, which has partially a braided character and is dominated by wet tundra. Thermokarst mounds were observed here especially

along riverbanks or road constructions. The mounds indicate the presence of ice-wedge polygons and thus relatively thick and ice-rich sediments. Most locations, especially in the central and lower valley, are covered with a peat horizon (Figure 4-8).

In the Khorogor Valley no assemblages of Edoma uplands and thermokarst depressions occur, although large parts of the valley have similar or lower elevations than the Bykovsky Peninsula. The conclusion from this important observation is, that there are only shallow sedimentary deposits in most parts of the central and lower Khorogor Valley, probably also containing less ground ice than the deposits on the Bykovsky Peninsula. Only in the lowest valley close to the Neelov Bay shore, assemblages of many small lakes occur, which are absent in the central and upper valley. This region has a relative sharp boundary to the central valley. The deposits are at least a few metres thick in this region (Figure 4-8: Khg-17, Neb-1).

By quantifying the coverage of various remotely sensed surface structures, the strong differences between the Bykovsky Peninsula and the Khorogor Valley became clear.

4.5.3 Terrain analysis

The DEM, a slope map, and several cross-sections were used for the spatial characterisation of the Khorogor Valley and the Bykovsky Peninsula in general and of individual structures identified by remote sensing in peculiar. The catchment area of the Khorogor Valley covers approximately 365 km^2. The two dominating rivers, the Khorogor and the Khatys-Yuryakh, originate from elevations at about 340 m and 330 m, respectively. Whereas the upper valley region is relatively narrow (Figure 4-6: A1-B1) and strongly dissected by the outcropping bedrocks, the wide central and lower valley is a plain with a very gentle general inclination towards the Neelov Bay in the NE, and a small tilt towards the Khorogor River at the south-eastern valley boundary (Figure 4-6: A2-B2, A3-B3, D-E). Almost all delly areas in the valley occur at slopes that are covered with fine-grained sediments (usually situated below 200 m a.s.l.), and that have slope inclinations of much less than 10° (Figure 4-12). Thus we assume these values as a pre-condition for the formation of dellies in the Khorogor Valley. The area with assemblages of small lakes that was identified with remote sensing in the lower valley is coincident with an even lower inclination angle than the average of the valley (Figure 4-6: lowest part of cross-section D-E).

Strong geomorphological dissection is observed for the landscape of the Bykovsky Peninsula. The maximum elevations of Edoma uplands on the Bykovsky Peninsula are about 43 m a.s.l.. No large difference in maximum elevations can be detected for the western and the eastern regions of the peninsula (Figure 4-7: G1-G2), thus we assume that the inclination of the Late Pleistocene accumulation plain was extremely small in the region. The Edomas in the

northern region (Figure 4-7: F2-F3) and the south-eastern region (Figure 4-7: F1-F2) have lower elevations of about 25 m, which is caused by Holocene erosion of the Edoma top at these narrow parts of the peninsula. About 46 % of the peninsula area consists of deep thermokarst depressions (Grosse et al., 2005), of which some form 4 agglomerated basins dividing the peninsula in W-E direction. The thermokarst depressions mostly have steep slopes and very low mean elevations of 1-8 m a.s.l.. The central parts of the peninsula are more compact (Figure 4-7: G1-G2) than the coastal areas (Figure 4-7: F1-F2 and F2-F3), which are incised additionally by highly frequent thermo-erosional valleys.

4.6

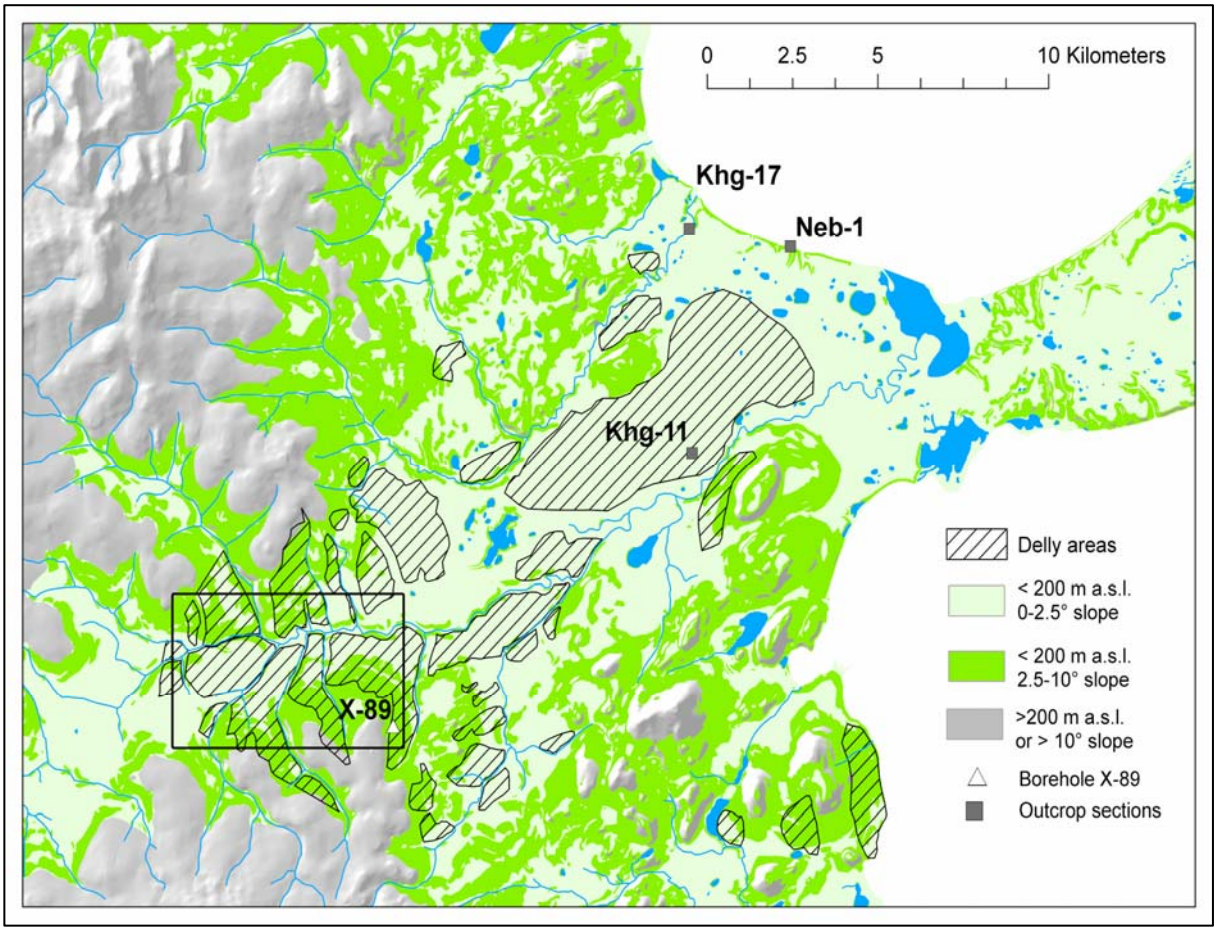

Figure 4-12: Slope map of the Khorogor Valley. The majority of delly areas is situated in regions with less than 2.5° slope inclination, and almost no dellies occur at slope inclinations higher than 10 °. The locations of the borehole X-89 and the three outcrop sections Khg-11, Khg-17 and Neb-1 are also shown. The black rectangle indicates the location of the CORONA image subset shown in figure 4-11.

Evolution of the landscape and discussion

From the numerous records available from stratigraphy, palaeo-environmental investigations, remote sensing and terrain surface analysis, a scheme of the evolution of the landscape in the investigation area was compiled, which is described in detail in the following subchapters. It covers the basal Pliocene-Early Pleistocene sediments as identified in boreholes and the main sequence with the Late Quaternary deposits. A graphical representation is summarising the developed scheme in Figure 4-13.

4.6.1 Pliocene – Early Pleistocene

The landscape was dominated by strong fluvial activity during a sedimentation period interpreted as Pliocene to Early Pleistocene (Kunitsky, 1989; Grigoriev, 1996). These deposits were evident in about 21 boreholes on the western and eastern Bykovsky Peninsula (e.g. Figure 4-9: 406/84, Figure 4-10: 317/83), but also several km offshore the Bykovsky Peninsula (e.g. Figure 4-10: 315/83) and Muostakh Island. Fluvial deposits below the Bykovsky Peninsula were detected from 9 m to >51 m b.s.l.. The rivers were capable to transport large amounts of medium- to coarse-grained sands and rounded gravels over wide distances from the Kharaulakh Ridge in the west to the mountain foreland in the east. The erosive strength of the rivers was probably supported by simultaneous tectonical uplift of the Karaulakh Ridge since the Oligocene (Imaev et al., 2000). Plant remains, grass roots, and shrub twigs in the sediments indicate, that the region was vegetated during this period. The sporadic occurrence of coal detritus in the sediments indicates varying sediment sources and thus river flow paths. Coal-bearing deposits were found for instance in the tertiary Sogo Graben several km south of the modern Bykovsky Peninsula (Figure 4-2). After this fluvial phase a large sedimentary gap is observed for the whole region. The causes of this gap are not clear, but most likely the strong tectonic activity in the region played a major role.

4.6.2 Early Weichselian (Zyryan Stadial)

The first sedimentation afterwards was that of the IC during the Zyryan, followed by Kargin and Sartan IC. During this entire period, a wide accumulation plain was developing in front of the Kharaulakh Ridge, probably enhanced by tectonic subsidence in the foreland. The general pattern of IC sedimentation was relatively stable for the whole Late Pleistocene (Zyryan, Kargin and Sartan).

The accumulation of the Zyryan IC started at about 80 ky BP (estimated by Meyer et al., 2002a), and resulted in 12-17 m thick ice-rich sediments. The fluvial energy was much lower than during the Early Pleistocene, and this first stage of IC sedimentation was dominated by

episodically shallow fluvial or alluvial floodplain-like facies with silty to fine-grained sandy deposits with graded bedding (Figure 4-9: 406/84; Figure 4-10: 317/83, MKh-main section). The deposits were found on the Bykovsky Peninsula in numerous boreholes and outcrop sections around the peninsula. Their elevation at Mamontovy Khayata is between 9 m b.s.l. and 8 m a.s.l.. Syngenetic ice wedges were capable to grow in these deposits and to form polygonal ground (Meyer et al., 2002a). The formation of soils and accumulation of organic matter was very weak (Schirrmeister et al., 2002b).

As main sedimentary source for the Bykovsky Peninsula IC we propose the Kharaulakh Ridge, and especially the Khorogor Valley. A high content of redeposited pre-Quaternary Pinaceae pollen especially in the Zyryan and Sartan IC sequence (Andreev et al., 2002) indicates the origin of the sediments in the nearby mountains of the Kharaulakh Ridge, where such pre-Quaternary deposits with Pinaceae pollen occur (Grinenko et al., 1998). Analyses of heavy minerals and rock fragments show the mineralogical similarity of Kharaulakh bedrocks (mainly Permian slates and sandstones) with various recent and Late Pleistocene sediments in the Khorogor Valley and the Bykovsky Peninsula IC deposits (Siegert et al., 2002). Similar results were received from investigations of mountain ranges and foreland IC in the Chekanovsky Ridge southeast of the Lena Delta (Schwamborn et al., 2002a; Schirrmeister et al., 2003a) and from Bol'shoy Lyakhovsky Island (Kunitsky et al., 2002), suggesting a strong genetic relationship between the mountain ranges and the foreland IC.

One main factor for the relatively small fluvial energy that was beneficial for the IC accumulation was probably the growth of a large Early Weichselian ice shield over Northern Europe and Western Siberia (Svendsen et al., 2004). The ice shield blocked the transport of moisture from the Atlantic to north-eastern Siberia and resulted in an increased aridity in these regions, which is documented in a variety of environmental proxies for the Bykovsky Peninsula, e.g. plant macro remains (Kienast et al., 2005) or insect remains (Sher et al., 2005). Although the Laptev Sea region and its low mountain ranges like the Kharaulakh Ridge were not glaciated during that time (Hubberten et al., 2004), extensive perennial snowfields existed on these mountains (Galabala, 1997). The supply of watercourses was probably substantially smaller during most time of the year except during the snowmelt, which led to intermittent and strongly seasonal sediment deposition. The high continentality with severe winters resulted in intensive nival weathering and erosion in connection with the formation of cryoplanation terraces and nival kars in the Kharaulakh mountains.

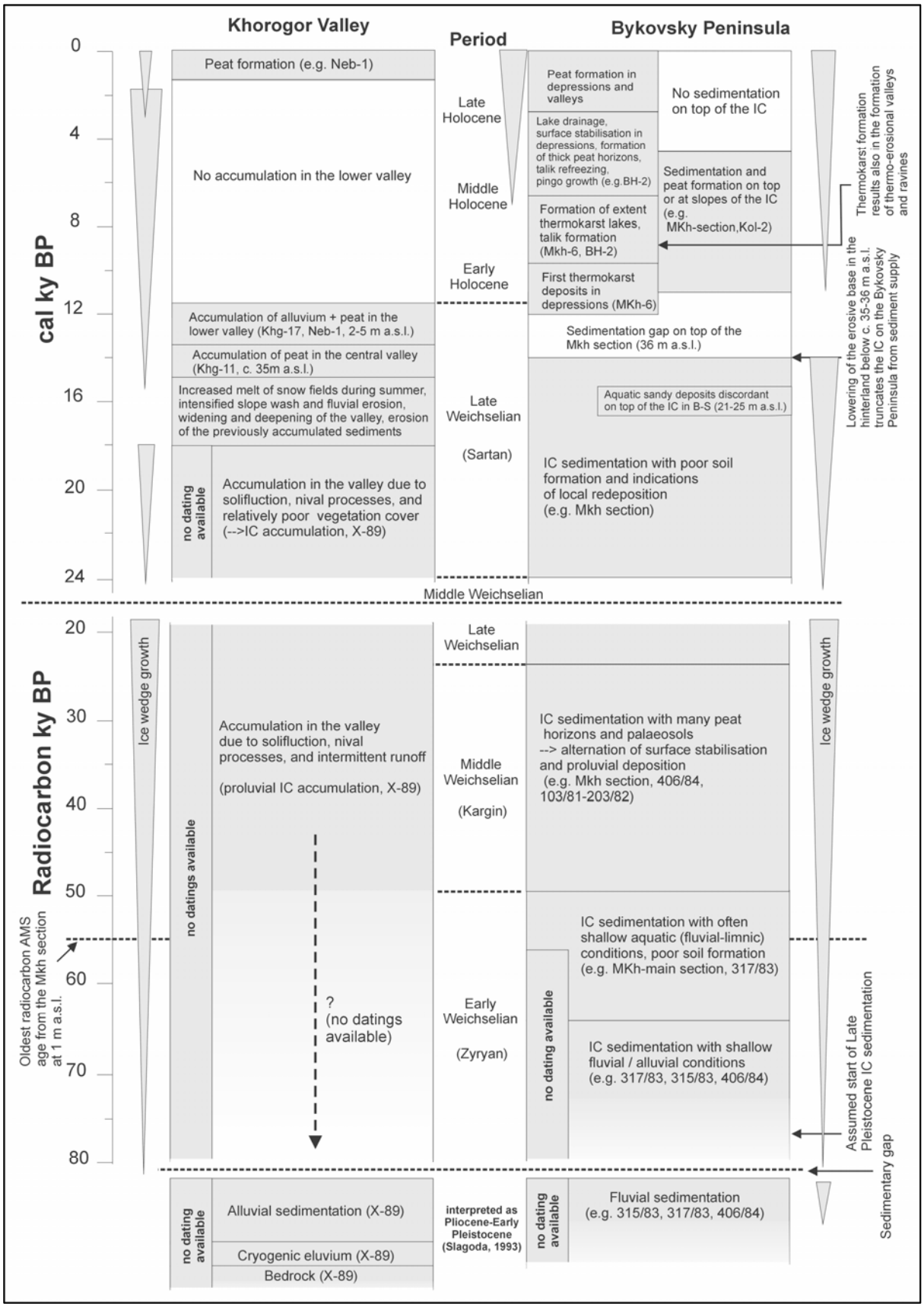

Figure 4-13: Schema of periglacial landscape development in the investigation area.

Large perennial snowfields accumulated in these structures and aeolian sediments were deposited with the snow. Aeolian deposition was widespread on the Eurasian continent during the Late Pleistocene (e.g. Rutter et al., 2003). During snowmelt in the quite warm summers (Kienast et al., 2005), slopewash and solifluction were strongly increased downslope of the snowfields. This was caused by the presence of the permafrost table close to the ground surface, which prevented the deep drainage of meltwater and resulted in supra-permafrost and above-surface drainage, and the increase of solifluction rates. Solifluction on permafrost grounds, so-called gelifluction, may already begin at slope angles as low as 1-3°, and is strongly dependent on the water content in the active layer (French, 1996). Many studies from periglacial regions show, that snowmelt has a strong impact on slope and surface erosion, often larger than summer precipitation can have (e.g. Lewkowicz, 1981; Stromquist, 1985). The surface wash in the Kharaulakh Ridge resulted in erosion and transport of fine-grained niveo-aeolian material from snowpatches and slopes towards the valleys. Similar processes, but in a smaller scale, were observed in the vicinity of present day snowfields in the Kharaulakh Ridge and other mountain ranges in the Laptev Sea region (Kunitsky, 1989; Kunitsky et al., 2002; Schirrmeister et al., 2003a). The remotely sensed dellies (Katasonova, 1963), or rills (Wilkinson & Bunting, 1975), are such drainage features on periglacial slopes with sedimentary cover and bad drainage conditions (Figure 4-11). Although the dellies itself are Holocene drainage features they indicate the presence of relatively thick ice-rich sediments, which are interpreted as Late Pleistocene (Figure 4-8: borehole X-89). We assume that comparable features developed in a much larger scale in the Late Pleistocene valleys of the Kharaulakh Ridge.

Additionally, the vegetation cover was probably much more fragmentary in the higher elevations and thus colder and more wind-exposed zones of the Kharaulakh mountains, resulting in easier erodibility of surface sediments.

4.6.3 Middle Weichselian (Kargin Interstadial)

During the Kargin Interstadial the IC accumulation in the foreland plain reached an elevation level (9-22 m a.s.l. at Mamontovy Khayata), at which the inclination and thus the relief energy of the accumulation plain was becoming to low for middle- to coarse-grained fluvial sedimentation. The sedimentation changed to more proluvial deposition. The strong climatic seasonality persisted, thus the highly seasonal runoff continued and mainly silty to fine-grained sandy sediments were deposited in the accumulation plain. Approximately 12-15 m sediments were accumulated at the Mamontovy Khayata section during the Kargin (50-28 ky BP) (Figure 4-10). Generally, the environmental conditions were rather unstable, and the

drainage of the tundra plain became poorer (Schirrmeister et al., 2002b). Well-developed palaeocryosol formation and intensive peat growth are evident for the Kargin period in almost all analysed profiles. The general geocryological conditions did not change, and syngenetic ice wedge growth was continued (Meyer et al., 2002a). The highly seasonal runoff persisting since the Zyryan was not capable to erode and transport all the provided sediments out of the mountains to the foreland plain, thus the valleys in the Kharaulakh Ridge became filled with sediments during the Zyryan, Kargin and Sartan. The borehole X-89 (Figure 4-8) and the extensive occurrence of dellies prove the presence of thick ice-rich sediments in the upper valley (Figure 4-11). We suggest, that these sediments are erosive remnants of an at least several metre thick Late Pleistocene sedimentary filling in the Khorogor Valley. The facial conditions were very similar to those on the foreland plain, although these proximal deposits have a higher content of coarse-grained sand and gravel (X-89). The ground-ice content is very high and comparable to the Bykovsky Peninsula IC. Ice wedges are also present in these deposits (X-89). This suggests favourable conditions for ice wedge growth in the upper valley not only in terms of climate, but also of hydrology and geomorphology. Large syngenetic ice wedges preferably grow in areas with low or no slope inclination. Even small slope inclinations lead to solifluction in fine-grained permafrost sediments (French, 1996), which prevents the growth of large ice wedges. This suggests smoother relief conditions than present in the upper valley during that period, resulting from the massive filling of the valley. Thus we propose, that IC-like sediments were also accumulated in the Khorogor Valley during the Late Pleistocene.

4.6.4 Late Weichselian (Sartan Stadial)

The IC of the Sartan period was characterised by ongoing proluvial sedimentation and local redeposition of fine-grained material in a poorly drained tundra plain in the Bykovsky Peninsula area. The climatic conditions were generally more arid (e.g. Hubberten et al., 2004) and dominated by strong seasonal temperature differences (Schirrmeister et al., 2002b). This resulted in a decrease of soil formation (Schirrmeister et al., 2002b) and the continuous growth of syngenetic ice wedges (Meyer et al., 2002a). With the accumulation of 13-15 m Sartan IC, an elevation of *c.* 36.5-39 m a.sl. was reached in the region of the Mamontovy Khayata site during the Sartan. A virtual accumulation plain plotted through the highest Edoma elevations (40-43 m a.s.l.) in the investigation area reveals the general small inclination of this plain. As the proposed main sediment source was the Kharaulakh Ridge and the Khorogor Valley, we assume that the Khorogor Valley was filled completely with IC-like deposits to at least similar elevations during the Sartan. The higher parts of the valley were

probably filled with IC-like deposits of at least several metre thickness, as is documented by the 15 m thick IC-like sediments in the upper valley (Figure 4-8: X-89, 160 m a.s.l.), which were interpreted as Sartan (Slagoda, 1993). The youngest ages for IC deposits on the Bykovsky Peninsula were dated between 14-15 cal ky BP (Figure 4-14), which coincides approximately with the begin of the Bølling/Allerød climatic period.

4.6.5 Transition period from Late Weichselian (Sartan Stadial) – Early Holocene

Major changes occurred in the landscape especially during the Late Sartan and Early Holocene. The trigger was probably the begin of a post-LGM climate amelioration in the region. Climatic changes in the region are for instance documented in a shift of the major winter precipitation source as recorded in ice wedges of the Late Sartan (Meyer et al., 2002a). Other indicators are the increase of herbs and a generally denser vegetation between *c.* 18-14 cal ky BP as inferred from pollen spectra (Andreev et al., 2002). Insect assemblages of the

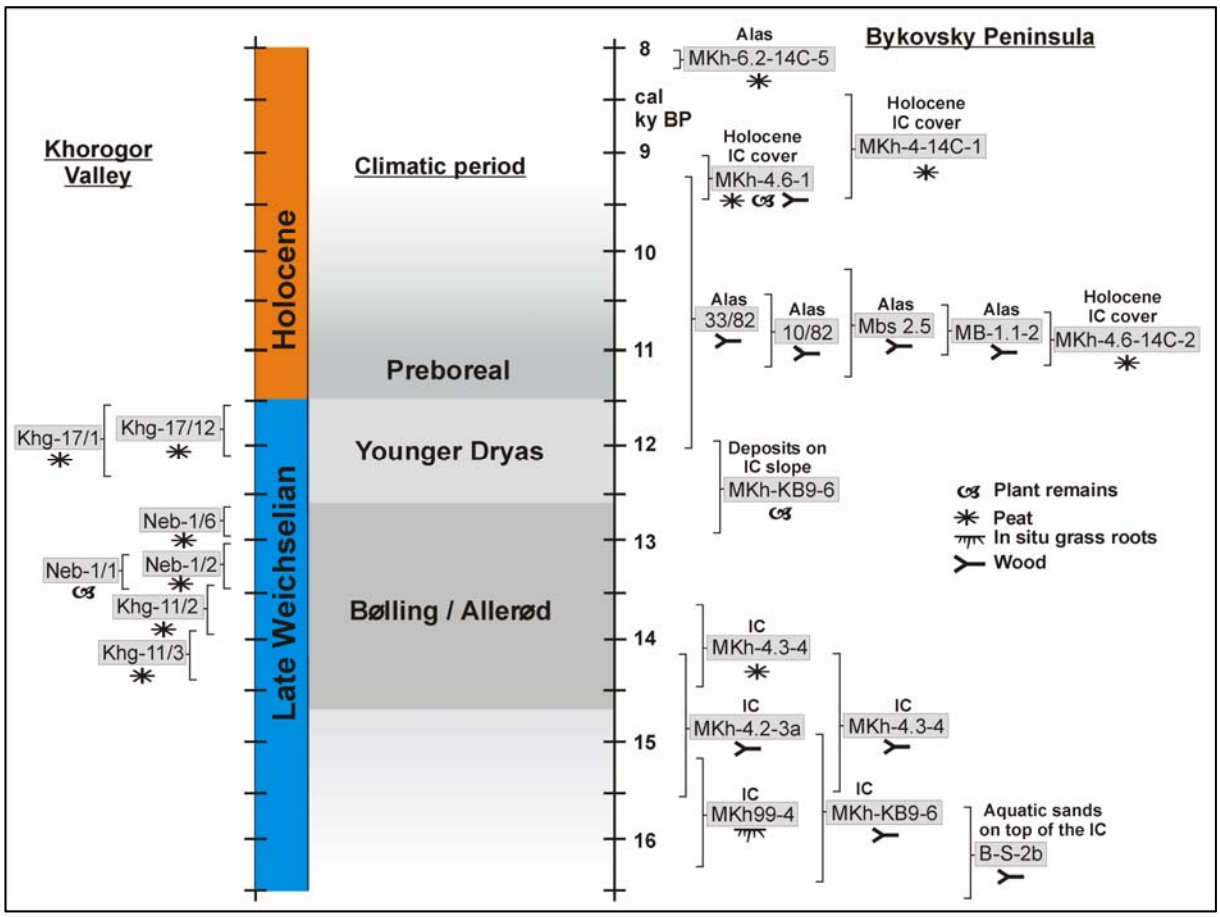

Figure 4-14: Available calibrated radiocarbon dates from the transition zone between the Late Glacial and the Early Holocene in the investigation area. The vertical bar for each dating is the 2-sigma error range. The deposits in the Khorogor Valley fit into the same time interval that is covered by a sedimentation gap on top of the Bykovsky Peninsula IC at Mamontovy Khayata. The datings are from Table 4-2 and from Schirrmeister et al. (2001). The boundaries of the climatic periods are based on greenland ice core data after Dansgaard (1993).

Late Sartan IC at Mamontovy Khayata indicate a sharp rise in summer temperatures and high aridity for the same period (Sher et al., 2005). Finally, the number of dated mammoth remains from the Laptev Sea region has a distinct rise in this period after a steadily decrease over the preceding 10 ky (Sher et al., 2005).

In the following period (*c.* 14-11 cal ky BP) after this initial climatic amelioration phase a sedimentation gap occurs on top of the Mamontovy Khayata IC at 36.5 m a.s.l., hence this important transition period is not recorded here (Figure 4-10; Figure 4-14) (Schirrmeister et al., 2002a; Sher et al., 2005).

We suggest, that this gap is possibly caused by a change in the hydrology of the hinterland, i.e. the Khorogor Valley. The preceding climate amelioration with increased summer temperatures most probably led to a more extensive melt of snowfields in the Kharaulakh mountains and resulted in increased seasonal discharge rates of melt water during the summers (compared to the periods before). The increased discharge caused intensified slopewash and stronger fluvial erosion of the deposits that were previously accumulated in the valleys. A hint for increased discharge rates during this period are e.g. shallow-fluvial sands found in a section of the northern Bykovsky Peninsula (Figure 4-10: profile B-S). They overlay the IC discordantly and their base was radiocarbon-dated to 16.6-15.7 cal ky BP (Table 4-2). We assume that the IC-like deposits in the Khorogor Valley were rapidly eroded by higher fluvial activity and thermal abrasion, caused by increased summer temperatures and a changing winter precipitation source during this climatic event between *c.* 18-14 cal ky BP. The Khorogor Valley has the largest catchment area in the region and thus the input of meltwater in the valley from the thawing of extensive snowfields would be quite high.

The idea on the filling and subsequent erosion in the Khorogor Valley is supported by Gravis (1969a, b), who intensively investigated periglacial slope processes in the NE Siberian Kular Range southeast of our investigation area. He assumes that periglacial slope processes like slope wash and solifluction interact and become dominant to each other depending on climatic conditions, especially temperature and precipitation. This results either in sediment accumulation within valleys, or erosion and valley deepening. Gravis (1969a, b) established a rhythmic sequence for the investigated Late Pleistocene deposits, whereas each glacial and interglacial period was divided into two phases of slope processes. During the first phase, valleys were mostly filled with sedimentary material, while during the second phase, the valley infill was mostly eroded, and valleys were deepened. Generally, the valley deepening and erosion was stronger during the interglacials. Gravis (1969a) suggests that during the early Sartan the valleys were filled due to an increase of solifluction. During the middle

Sartan this trend continued with a higher solifluction and minor slope wash. During the late Sartan, solifluction decreased, slope wash became dominant and valley deepening and widening took place. This process was partly reversed during the Early Holocene, when accumulation starts again in valleys. We agree with this hypothesis and find similar patterns in the Khorogor Valley at least for the late Sartan and Early Holocene periods.

The erosive base in the central Khorogor Valley was lowered below 35 m a.s.l. around *c.* 14.4 cal ky BP, when thin alluvial sediments above weathered bedrock were covered with a 1 m thick peat horizon at Khg-11 (Figure 4-8, 4-6). A new pollen record from this peat suggest dense shrub vegetation (Betula nana and Salix) in the valley and thus a more ameliorated climate, correlating to the early-middle Bølling/Allerød period. The elevation and age of this deposit is approximately coincident with the sedimentation gap on the Mamontovy Khayata IC. Therefore we suggest that the lowering of the erosive base by increased fluvial activity in the hinterland (i.e. in the Khorogor Valley) forced the truncation of the Bykovsky accumulation plain from the main sediment supply in the Kharaulakh Ridge, and resulted in a sedimentation stop on the top of the Bykovsky Peninsula IC. The erosive base reached the lower valley at *c.* 13.5 cal ky BP, when alluvial silty fine-grained sands with peat inclusions were accumulated at the site Neb-1 during the middle-late Bølling/Allerød period (Figure 4-8) These sediment is probably reworked material from the eroded IC deposits in the Khorogor Valley. Pollen and spore data from this site suggest the presence of disturbed soils, probably due to a more exposed position of the site at the valley mouth. The presence of large epigenetic ice wedges indicates relative stable surface conditions probably during the following Younger Dryas cold period. The upper part of Neb-1 and the lower sequence of Khg-17 (Figure 4-8) have much lower pollen concentrations. They are dominated by Equisetum and contain high amounts of dung-inhabiting Sordariaceae spores, which probably may indicate the presence of grazing herds in the region during the Younger Dryas. The pollen spectra from the middle part of Khg-17 already documents the Holocene climate amelioration, and the upper part reflects Holocene shrub tundra vegetation.

Finally, no IC deposits were preserved in the lower and central Khorogor Valley. IC was partially preserved on slopes in the upper valley.

4.6.6 Early Holocene

The early Holocene is characterised by the strongest changes in the investigated landscape.

The strong climatic warming and increase of precipitation in the region during the Early Holocene is well-documented in a wide range of palaeo-environmental proxies in the Mamontovy Khayata sequence and adjacent thermokarst deposits (Andreev et al., 2002;

Schirrmeister et al., 2002b; Sher et al., 2005). Ice wedge growth was limited in this period (Meyer et al., 2002a). In an initial stage, probably at around 12 cal ky BP, the higher humidity and the poor drainage conditions in the flat tundra plain resulted in the formation of small water bodies in shallow relief depressions in the Bykovsky accumulation plain. They rapidly increased in size, and high summer temperatures led to a strong input of heat energy into the water. Thermokarst subsidence began below these ponds, and continued as a self-enforcing effect due to the redirection of runoff towards the newly formed depressions. This initial phase of thermokarst subsidence and lake growing must have happened very rapidly. Well developed thermokarst deposits appear already at *c.* 11.5 cal ky BP on the Bykovsky Peninsula (Figure 4-14; 4-10: combined profiles MKh-6). The landscape was already strongly dissected at that time and sedimentary processes, now dominated by very local erosion, transport and deposition, clearly differed from the Late Pleistocene period before. Definitely this climatic and geomorphic change had also a strong influence on local biocoenoses, e.g. by generating wind-protected habitats in depressions and valleys with shrub and tree tundra vegetation, or by the favouring of wetness adapted plants.

The rapid subsidence of thermokarst depressions and the formation of steep slopes resulted in the massive reworking of IC material by solifluction and slope wash, and the deposition of fine- to coarse-grained subaerial thermokarst deposits (Figure 4-10: combined profile MKh-6). Lacustrine silty-sandy thermokarst deposits were accumulated in thermokarst lakes. They are situated directly above the IC deposits, which have been turned into a typical taberal (first thawed and then subsequently refrozen) sediment due to talik formation below the lake (Figure 4-10: pingo sediment core BH-2). The thermokarst depressions have often subsided more than 30 m, thus their mean elevation is only sligthly above the present day sea level. The thermokarst development climaxed in the Early Holocene Optimum, when thermokarst lakes reached their maximum extent in the region around *c.* 7-5 cal ky BP. Some depressions coalesced by lateral extension and formed large basins crossing the entire peninsula from west to east. We suggest that these large basins occur at locations where the thermal, hydrological, and sedimentological properties were favouring the formation of these east-west-crossing basins, e.g. by the presence of coarser-grained deposits of small Late Pleistocene streams or shallow stream valleys that possibly drained the accumulation plain from west to east. An indicator for this hypothesis is probably the presence of coarse-grained sands with graded bedding in the sediment sequences of some thermokarst depressions (e.g. Figure 4-10: combined profile MKh-6, BH-2).

The subsidence of large depressions was accompanied by the formation of thermo-erosional

valleys, which mostly developed above the Late Pleistocene ice-wedge net. These extensive valley networks often radially drained the remaining IC tops (Edomas) towards existing depressions. Edomas with lacking or poorer drainage conditions were disturbed locally by small-scale thermokarst features, which deposited peat-rich sediments on top of the IC during since *c.* 11 cal ky BP. At the Mamontovy Khayata site the Holocene cover is up to 2 m thick (*c.* 35-37 m a.s.l.) and ranges from 11-6 cal ky BP in local thermokarst deposits on the top of the IC (Figure 4-10: MKh-main section).

No Early Holocene deposits are documented in the Khorogor Valley.

4.6.7 Middle-Late Holocene

After the Early Holocene Optimum a general climate deterioration is indicated by the decline in thermokarst development, the drainage or silting-up of thermokarst lakes, and the refreezing of lake taliks. Other proxies that suggest a climate deterioration are the decreasing content of tree pollen (Andreev et al., 2002) and the restart of ice wedge growth in subaerial thermokarst depressions and thermo-erosional valleys (Meyer et al., 2002a).

Two phases of surface stabilisation are suggested by the accumulation of thick peat deposits in depressions and valleys of the Bykovsky Peninsula. One is between *c.* 6-3 cal ky BP and another one between *c.* 1.5-0.9 cal ky BP (Table 4-2; Schirrmeister et al., 2002a).

The presence of several pingos on the Bykovsky Peninsula proves the refreezing of lake taliks with the beginning climate deterioration after the Holocene Optimum. Approximately around 5 cal ky BP the Laptev Sea transgression reached its Holocene high-stand (Bauch et al., 2001). The presently observed thermo-erosional cirques along the shore are significant younger, as coastal erosion rates for the ice-rich permafrost coasts are high with several metres/year (Rachold, 2000). Several former terrestrial thermokarst depressions developed to thermokarst lagoons due to coastal erosion around the Bykovsky Peninsula in the Late Holocene. This development is exemplary for large parts of the Laptev Sea shelf during the Holocene (Romanovskii et al., 2004).

The Neelov Bay and the Tiksi Bay have probably formed during the Middle-Late Holocene by IC erosion and inundation of thermokarst depressions (Figure 4-4). The Bykovsky Channel, a major outlet from the Lena Delta, flows towards the Neelov Bay and probably played an important role for IC erosion and inundation in the Neelov Bay area.

The Khorogor River accumulated a delta in the Safroneeva Lagoon south of the Kolychev Isthmus during the Late Holocene. The truncation of this delta from water and sediment supply by a shift of the Khorogor River bed occurred probably in subrecent times. Since then the new active delta was accumulating in a lagoon north of the isthmus. The general relief in

this area is very gently. This indicates that even small geomorphic changes by whatever reasons (thermokarst subsidence; neotectonics; ice-jams) can have a large effect on the course of stream beds in such flat tundra landscapes and thus on the sedimentation pattern in the foreland.

All investigated outcrops and boreholes in the Khorogor Valley were covered by a peat horizon of varying thickness. Although these boggy deposits have Late Sartan age in the central valley (Figure 4-8: Khg-11), peat with clearly Late Holocene age was identified in the lower valley (Figure 4-8: Neb-1). The age of the 2 m thick peat cover at the site (X-89) in the upper valley is unknown. No noteworthy sedimentation in the valley is documented for the period between the Late Sartan and the Late Holocene. This indicates the stabilisation of slopes and plains, a general poorer sediment supply than in the glacial periods before, and the dominance of fluvial erosion for this period.

4.7 Conclusions

We successfully applied sediment studies, remote sensing and terrain modelling for the reconstruction of the evolution of a periglacial landscape in NE Siberia during the Late Quaternary. The combination of this wide variety of data types and sources was very beneficial for the reconstruction approach. Remote sensing and terrain modelling were used for the up-scaling of field data. Especially these applications can be further expanded with the advance of new satellite sensors and the volumetric modelling of geologic/geomorphic processes, respectively. The compiled cryolithological database of more than 170 boreholes, outcrops and other sample data will be very useful for various investigations and modelling approaches addressing the periglacial Bykovsky Peninsula, which is a key site for permafrost research and palaeo-environmental investigations for more than 200 years.

The Late Pleistocene IC deposits of the Bykovsky Peninsula were closely connected to sedimentary processes under highly continental climate conditions in the nearby Kharaulakh Ridge and its valleys, i.e. the Khorogor Valley. Beyond the general climatic influence, especially the hydrology in the mountainous hinterland and on the accumulation plain played a major role for the IC deposition during the Late Pleistocene and the IC degradation during the Holocene. The Late Pleistocene hydrology in the region was dominated by seasonal slope wash and melt water brooks both originating from the meltwater of extensive perennial snowfields in the mountains. It is suggested, that the IC on the Bykovsky Peninsula is a distal form of deposits originating in the Kharaulakh Ridge and its valleys. Major components in the IC genesis are niveo-aeolian processes in association with snowfields, strongly seasonal slope

processes like slope wash and solifluction, and seasonally alluvial or proluvial processes on an accumulation plain in the mountain foreland. As a result from these processes the Khorogor Valley was at least partially filled with IC-like deposits during the Late Pleistocene and was thus part of the gently inclined accumulation plain in the mountain foreland. The valley infill was eroded during the Late Sartan between *c.* 18-13.5 cal ky BP, when fluvial activity was high due to higher post-LGM summer temperatures and increased seasonal meltwater release from snowfields. The sedimentation gap on top of the Mamontovy Khayata outcrop section between *c.* 14-11 cal ky BP can be attributed to the truncation of the Bykovsky accumulation plain from sediment supply of the Kharaulakh Ridge as a result of fluvial erosion in the hinterland, i.e. in the Khorogor Valley. The palaeo-environmental information derived from the new outcrops in the central and lower Khorogor Valley cover approximately the Bølling/Allerød and the Younger Dryas periods, and are very useful for closing the information gap in the Mamontovy Khayata section at this important climatic transition zone. Since that period, the slopes and plains in the Khorogor Valley are relatively stable, the fluvial activity remained high, and no major accumulation took place. This indicates fundamental differences between Late Pleistocene and recent environmental variables in terms of snow accumulation, weathering, erosion and sediment transport in the Khorogor Valley, which can probably be extrapolated to the entire Kharaulakh Ridge and also to other mountain ranges in the Laptev Sea region.

The combination of arid climatic conditions and strongly seasonal water supply seems to be an important factor for the IC accumulation and the fossil biocoenoses found in the deposits. The assumption of strong seasonality in hydrology possibly can solve the problem of some contrary bio-and climate indicators in the IC archive (e.g. the occurrence of abundant green algae remains ‘simultaneous’ with proxies for general arid conditions). We assume that the palaeogeographical and geomorphological characteristics of the investigated periglacial landscape complex were directly influencing the development of the biocoenoses in the region.

With begin of the Holocene, the former extensive accumulation plain was completely reshaped to a landscape dominated by extensive permafrost degradation structures. Thermokarst and thermo-erosion were the dominant processes in the Holocene, leading to lake formation, ground subsidence, and the formation of distinct depressions. It is suggested that initial thermokarst preferentially started in previously existing negative relief forms like shallow stream beds, or above anomalous ground e.g. in terms of lithology or cryology. The thermally induced landscape reshaping had enormous influence on the hydrology, the

sediment deposition, and on the composition of biocoenoses. The maximum thermokarst activity was during the Early Holocene Optimum, when the largest lakes existed. Afterwards, climate deterioration lead to lake shrinking and talik refreezing. The Late Holocene outline of the peninsula was shaped by a combination of thermokarst, thermo-erosion, thermo-abrasion, coastal erosion, and marine inundation.

The role of neotectonics on the regional landscape evolution has still to be addressed with more intensive research.

A similar pattern of IC distribution including low mountain ranges and gently inclined accumulation plains in their foreland can be observed also in other regions of the Laptev Sea. We suggest that the processes leading to the formation of IC in these landscapes were very similar to the processes described in this paper for the Bykovsky Peninsula and the Kharaulakh Ridge. These ideas are also backed by own fieldwork on Bol'shoy Lyakhovsky Island with the Khaptagai Tas and other mountains (Schirrmeister et al., 2000; Kunitsky et al., 2002), in the western Lena Delta in front of the Chekanovsky Ridge (Schirrmeister et al., 2003a), around Cape Svyatoi Nos, on Stolbovoy Island, on Belkovsky Island and on Kotelny Island (all: Schirrmeister et al., 2003b), and in the Anabar-Olenek lowland in front of the Pronchishchev Ridge (Schirrmeister et al., 2004).

5. Synthesis

5.1 Intention

Palaeoclimate reconstructions in Arctic regions have revealed that northern environments were rather sensible to climatic change during the Late Quaternary and reacted strong on disturbances (e.g. Dansgaard et al., 1993; Thiede et al., 2001; Thiede et al., 2004). Additionally, most global climate models predict that northern high-latitude environments will be affected by stronger disturbances than lower latitude environments under current global change scenarios (ACIA, 2004).

Particularly landscapes dominated by ice-rich permafrost deposits are sensible to climatic change in terms of temperature and precipitation. Such deposits were widely distributed on the shallow non-glaciated Late Pleistocene shelves in Northeast Siberia, where they are called Ice Complex (IC). The use of the IC for the reconstruction of past environmental changes, and in particular their causes, consequences, and chronologies during the last glacial-interglacial cycle, has been an important scientific goal for many decades (Table 4-1), as these deposits provide an unique archive for the northeast Siberian region. Only recently, the geochronology of the IC key site Mamontovy Khayata on the Bykovsky Peninsula became precise enough to make detailed palaeo-environmental reconstructions for this site (e.g. Andreev et al., 2002; Meier et al., 2002a; Schirrmeister et al., 2002a, b; Sher et al., 2005) and to draw broader conclusions for the Late Quaternary environmental development in the region (e.g. Schirrmeister et al., 2002b; Hubberten et al., 2004; Sher et al., 2005). The IC deposits were strongly degraded and destroyed by thermokarst and marine inundation of the shelf areas during the Holocene (e.g. Romanovskii et al., 2000, 2004), thus only thermokarst-dominated remnants of these deposits survived in the modern coastal regions. The quantification of these changes that happened due to degradation of the IC by thermokarst during the Holocene is still in the beginning. The main thermokarst development occurred within a very short time period in the Early Holocene, which was characterised by a climatic shift towards warmer winters (e.g. Andreev, et al., 2002; Meyer et al., 2002a, b), and especially towards more precipitation in the previously very arid region (Schirrmeister et al., 2002b).

The dominant features of this change were energy and matter fluxes on various scales connected to extensive thermokarst subsidence (e.g. Romanovskii et al., 2000), thermo-erosion and coastal erosion (e.g. Rachold et al., 2000). The quantification of fluxes of sediment and freshwater delivers important variables for environmental modelling of the past landscape changes. These variables are necessary for the development of predictive landscape

models. As the IC sediments are very organic-rich (e.g. Schirrmeister et al., 2002b), the modelling of carbon fluxes connected to permafrost-degradation (organic matter, methane, carbon dioxide) is important for the enhancement of climate models.

Within this context, the focus of this work was the characterisation of periglacial landscapes in Northeast Siberia in their present state, in particular the quantification of surface structures and processes. Remote sensing and terrain modelling were evaluated as main tools for this task, and as tools for supplementing and up-scaling existing palaeo-environmental reconstructions in the key sites. Thus, a variety of techniques based on the composition of remote sensing, field work, and terrain analysis were developed for the analysis of periglacial landscapes in two key regions in the Laptev Sea coastal lowland.

5.2 Methods and techniques

The application of a combination of remote sensing and terrain modelling or GIS-based analyses is widely recognised in geomorphological investigations (e.g. Florinsky, 1998; Walsh et al., 1998). Some authors suggest automated classifications for various geomorphological structures or elements (e.g. Brown et al., 1998a; Giles et al., 1998; Wulder et al., 2004). A few approaches investigate processes connected to periglacial environments, but almost all of them consider alpine regions only (Etzelmüller et al., 2001; Gude et al., 2002; Bartsch et al., 2004). Approaches in the observation of periglacial lowland landscapes with remotely sensed images focus predominantly on vegetation classification and vegetation change on various scales (e.g. Walker, 1999; Brook & Kenkel, 2002; Gould et al., 2002; Hope et al., 2003; Jia et al., 2003; Stow et al., 2004). Some of these approaches incorporate rule- or terrain-based stratification, or general GIS-based spatial analysis (Joria & Jorgenson, 1996; Virtanen et al., 2004). Nevertheless, their focus is still on the analysis of the recent distribution of vegetation classes, or the change in vegetation distribution or biomass. Currently there is no approach for the classification of periglacial lowland relief and the identification of thermokarst-affected terrain with the method of remote sensing and terrain modelling.

Within this work, data originating from different sources and types (remote sensing, DEM, and field work), were successfully implemented into a GIS for each investigation area. GIS-based methods proved very efficient for data handling, integration, and conversion, and were thus used in all stages of data processing and analysis. Additionally, GIS-tools were applied for various spatial analyses.

Two different optical sensors (CORONA, Landsat-7) were used for the detailed

characterisation of periglacial lowland landscapes, i.e. geomorphology and hydrology. For the first time a method was developed for the application of high-resolution panchromatic CORONA satellite photography in periglacial research. The images of the CORONA program, which were classified and poorly known before 1995, proved so a qualified tool for the special needs in high-resolution remote sensing of remote Arctic periglacial environments. Some advantages of this imagery against aerial photography or commercial high-resolution satellite images is the easy and cheap availability, a larger ground coverage, and a relatively high temporal coverage between *c.* 1960-1980. These factors make them the preferable tool for certain tasks in periglacial research in remote areas, e.g. for expedition/field campaign planning, the detailed but large-scale mapping of thermokarst geomorphology and hydrology, or the detection of morphological changes over the last 45 years. Thus, beyond the geomorphological and hydrological mapping proposed in chapter 2, change detection of e.g. arctic permafrost coasts is another promising application for this imagery. The CORONA-based mapping of periglacial geomorphology on the Bykovsky Peninsula and in the Khorogor Valley, in particular of permafrost-degradation structures, was done manually. Additionally, the implementation of a relatively straightforward image classification into water/non-water pixels was demonstrated for the CORONA images.

CORONA images were also very useful for the accuracy evaluation of the Landsat-7-based classification conducted for the Mamontovy Klyk coastal lowland region in chapter 3. Imagery from the multispectral Landsat-7 Enhanced Thematic Mapper (ETM+) sensor were used in several ways. In chapter 3, this imagery was used in combination with digital terrain data for a supervised classification of terrain surface classes. The methodology and the classification result with 79 % overall accuracy are very promising and the transferability of the technique should be tested in other regions with similar thermokarst-dominated lowlands. Other classification approaches, i.e. for vegetation classification in tundra environments reported comparable classification accuracies mostly in the range from 60-85 % overall accuracy (e.g. Joria & Jorgenson, 1996; Virtanen et al., 2004). The most misclassification in our approach was identified for classes which are spectrally and genetically very similar and which are similarly interpreted in terms of relevance for thermokarst, thus the misclassification is not profoundly. The supervised classification method involves the use of field-based ground data, field knowledge, CORONA-derived ground data, and a medium-resolution digital elevation model in a maximum likelihood classification process. GIS-based rules, in particular pre- and post-classification image stratification, were successfully implemented to enhance the classification result.

Another promising method for the investigation of periglacial landscapes by remote sensing was the virtual merging of spatially high-resolution CORONA data with multispectral Landsat-7 data within a GIS as semitransparent image overlays. This technique strongly enhanced the visual identification and interpretability of distinct periglacial structures for mapping purposes.

Medium-resolution DEM were incorporated in all these remote sensing approaches. They were derived from scanned, geo-referenced and manually digitised topographic maps 1:100,000. The DEM were produced as raster grids with cell sizes of 30 m and 15 m for the Cape Mamontovy Klyk region and the Bykovsky Peninsula/Khorogor Valley area, respectively. The quality of these DEM was acceptable for the regional geomorphological approach of this work, but should be higher for special tasks, e.g. hydrological modelling. Secondary parameter, like slope maps, hillshade maps, or cross-sections were derived from the DEM to enhance mapping, classification, or field data interpretation.

In combination with a large amount of cryolithological field data that was compiled in a extensive database for the Bykovsky Peninsula and the Khorogor Valley, remote sensing was successfully used as supplementary tool for the reconstruction of the landscape evolution in the region during the Late Quaternary. In particular, CORONA images were used for the derivation of several landscape stages by the analysis of spatial relations of identified surface structures. One of the important conclusions from this investigation is, that the combination of remote sensing techniques, cryolithological field data and terrain modelling is very useful for the reconstruction of periglacial lowland landscapes.

5.3 Results

5.3.1 Periglacial surface structures and thermokarst quantification

The spatial parameters of thermokarst-affected terrain, in particular thermokarst depressions, thermokarst lakes, thermokarst lagoons, and thermo-erosional valleys were investigated for the Bykovsky Peninsula and the Khorogor Valley in the eastern Laptev Sea. They were analysed by means of spatially high-resolution CORONA satellite imagery and spatially analysis tool provided by a GIS software package. About 53.1 % of the peninsula are affected by deep thermokarst subsidence and thermo-erosion (thermokarst depressions, thermo-erosional valleys, thermo-erosional cirques). The subsidence was often down to near sea level, or in some cases even below, which resulted in the formation of thermokarst lagoons. In most places of the Bykovsky Peninsula this means 30-40 m thaw settlement in connection with erosion. Although the general thermokarst seems to have stopped since the Middle-Late

Holocene, the peninsula will be separated into several islands in near future due to ongoing thermo-erosion along the steep slopes of subsidence structures and the rapid coastal erosion.
A similar picture was revealed by the investigation of the Cape Mamontov Klyk region in the western Laptev Sea. The complete terrain surface classification resulted not only in the identification of deep thermokarst structures like in the manual mapping approach for the Bykovsky Peninsula, but also in the identification of extensive slope areas. These slopes towards thermo-erosional valleys or thermokarst depressions represent a large part of the thermokarst-affected terrain in the investigation area. Including all surfaces where the IC is degraded to some degree, at least 78 % of the investigated terrain of the coastal plain is affected by thermokarst and connected processes. By excluding the slope areas (which were not quantified on the Bykovsky Peninsula), 48.7 % of the region is affected by deep thermokarst. This value is very comparable to the 53.1 % value of the Bykovsky Peninsula.

5.3.2 Reconstruction of the Palaeo-landscape evolution

Generally, remotely sensed periglacial surface structures and cryolithological field information were used as indicators for the differentiation between individual phases of the periglacial landscape development. Both investigated regions represent erosional remains of an extensive tundra-steppe accumulation plain that has developed on the shallow subaerial Laptev Sea shelf during the Late Pleistocene. The palaeo-landscape development was investigated in detail only for the Bykovsky Peninsula and the Khorogor Valley. Very similar genetic processes as identified in this investigation area can be assumed for most locations in the Laptev Sea region where low mountain ranges in the hinterland and IC accumulation plains in the foreland occur. Such assemblages are found for the Kharaulakh Ridge (SE of the Lena Delta), the Chekanovsky Ridge (SW of the Lena Delta), the Pronchishchev Ridge (Lena-Anabar lowland), the Svyatoi Nos region (eastern Laptev Sea), and the New Siberian Islands. First investigations from some of these regions suggest the correctness of the findings in this work (e.g. Schirrmeister et al., 2000; Kunitsky et al., 2002; Schirrmeister et al., 2003a, b; Schirrmeister et al., 2004).
In a sedimentation phase before the Late Pleistocene (interpreted as Pliocene-Early Pleistocene by Slagoda, 1993), the region was dominated by strong fluvial activity in the mountain foreland. Between this period and the following IC sedimentation a large gap in the sedimentary record occurs, which possibly is related to tectonic activity in this region close to the Laptev Sea rift. On the Bykovsky Peninsula the accumulation of the ice- and organic-rich IC began around 80 ky BP (extrapolated by Meyer et al., 2002a), and was relatively continuously deposited until *c.* 14 cal ky BP, thus covering the Zyryan stadial, Kargin

interstadial and Sartan stadial periods (Schirrmeister et al., 2002b). The cryolithological investigations suggest a very close genetic relationship between the low mountain ranges and these deposits in the foreland accumulation plains. One of the most important factors for the palaeo-environmental development in this generally highly continental region (e.g. Treshnikov, 1985) was water in its various appearances in periglacial landscapes (ground ice, surface runoff, supra-permafrost runoff, lakes and ponds, snow accumulations). The low mountain ranges in the dry region were not glaciated during the Late Pleistocene but characterised by extensive snowfields (Galabala, 1997; Hubberten et al., 2004). Thus the landscape was characterised by a strongly seasonal and braided runoff fed mostly by snowmelt from the snowfields in the mountains. It is assumed that the snowfields, related niveo-aeolian processes, and the special runoff conditions were a precondition for the formation of the Late Pleistocene IC deposits in the Laptev Sea coastal lowlands (Kunitsky, 1989). At the transition from the Pleistocene to the Holocene, the change in global climatic patterns resulted also in rapid and strong regional changes in the investigation areas. First signs were already recorded for the latest Late Weichselian, when increased summer temperatures inferred from the Mamontovy Khayata palaeo-climate archive (Sher et al., 2005) probably led to the increase of slopewash and runoff rates in the Kharaulakh mountains between *c.* 18-14 cal ky BP and subsequently resulted in the erosion of Late Pleistocene sedimentary valley infill. Similar valley processes with strong relation to changes in moisture and runoff are reported from other periglacial regions (e.g. Gravis, 1969a, b; Mann et al., 2002). The IC sedimentation on the Bykovsky Peninsula ends at about 14 cal ky BP (Schirrmeister et al., 2002b). It is suggested that the main cause was the ongoing fluvial erosion in the hinterland and the subsequent truncation of the Bykovsky region from sediment supply. The main cause for the regional climatic amelioration during this time was probably the ongoing decay of the Eurasian ice sheet and the subsequent change in global climatic patterns, leading to a change in the source region of air masses, and subsequently to a rise in mean annual air temperatures, increased precipitation, and higher runoff rates. After a short period of climate deterioration during the Younger Dryas, a further push of climate amelioration occurred in the Early Holocene (e.g. Andreev et al., 2002; Schirrmeister et al., 2002b). It is suggested that these conditions initiated a chain reaction in the shallow and poorly drained accumulation plain consisting of ice-rich IC deposits. Large water bodies were forming due to increased runoff from snowfields in the mountains and higher precipitation rates. The initial thermokarst subsidence below these water bodies resulted in a redirection of the previously braided and strongly seasonal hydrological regime in the plain towards the new

depressions, which further increased the thermokarst subsidence and supported thermo-erosion and slope processes. These led to further lateral growth of the depressions. Various deposits were accumulated in the depressions (peat, limnic sands, slope deposits) and deep taliks were formed below the lakes. After this phase of intensive thermokarst during the Early Holocene, a climate deterioration was recorded since the Middle Holocene (Andreev et al., 2002; Schirrmeister et al., 2002b), which led to lake shrinking, talik refreezing, pingo up-heave, and the restart of ice wedge growth (Meyer et al., 2002a) in the then subaerial parts of depressions. Finally, the Holocene marine transgression reached the investigated region during the Late Holocene (Bauch et al., 2001) and transformed it to a coastal lowland area with thermokarst lagoons, thermo-erosional cirques along the coast, and deltaic sedimentation at the Khorogor River mouth. According to Romanovskii et al. (2004) the thermokarst relief played a major role in the rapid inundation of the shelf landscape.

5.4 Outlook

5.4.1 Further investigations of important processes

The dominant factor for the landscape evolution in the investigated periglacial regions was water. The low mountain ranges were not glaciated during the Late Pleistocene due to a strongly continental climate with generally dry conditions, but extensive snowfields existed. The extensive perennial snowfields are considered an embryonic equivalent to the large ice sheets in the western regions of North-Eurasia (Galabala, 1997). The snowfields were an important factor for weathering, erosion, and the supply of melt water for sediment transport to the mountain forelands (Kunitsky, 1989). Niveo-aeolian processes around the snowfields, and the seasonal and braided runoff from these snowfields were a main source and pre-condition for the IC deposits in the foreland. Until now, the spatial and temporal distribution of the snowfields is poorly known. Thus, the investigation of the type and extent of these snowfields as indicated by numerous nival kars or cryoplanation terraces in the mountain ranges of the Laptev Sea region is extremely important to understand and reconstruct the genesis of the IC deposits, the evolution of the shelf landscapes, and the general palaeo-environmental conditions during the Late Pleistocene. Additionally, to understand snowfield-related processes acting during the Late Pleistocene, it is necessary to investigate in detail modern perennial snowfields, associated nival processes, and matter and energy balances around these snowfields. Conclusions from such investigations could be adapted to large regions of the East-Siberian Beringia region.

Climatically forced change disturbed the established Late Pleistocene hydrological pattern by

increased temperatures and precipitation, and intensified runoff rates from snowfields. The climatic amelioration in the Early Holocene led especially to the reformation of hydrological processes, and initiated rapid and extensive thermokarst with a strong influence on the landscape and the regional environment. Until now, only a few sites with field investigations cover this transition period in the Laptev Sea region. Mostly, the records are hampered by gaps in the sedimentary record due to the nature of this event of extensive landscape re-shaping. For a detailed palaeo-environmental analysis of this period it is necessary to search for useful sedimentary archives covering this time. Of special interest would be the timing and the onset of thermokarst subsidence, the formation of thermokarst lakes, and the lateral extension and agglomeration of thermokarst depressions. Such information are very useful for the regional modelling of thermokarst evolution and provide additional data for the large-scale modelling of energy and matter fluxes associated with widespread thermokarst. Such data would also be of interest for the modelling of permafrost-dominated landscape under future climate change scenarios.

The quantification of thermokarst in large regions of the Arctic is still based on estimations, not on spatial measurements. The results would be of major interest for Arctic coastal dynamics research in terms of shore line dynamics and sediment input into the sea (e.g. Rachold et al., 2005), and for past and modern greenhouse gas balancing in the Arctic in terms of organic carbon and wetland balances (e.g. Christensen, 1993; Callaghan et al., 2004).

5.4.2 Future tasks for the observation and monitoring of change in periglacial landscapes

The general quantification and monitoring of change in periglacial environments includes especially the investigation of vegetation, hydrology, and matter fluxes from permafrost degradation. For all three tasks the application of remote sensing and terrain modelling is necessary in particular for the upgrading of local field measurements to larger areas. This is also a precondition for modelling future change in these landscapes.

Therefore, the next step should focus on one of two main directions: The increase in the level of detail and precision of the available approaches and thus the concentration on keysites, or the increase in spatial coverage and thus the application of the currently available approaches to larger regions.

The first idea focuses on the absolute necessity to understand small-scale processes in periglacial landscapes. Small-scale processes are still poorly investigated and there are still uncertainties about how they will react under global change scenarios and how possible reactions may influence the environment on various scales. Such processes are e.g. the flux of

sediment and organic matter in context with thermokarst, thermo-erosion or coastal erosion, the complex hydrology in permafrost-dominated areas, or biological interactions with the landscape. Thus, for the precise analysis, monitoring, and modelling of local periglacial landscapes it is desirable to increase the resolution of remote sensing (spatial, spectral and/or temporal) and terrain modelling (spatial and/or temporal). Such research must be concentrated on key sites with observatory characteristics. They should have several preconditions:

- The site location and the related environmental conditions are significant when compared with a large-scale, at least regional context. This assures the potentiality to up-scale achieved results to larger regions and support the answering of questions concerning the past and present environmental changes in the whole Arctic.
- Multi-disciplinary research is conducted at the site (e.g. geocryological research, palaeo-environmental investigations, hydrology, soil science, botany, ecology, micrometeorology), thus synergistic effects for remotely sensed and modelled analyses of landscape processes will result.
- The site must be relatively easily accessible to conduct investigations and measurements throughout the year, and over a period of at least several years.
- The site has an extent, which is manageable in terms of expected data quantity for high-precision observation, monitoring and modelling.
- The site must not be subject to legal restrictions in terms of data policy for high-precision remote sensing, terrain modelling and field work.

Appropriate remote sensing tools for such key sites in Arctic latitudes include presently operated high-resolution satellite or airborne sensors, which are capable to acquire data in a wide variety of wavelengths in multi- or hyperspectral mode (e.g. Ikonos, Quickbird, Spot, Terra-Aster, Chris-Proba, EO-1 Hyperion). Multi-sensor investigations, e.g. the combination of optical with radar data, are also desirable. Upcoming satellite missions in the next years, which are of interest for such observatory sites include e.g. hyperspectral sensors or high-resolution radar sensors (e.g. TerraSAR-X). Additionally, to integrate the high-resolution imagery with proper elevation models and to conduct terrain modelling on the same scale as the remotely sensed images, it is necessary to establish excellent elevation data sets for the key sites. Very high-resolution elevation data can be achieved by DEM generation from small-scale topographic maps, range finding airborne Light Detection And Ranging (LiDAR) data (e.g. Woolard & Colby, 2002; MacMillan et al., 2003; Töyrä et al., 2003) or Interferometric Synthetic Aperture Radar (InSAR) data (e.g. Catani et al., 2005). The acquisition of old data (e.g. CORONA or aerial imagery) and the recurrent acquisition of new

data would be a pre-condition for highly precise modelling and detection of volumetric or general surface changes at key sites. This data can be used for the determination of past and present volume fluxes of sediments and organic matter due to thermokarst, thermal erosion and coastal erosion and for the prediction of future developments under global change scenarios. In the Laptev Sea region, such a site could probably be the Bykovsky Peninsula, for which a comprehensive cryolithological database and a landscape evolution model was developed in this work. The peninsula is also close to the city of Tiksi and thus relative easily to access for field measurements. Another site could be the Samoylov Island and the adjacent Kurungnakh Island in the Lena Delta, where a polar research station and several environmental observatories are already operated.

The second idea focuses on the quantification of thermokarst and thermo-erosion in the extensive permafrost-dominated coastal lowlands of the Arctic. Currently, there are no precise quantifications on the extent and distribution of these permafrost-degradation processes over large regions, and the extent of matter fluxes connected to these processes. This approach could be based on the already developed techniques, using Landsat-7 ETM+ data, digital elevation models derived from 1:100,000 topographic maps, and basic cryolithological data. The existing approach can be further enhanced, e.g. by the inclusion of detailed vegetation and soil data, by using field spectrometry for ground date collection, or by incorporation of additional radar data. It would be useful to develop a catalogue of characteristics for typical periglacial surface features, including vegetation, soils, hydrology, spectral properties, cryolithology, and spatial parameters (size, elevation, slope, morphometry, etc.). The enhanced approach should be transferred from the key sites to larger regions to test its general applicability and the potential for up-scaling the local results. These test regions should not be limited to the Laptev Sea coastal lowland area, as other regions with extensive thermokarst-affected terrain exist especially along the coasts of the East Siberian, Chukchi, and Beaufourt Seas, and also in central Yakutia. A limiting factor for this approach is the availability of appropriate elevation data with good enough resolution for most regions in the Arctic. Thus, a downgrade in general spatial resolution for the observation and quantification of thermokarst would be a possible solution. The general requirements include the acquisition of medium- to high-resolution digital elevation models from selected regions, of Landsat-7 or comparable multispectral data, and of additional data sources like vegetation maps, geological maps or radar satellite data.

6. References

ACIA (2004). Impacts of a warming Arctic. Arctic Climate Impact Assessment. Cambridge University Press: pp. 146.

Adams, M. (1807). Some account of a journey to the Frozen Sea, and of the discovery of the remains of a Mammoth. Philosophical Magazin 29, 141-143.

Allard, M., Caron, S., & Begin, Y. (1996). Climate and ecological controls on ice segregation and thermokarst: the case study of a permafrost plateau in Northern Quebec. Permafrost & Periglacial Processes 7, 207-227.

Altmaier, A., & Kany, C. (2002). Digital surface model generation from CORONA satellite images. ISPRS Journal of Photogrammetry and Remote Sensing 56, 221-235.

Andreev, A. A., Manley, W. F., Ingolfsson, O., & Forman, S. L. (2001). Environmental changes on Yugorski Peninsula, Kara Sea, Russia, during the last 12,800 radiocarbon years. Global and Planetary Change 31, 255-264.

Andreev, A. A., Schirrmeister, L., Siegert, C., Bobrov, A. A., Demske, D., Seiffert, M., & Hubberten, H.-W. (2002). Paleoenvironmental changes in north-eastern Siberia during the Late Quaternary – Evidence from Pollen Records of the Bykovsky Peninsula. Polarforschung 70, 13-25.

Andreev, A. A., Grosse, G., Schirrmeister, L., Kuzmina, S. A., Novenko, E. Y., Bobrov, A. A., Tarasov, P. E., Kuznetsova, T. V., Krbetschek, M. R., Meyer, H., & Kunitsky, V. V. (2004). Late Saalian and Eemian palaeoenvironmental history of the Bol'shoy Lyakhovsky Island (Laptev Sea region, Arctic Siberia). Boreas 33, 319-348.

Are, F., & Reimnitz, E. (2000). An Overview of the Lena Delta Setting: Geology, Tectonics, Geomorphology, and Hydrology. Journal of Costal Research 16, 1083-1093.

Are, F.E. (1999). The role of coastal retreat for sedimentation in the Laptev Sea. In: Kassens, H., Bauch, H.A., Dmitrenko, I.A., Eicken, H., Hubberten, H.-W., Melles, M., Thiede, J., Timokhov, L.A. (eds.). Land–Ocean Systems in the Siberian Arctic: Dynamics and History. Springer-Verlag, Berlin, Heidelberg, New York, 287-295.

Bartsch, A., Gude, M., Jonasson, C., & Scherer, D. (2004). Identification of geomorphic process units in Kärkevagge, northern Sweden, by remote sensing and digital terrain analysis. Geografiska Annaler, Series A: Physical Geography 84, 171-178.

Bauch, H. A., Mueller-Lupp, T., Taldenkova, E., Spielhagen, R.F., Kassens, H., Grootes, P.M., Thiede, J., Heinemeier, J., & Petryashov, V.V. (2001). Chronology of the Holocene transgression at the North Siberian margin. Global and Planetary Change 31, 125-139.

Bauch, H. A., & Kassens, H. (eds.)(in press). Arctic Siberian shelf environments. Special issue, Global and Planetary Change.

Beaulieu, N., & Allard, M. (2003). The impact of climate change on an emerging coastline affected by discontinuous permafrost: Manitounuk Strait, northern Quebec. Canadian Journal of Earth Sciences 40, 1393-1404.

Bindschadler, R., & Vornberger, P. (1998). Changes in the West Antarctic Ice Sheet since 1963 from Declassified Satellite Photography. Science 279, 689-692.

Black, R. F. (1969). Thaw depressions and thaw lakes – a review. Biuletyn Peryglacjalny 19, 131-150.

Bobrov, A. A., Andreev, A. A, Schirrmeister, L., & Siegert, C. (2004). Testate amoebae (Protozoa: Testacealobosea and Testaceafilosea) as bioindicators in the Late Quaternary deposits of the Bykovsky Peninsula, Laptev Sea, Russia. Palaeogeography Palaeoclimatology Palaeoecology 209, 165– 181.

Boike, J., & Yoshikawa, K. (2003). Mapping of periglacial geomorphology using kite/balloon aerial photography. Permafrost and Periglacial Processes 14, 81-85.

Bolshiyanov, D., & Makarov A. (2004). Geomorphologic route along the Urasalakh River. In: Schirrmeister, L., Grigoriev, M. N., Kutzbach, L., Wagner, D., and Bolshiyanov, D. (eds.). Russian-German Cooperation System Laptev Sea: The Expedition Lena-Anabar 2003. Reports on Polar and Marine Research 489, 67-74.

Brigham-Grette, J. (2001). New perspectives on Beringian Quaternary paleogeography, stratigraphy, and glacial history. Quaternary Science Reviews 20, 15-24.

Brook, R. K., & Kenkel, N. C. (2002). A multivariate approach to vegetation mapping of Manitoba's Hudson Bay Lowlands. International Journal of Remote Sensing 23, 4761-4776.

Brown, D. G., Lusch, D. P., & Duda, K. A. (1998a). Supervised classification of types of glaciated landscapes using digital elevation data. Geomorphology 21, 233-250.

Brown, J., Ferrians Jr., O. J., Heginbottom, J. A., & Melnikov, E. S. (1998b). Circum-Arctic Map of Permafrost and Ground-Ice Conditions. In: Parsons, M., Zhang, T. (eds.) (2003). International Permafrost Association Standing Committee on Data Information and Communication (comp.). Circumpolar Active-Layer Permafrost System, Version 2.0. Boulder, CO: National Snow and Ice Data Center/World Data Center for Glaciology. CD-ROM.

Cabot, E. S. (1947). The northern Alaskan coastal plain interpreted from aerial photographs. The Geographical Review 37, 639-648.

Callaghan, T. V., Bjorn, L. O., Chernov, Y., Chapin, T., Christensen, T. R., Huntley, B., Ims, R. A., Johansson, M., Jolly, D., Jonasson, S., Matveyeva, N., Panikov, N., Oechel, W., Shaver, G., Schaphoff, S., & Sitch, S. (2004). Effects of changes in climate on landscape and regional processes, and feedbacks to the climate system. Ambio 33, 459-468.

Carson, C. E., & Hussey, K. M. (1962). The oriented lakes of arctic Alaska. Journal of Geology 70, 417-439.

Catani, F., Farina, P., Moretti, S., Nico, G., & Strozzi, T. (2005). On the application of SAR interferometry to geomorphological studies: estimation of landform attributes and mass movements. Geomorphology 66, 119-131.

Chapin, F. S., Mcguire, A. D., Randerson, J., Pielke, R., Baldocchi, D., Hobbie, S. E., Roulet, N., Eugster, W., Kasischke, E., Rastetter, E. B., Zimov, S. A., & Running S. W. (2000). Arctic and boreal ecosystems of western North America as components of the climate system. Global Change Biology 6, 211-223.

Chavez, P. S. (1996). Image-based atmospheric corrections - revisited and improved. Photogrammetric Engineering and Remote Sensing 62, 1025-36.

Christensen, T. R. (1993). Methane emission from Arctic tundra. Biogeochemistry 21, 117-139.

Christensen, T. R., & Cox, P. (1995). Response of methane emission from arctic tundra to climate change: Results from a model simulation. Tellus 47B, 301-310.

Clark, P. U., & Mix, A. C. (2002). Ice sheets and sea level of the Last Glacial Maximum. Quaternary Science Reviews 21, 1-7.

Conrad, R. (1989). Control of methane production in terrestrial ecosystems. In: Andrae, M. O., & Schimel, D. S. (eds.). Exchange of trace gases between terrestrial ecosystems and the atmosphere. John Wiley and Sons. 39-58.

Coté, M. M., & Burn, C. R. (2002). The oriented lakes of Tuktoyaktuk Peninsula, western Arctic coast, Canada: a GIS-based analysis. Permafrost and Periglacial Processes 13, 61-70.

Czudek, T., & Demek, J. (1970). Thermokarst in Siberia and its influence on the development of lowland relief. Quaternary Research 1, 103-120.

Dansgaard, W., Johnson, S. J., Clausen, A. B., Dahl-Jensen, D., Gundestrup, N. S., Hammer, C. U., Hvidberg, C. S., Steffensen, J. P., Sveinbjornsdottir, A. E., Jouzel, J., & Bond, G. (1993). Evidence for general instability of past climate from a 250-kyr ice-core record. Nature 364, 218-220.

Drachev, S. S., Savostin, L. A., Groshev, V. G., & Bruni, I. E. (1998). Structure and geology of the continental shelf of the Laptev Sea, Eastern Russian Arctic. Tectonophysics 298, 357-393.

Drachev, S. S., Johnson, G. L., Laxon, S. W., McAdoo, D. C., & Kassens, H. (1999). Main structural elements of Eastern Russian Arctic continental margin derived from satellite gravity and multichannel seismic reflection data. In: Kassens, H., Bauch, H. A., Dmitrenko, I. A., Eicken, H., Hubberten, H.-W., Melles, M., Thiede, J., & Timokhov, L. A. (eds.). Land–Ocean Systems in the Siberian Arctic: Dynamics and History. Springer-Verlag, Berlin, Heidelberg, New York, 667–682.

Eisner, W. R., Bockheim, J. G., Hinkel, K. M., Brown, T. A., Nelson, F. E., Peterson, K .M., & Jones, B. M. (2005). Paleoenvironmental analyses of an organic deposit from an erosional landscape remnant, Arctic Coastal Plain of Alaska. Palaeogeography Palaeoclimatology Palaeoecology 217, 187-204.

Eissmann, L. (2002). Quaternary geology of eastern Germany (Saxony, Saxon-Anhalt, South Brandenburg, Thuringia), type area of the Elsterian and Saalian Stages in Europe. Quaternary Science Reviews 21, 1275-1346.

Ermolin, E., De Angelis, H., & Skvarca, P. (2002). Mapping of permafrost on Vega Island, Antarctic Peninsula, using satellite images and aerial photography. Annals of Glaciology 34, 184-188.

Etzelmüller, B., Ødegård, R. S, Berthling, I., & Sollid, J. L. (2001). Terrain parameters and remote sensing data in the analysis of permafrost distribution and periglacial processes: principles and examples from southern Norway. Permafrost & Periglacial Processes 12: 79-92.

Everdingen, R.v. (ed.) (1998, revised 2002). Multi-language Glossary of Permafrost and Related Ground-Ice Terms. In: Parsons, M., Zhang, T. (eds.) (2003). International Permafrost Association Standing Committee on Data Information and Communication (comp.). Circumpolar Active-Layer Permafrost System, Version 2.0. Boulder, CO: National Snow and Ice Data Center/World Data Center for Glaciology. CD-ROM.

Fairbanks, R. G. (1989). A 17,000-year glacio-eustatic sea level record: influence of glacial melting rates on the Younger Dryas event and deep-ocean circulation. Nature 342, 637 - 642.

Fartyshev, A. I. (1993). The peculiarities of Laptev Sea littoral-shelf cryolithozone. Moscow, Nauka. pp. 135. (in Russian).

Fedorov, A. N. (1996). Effects of Recent Climate Change on Permafrost Landscapes in Central Sakha. Polar Geography 20, 99-108.

Florinsky, I. V. (1998). Combined analysis of digital terrain models and remotely sensed data in landscape investigations. Progress in Physical Geography 22, 33-60.

Franke, D., Hinz, K., & Oncken, O. (2001). The Laptev Sea Rift. Marine and Petroleum Geology 18, 1083-1127.

French, H. M. (1974). Active thermokarst processes, eastern Banks Island, Western Canadian Arctic. Canadian Journal of Earth Science 11, 785-794.

French, H. M. (1996). The Periglacial Environment. 2nd ed. Longman: Harlow. pp. 341.

French, H. M. (1999). Past and present permafrost as an indicator of climate change. Polar Research 18, 269-274.

Frost, R. E. (1963). Photointerpretation in the arctic and subarctic. In: First International Conference on Permafrost. National Research Council. Publication 1287.

Galabala, R. O. (1997). Pereletki and the initiation of glaciation in Siberia. Quaternary International 41-42, 27-32.

Gavrilov, A. V., Romanovskii, N. N., Romanovsky, V. E., Hubberten, H.-W., & Tumskoy, V. E. (2003). Reconstruction of Ice Complex Remnants on the Eastern Siberian Arctic Shelf. Permafrost and Periglacial Processes 14, 187–198.

Geological Map Tiksi (1986). R-52-III-IV (Tiksi). 1:200.000. Ministry of Geology, Leningrad, USSR.

Geological Map Ulakhan-Yunkyur (1986). Olenekskaya Seria, S-50-XXI, XXII, XXIII, XXIV (os. Ulakhan-Yunkyur). 1:200.000. Ministry of Geology, Leningrad, USSR.

Giles, P. T., & Franklin, S. E. (1998). An automated approach to the classification of the slope units using digital data. Geomorphology 21, 251-264.

GLOBE Task Team. (1999). The Global Land One-kilometer Base Elevation (GLOBE) Digital Elevation Model, Version 1.0. National Oceanic and Atmospheric Administration, National Geophysical Data Center, 325 Broadway, Boulder, Colorado 80303, U.S.A. URL: http://www.ngdc.noaa.gov/seg/topo/globe.shtml.

Goossens, R., De Man, J., & De Dapper. M. (2000). Research on the possibilities of CORONA-satellite-data to replace conventional aerial photographs in Geo-archaeological studies, practised on Sai (Sudan). In: A decade of Trans-European Remote Sensing Cooperation, Buchroitner, C. (ed). 2001. Balkema Publishers: Lisse/Netherlands, 257-262.

Gorham, E. (1991). Northern Peatlands: Role in the Carbon Cycle and Probable Responses to Climatic Warming. Ecological Applications 1, 182–195.

Gould, W. A., Edlund, S., Zoltai, S., Raynolds, M., Walker, D. A., & Maier, H. (2002). Canadian Arctic vegetation mapping. International Journal of Remote Sensing 23, 4597-4609.

Goward, S. N., Masek, J. G., Williams, D. L., Irons, J. R., & Thompson, R.J. (2001). The Landsat 7 mission: Terrestrial research and applications for the 21st century. Remote Sensing of Environment 78, 3–12.

Gravis, G. F. (1969a). Slope Deposits in Yakutia. Nauka, Moscow: pp. 128. (in Russian).

Gravis, G. F. (1969b). Fossil slope deposits in the northern Arctic asymmetrical valleys. Biuletyn Peryglacjalny 20.

Grigoriev, N. F. (1966). Perennially frozen rocks of the coastal zone of Yakutia. Nauka, Moscow. pp. 180. (in Russian).

Grigoriev, M. N. (1993). Cryomorphogenesis in the Lena Delta. Permafrost Institute Press, Yakutsk. pp. 176. (in Russian).

Grigoriev, M. N., Imaev, V. S., Kozmin, B. M., Kunitsky, V. V., Larionov, A. G., Mikulenko, K. I., Skrjabin, R. M., & Timirsin, K. V. (1996). Geology, seismicity and cryogenic processes in the arctic areas of western Yakutia. Yakutian Scientific Centre SB RAS, Yakutsk. pp. 80. (in Russian).

Grigoriev, M. N., Rachold, V., Bolshiyanov, D., Pfeiffer, E.-M., Schirrmeister, L., Wagner, D., & Hubberten, H.-W. (eds.) (2003). Russian-German Cooperation “System Laptev Sea” The Expedition Lena 2002. AWI Reports on Polar and Marine Research 466, 1-341.

Grinenko, O. V., & Imaev, V. S., (1989). Cenozoic thrusts of the northern part of the Kharaulakh Ridge. Geology and Geophysics 5, 121–123. (in Russian).

Grinenko, O. V., Sergeenko, A. I., Belolyubskiy, I. N. (1998). Regional stratigraphic chart for the Paleogene and Neogene deposits in Eastern Yakutia and the explanatory note. In: Paleogene and Neogene in Northeastern Russia, Part 2. Yakutsk. 5–30. (in Russian).

Grosse, G., Schirrmeister, L., Kunitsky, V. V., & Dereviagyn, A. Y. (2003). Periglacial features around Tiksi. Reports on Polar and Marine Research 466, 137-191.

Grosse, G., Schirrmeister, L., Kunitsky, V. V., & Hubberten, H.-W. (2005, in press). The use of CORONA images in remote sensing of periglacial geomorphology: an illustration from the NE Siberian coast. Permafrost and Periglacial Processes 16.

Grosse, G., Schirrmeister, L., & Malthus, T.J. (submitted). Application of Landsat-7 satellite data and GIS for the quantification of thermokarst-affected terrain types in the periglacial Lena-Anabar coastal lowland. Polar Research.

Grosse, G., Krbetschek, M. R., Schirrmeister, L. (in preparation). Luminescence dating (IRSL) of sediments from permafrost sequences in NE-Siberia.

Grosswald, M. G. (1983). Glaciation of continental shelves. In: Itogi nauki i tekhniki. VINITI. Paleogeografiya. Vyp. 1. M., VINITI, 1-165. (in Russian).

Grosswald, M. G. (1998). Late-Weichselian ice sheets in Arctic and Pacific Siberia. Quaternary International 45-46, 3-18.

Gude, M., G. Daut, Dietrich, S., Mäusbacher, R., Jonasson, C., Bartsch, A., & Scherer, D. (2002). Towards an integration of process measurements, archive analysis and modelling in geomorphology - the Kärkevagge experimental site, Abisko area, northern Sweden. Geografiska Annaler Series A: Physical Geography 84, 205-212.

Gusev, A. I. (1958). To the stratigraphy of Quaternary deposits of western part of the Coastal plain. Sbornik statey po geologii Arktiki., vyp. 5. Trudy NIIGA, t. 80, N 5, L., 79-86. (in Russian).

Guthrie, R. D. (2001). Origin and causes of the mammoth steppe: a story of cloud cover, woolly mammal tooth pits, buckles, and inside-out Beringia. Quaternary Science Reviews 20. 549-574.

Hinkel, K. M., Eisner, W. R., Bockheim, J. G., Frederick, E. N., Peterson, K. M., & Dai, X. (2003). Spatial extent, age, and carbon stocks in drained thaw lake basins on the Barrow Peninsula, Alaska. Arctic, Antarctic and Alpine Research 35, 291-300.

Holmes, M. L., & Creager, J. S. (1974). Holocene History of the Laptev Sea Continental Shelf. In: Herman, Y. (ed.). Marine Geology and Oceanography. Springer-Verlag, New York. 211-229.

Hope, A. S., Boynton, W. L., & Stow, D. A. (2003). Interannual growth dynamics of vegetation in the Kuparuk Riverwatershed, Alaska, based on the Normalized Difference Vegetation Index. International Journal of Remote Sensing 24, 3413-3425.

Hopkins, D. M. (1949). Thaw lakes and thaw sinks in the Imuruk Lake area, Seward Peninsula. Journal of Geology 57, 119-131.

Hubberten, H.-W., Andreev, A., Astakhov, V. I., Demidov, I., Dowdeswell, J. A., Henriksen, M., Hjort, C., Houmark-Nielsen, M., Jakobsson, M., Larsen, E., Lunkka, J. P., Lysså, A., Mangerud, J., Möller, P., Saarnisto, M., Schirrmeister, L., Sher, A. V., Siegert, C., Siegert, M. J., & Svendsen, J. I. (2004). The periglacial climate and environment in northern Eurasia during the last glaciation (LGM). Quaternary Science Reviews 23, 1333-1357.

Hutchinson, M. F. (1989). A new procedure for gridding elevation and stream line data with automatic removal of spurious pits. Journal of Hydrology 106, 211-232.

Imaev, V. S., Imaeva, L. P. & Koz'min, B. M. (2000). Seismotektonika Yakutii. GEOS, Moscow, pp. 226. (in Russian).

Ivanov, O. A. (1972). Stratigraphy and correlation of Neogene and Quaternary deposits in the subarctic plains of East Yakutia. In: Problems of Quaternary Period Research. Moscow, Nauka, 202-211. (in Russian).

Jakobsson, M., Cherkis, N. Z., Woodward, J., Macnab, R., & Coakley, B. (2000). A new grid of Arctic bathymetry: A significant resource for scientists and mapmakers. EOS Transactions, American Geophysical Union 81, 89, 93, 96.

Jia, G. J., Epstein, H. E., & Walker, D. A. (2003). Greening of arctic Alaska, 1981–2001. Geophysical Research Letters 30, 2067.

Jorgenson, M. T., Racine, C. H., Walters, J. C., & Osterkamp, T. E. (2001). Permafrost Degradation and Ecological Changes Associated with a Warming Climate in Central Alaska. Climatic Change 48, 551-579.

Joria, P. E., & Jorgenson, J. C. (1996). Comparison of Three Methods for Mapping Tundra with Landsat Digital Data. Photogrammetric Engineering & Remote Sensing 62, 163-169.

Kaplina, T. N. (1981). History of permafrost in Northern Yakutia during the Late Cenozoic. In: History of the development of perennial frozen deposits in Eurasia. Moscow, Nauka: 153-181. (in Russian).

Kaplina, T. N., & Lozhkin, A. V. (1985). Age and History of Accumulation of the "Ice Complex" of the Maritime Lowlands of Yakutiya. In: Late Quaternary Environments of the Soviet Union. Minneapolis, Univ. Minnesota Press. 147-151.

Kassens, H., Bauch, H. A., Dmitrenko, I. A., Eicken, H., Hubberten, H.-W., Melles, M., Thiede, J., & Timokhov, L. A. (eds.) (1999). Land–Ocean Systems in the Siberian Arctic: Dynamics and History. Springer-Verlag, Berlin, Heidelberg, New York. pp. 711.

Katasonov, E. M. (1954). Lithology of the perennially frozen Quaternary deposits (cryolithology) of the Yana Lowland. Doctoral thesis, Obruchev Permafrost Institute, Moscow. (in Russian).

Katasonova, E. G. (1963). The role of thermokarst in the development of delly. In: Conditions and special features of the formation of frozen horizons in Siberia and in Far-East. Moscow, Isd-vo AN SSSR, 81-100. (in Russian).

Kayalaynen, V. I., & Kulakov, Yu. N. (1966). To the questions of paleogeography of the Yana-Indigirka coastal lowland during the Neogene-Quaternary period. In: Saks V.N. (ed.). Quaternary Period in Siberia. Moscow, Nauka, 274-282 (in Russian).

Kennedy, D. (1998). Declassified satellite photographs and archaeology in the Middle East: case studies from Turkey. Antiquity 72, 553-561.

Kholodov, A. L, Rivkina, E. M., Gilichinsky, D. A., Fyodorov-Davydov, D. G., Gubin, S. V., Sorokovikov, V. A., Ostroumov, V. E., & Maksimovich, S. V. (2003). Estimation of the organic carbon input into Arctic ocean due to erosion of Laptev and East-Siberian seashore. Kriosfera Zemlii 7, 3-12. (in Russian).

Kienast, F., Schirrmeister, L., Siegert, C., & Tarasov, P. (2005). Palaeobotanical evidence for warm summers in the East Siberian Arctic during the last cold stage.- Quaternary Research, in press: doi:10.1016/j.yqres.2005.01.

Kienel, U., Siegert, Ch., Hahne, J. (1999). Late Quaternary palaeoenvironmental reconstructions from a permafrost sequence (North Siberian Lowland, SE Taymyr Peninsula) - a multidisciplinary case study. Boreas 28, 181-193.

Kleiber, H. P., & Niessen, F. (1999). Late Pleistocene paleoriver channels on the Laptev Sea shelf - Implications from sub-bottom profiling. In: Kassens, H., Bauch, H.A., Dmitrenko, I.A., Eicken, H., Hubberten, H.-W., Melles, M., Thiede, J., & Timokhov, L.A. (eds.). Land–Ocean Systems in the Siberian Arctic: Dynamics and History. Springer-Verlag, Berlin, Heidelberg, New York, 657–665.

Kondratjeva, K. A., Krutsky, S. F., & Romanovskii, N. N. (1993). Changes in the extent of permafrost during the Late Quaternary Period in the territory of the former Soviet Union. Permafrost and Periglacial Processes 4, 113-119.

Konishev, V. N., Kolesnikov, S. F. (1981). Specialities of structure and composition of late Cenozoic deposits in the section of Oyogossky Yar. In: Problems of cryolithology, Vil IX. MGU Publishing, Moscow. 107-117. (in Russian).

Krbetschek, M. R., Gonser, G., & Schwamborn, G. (2002). Luminescence dating results of sediment sequences of the Lena delta. Polarforschung 70, 83-88.

Kunitsky, V. V. (1989). Cryolithogenesis of the lower Lena. Permafrost Institute, Academy of Science USSR, Siberian Branch, Yakutsk. pp. 162. (in Russian).

Kunitsky, V. V. (1996). Chemical composition of continuously grown ice wedges of the Ice Complex. In: Cryolithozone and groundwater of Siberia, part I: Morphology of the cryolithozone. Publications of Melnikov Permafrost Institute Yakutsk, Russian Academy of Science, Siberian Branch, Yakutsk. 93-117. (in Russian).

Kunitsky, V. V. (1998). The Ice Complex and cryoplanation terraces on Big Lyakhovsky Island. In: Kamensky, R. M., Kunitsky, V. V., Olovin, B. A., & Shepelev, V. V. (eds.). Problems of geocryology - collected paper. Russian Academy of Science, Siberian Branch, Permafrost Institute Yakutsk. 60-72. (in Russian).

Kunitsky, V. V., Schirrmeister, L., Grosse, G., & Kienast, F. (2002). Snow patches in nival landscapes and their role for the Ice Complex formation in the Laptev Sea coastal lowlands. Polarforschung 70, 53-67.

Lavrushin, Yu. A. (1962). Stratigraphy and some peculiarities of Quaternary deposits formation in the lower reaches of the Indigirka River. Izvestiya AN SSSR, Ser. Geol. 2, 73-87 (in Russian).

Leachtenauer, J. C., Daniel, K., & Vogl, P. T. (1998). Digitising satellite imagery: Quality and cost considerations. Photogrammetric Engineering & Remote Sensing 64, 29-34.

Leverington, D. W., & Duguay, C. R. (1997). A Neural Network Method to Determine the Presence or Absence of Permafrost near Mayo, Yukon Territory, Canada. Permafrost and Periglacial Processes 8, 205-215.

Lewkowicz, A. G. (1981). A study of slopewash processes in the continuous permafrost zone, Western Canadian Arctic. Unpublished Ph.D. thesis, University of Ottawa, Ottawa, Canada.

Lewkowicz, A. G., & Duguay, C. R. (1999). Detection of Permafrost Features Using SPOT Panchromatic Imagery, Fosheim Peninsula, Ellesmere Island, N.W.T.. Canadian Journal of Remote Sensing 25, 33-44.

Lewkowicz, A. G., & Kokelj, S. V. (2002). Slope sediment yield in arid lowland continuous permafrost environments, Canadian Arctic Archipelago. Catena 46, 261-283.

Li, X., Cheng, G., & Chen, X. (1998). Response of permafrost to global change on the Qinghai-Xizang Plateau; a GIS-aided model. Collection Nordicana 57, 657-661.

Lorenz, H. (2004). Integration of CORONA and Landsat Thematic Mapper data for bedrock geological studies in the high Arctic. International Journal of Remote Sensing 25, 5143 - 5162.

Luoto, M. & Seppälä, M. (2003). Thermokarst ponds as indicators of the former distribution of palsas in Finnish lapland. Permafrost and Periglacial Processes 14, 19-27.

Mackay, J. R. (1962). Pingos of the Pleistocene Mackenzie Delta area. Geographical Bulletin 18, 21-63.

Mackay, J. R. (1963). The Mackenzie Delta area, N.W.T. Geographical Branch Memoir. Department of Mines and Technical Surveys, Ottawa. pp. 202.

MacMillan, R. A., Martin, T. C., Earle, T. J., & McNabb, D. H. (2003). Automated analysis and classification of landforms using high-resolution digital elevation data: applications and issues. Canadian Journal of Remote Sensing 29, 592-606.

Mann, D. H., Peteet, D. M., Reanier, R. E., & Kunz, M. L. (2002). Responses of an arctic landscape to Lateglacial and early Holocene climatic changes: the importance of moisture. Quaternary Science Reviews 21, 997-1021.

Meyer, H., Dereviagin, A. Y., Siegert, C., & Hubberten, H.-W. (2002a). Paleoclimate studies on Bykovsky Peninsula, North Siberia - hydrogen and oxygen isotopes in ground ice. Polarforschung 70, 37-51.

Meyer, H., Dereviagin, A., Siegert, C., Schirrmeister, L., & Hubberten, H.-W. (2002b). Palaeoclimate reconstruction on Big Lyakhovsky Island, north Siberia - hydrogen and oxygen isotopes in ice wedges. Permafrost and Periglacial Processes 13, 91-105.

Mollard, J. D. (2000). Ice-shaped ring-forms in Western Canada: their airphoto expressions and manifold polygenetic origins. Quaternary International 68-71, 187-198.

Morrissey, L. A., Strong, L., & Card, D. H. (1986). Mapping permafrost in the boreal forest with thematic mapper satellite data. Photogrammetric Engineering and Remote Sensing 52, 1513-1520.

Murton, J.B. (1996). Thermokarst-lake-basin sediments, Tuktoyaktuk coastlands, western arctic Canada. Sedimentology 43, 737-760.

Nagaoka, D. (1994). Properties of Ice Complex deposits in Eastern Siberia. In: Inoue, G. (ed.). Proceedings of the 2nd Symposium on the Joint Siberian Permafrost Studies between Japan and Russia, 1993. Tsukuba, Japan. 14-18.

Nagaoka, D., Saijo, K., & Fukuda, M. (1995). Sedimental environment of the Edoma in high Arctic eastern Siberia; In: Takahashi, K., Osawa, A., & Kanazawa, Y. (eds.): Proceedings of the 3rd Symposium on the Joint Siberian Permafrost Studies between Japan and Russia in 1994 , 30-31 January 1995, Sapporo, Hokkaido University Press, Japan. 8-13.

Nikolsky, P. A., Basilyan, A. Ye., & Simakova, A. N. (1999). New stratigraphical data of upper Cenozoic deposits in the area of Cape Svyatoi Nos (coast of the Laptev Sea). In: Landscape-climate change, fauna and man during Late Pleistocene and Holocene. Moscow, IGRAN. 51-60. (in Russian).

Osterkamp, T. E., & Romanovsky, V. E. (1999). Evidence for warming and thawing of discontinuous permafrost in Alaska. Permafrost and Periglacial Processes 10, 17-37.

Pavlov, A. V. (1994). Current changes of climate and permafrost in the Arctic and sub- Arctic of Russia. Permafrost & Periglacial Processes 5, 101-110.

Payette, S., Delwaide, A., Caccianiga, M., & Beauchemin, M. (2004). Accelerated thawing of subarctic peatland permafrost over the last 50 years. Geophysical Research Letters 31, doi:10.1029/2004GL020358.

Peddle, D. R., & Franklin, S. E. (1993). Classification of permafrost active layer from remote sensed and topographic evidence. Remote Sensing of Environment 44, 67-80.

Philip, G., Donoghue, D., Beck, A., & Galiatsatos, N. (2002). CORONA satellite photography: An archaeological application from the Middle East. Antiquity 76, 109–118.

Pisaric, M. F. J., MacDonald, G. M., Velichko, A. A., Cwynar, L. C. (2001). The Lateglacial and Postglacial vegetation history of the northwestern limits of Beringia, based on pollen, stomate and tree stump evidence. Quaternary Science Reviews 20, 235-245.

Pollard, W. H., & French, H. M. (1980). A first approximation of the volume of ground ice, Richards Island, Pleistocene Mackenzie delta, Northwest Territories, Canada. Canadian Geotechnical Journal 17. 509-516.

Popov, A. I., (1953). Features of lithogenesis of alluvial plains under the conditions of cold climate. Izvestiya AN SSSR, Ser. Geogr. 2, 29-41 (in Russian).

Popov, A. I. (1969). Underground ice in the Quaternary deposits of the Yana-Indigirka Lowland as a genetic and stratigraphic indicator. In: Pewe, T. L. (ed.). The Periglacial Environment, Past and Present. McGill-Queen's University Press, Montreal, 55-64

Rachold, V., Grigoriev, M. N., Are, F. E., Solomon, S., Reimnitz, E., Kassens, H., Antonow, M. (2000). Coastal erosion vs riverine sediment discharge in the Arctic Shelf seas. International Journal of Earth Sciences 89, 450-460.

Rachold, V. (ed.) (2002). The modern and ancient terrestrial and coastal environment of the Laptev Sea region, Siberian Arctic. Polarforschung 70, 1-157.

Rachold, V., Are, F. E., Atkinson, D. E., Cherkashov, G., & Solomon, S. M. (2005). Arctic Coastal Dynamics (ACD) – An Introduction; Geo-Marine Letters, DOI: 10.1007/s00367-004-0187-9.

Rees, W. G., Williams, M., & Vitebsky, P. (2003). Mapping land cover change in a reindeer herding area of the Russian Arctic using Landsat TM and ETM+ imagery and indigenous knowledge. Remote Sensing of Environment 85, 441-452.

Rigina O. (2003). Detection of boreal forest decline with high-resolution panchromatic satellite imagery. International Journal of Remote Sensing 24, 1895-1912.

Romanovskii, N. N. (1958a). Paleogeographic conditions of formation of the Quaternary deposits on Bol'shoy Lyakhovsky Island (Novosibirsky Islands). In: Questions of Physical Geography of Polar Region; Faculty of Geography, Publications of Moscow State University, 80-88. (in Russian).

Romanovskii, N. N. (1958b). New data about the construction of Quaternary deposits on Bol'shoy Lyakhovsky Island (Novosibirsky Islands). In: Science College Report, Moscow. Geological-Geographical Serie 2, 243-248. (in Russian).

Romanovskii, N. N. (1961). Erosion-thermokarst basins in the northern marine plains of Yakutia and the New Siberian Islands. Merzlotnye issledovaniya. Sbornik statey 1, 124-144. (in Russian).

Romanovskii, N. N. (1993). Fundamentals of cryogenesis of the lithosphere. (Osnowi kriogenesa litosfery). University Press, Moscow State University: pp. 336. (in Russian).

Romanovskii, N. N., Hubberten, H.-W., Gavrilov, A. V., Tumskoy, V.E., Tipenko, G. S., Grigoriev, M. N., & Siegert, Ch. (2000). Thermokarst and Land-Ocean Interactions, Laptev Sea Region, Russia. Permafrost and Periglacial Processes 11, 137-152.

Romanovskii, N. N., Hubberten, H.-W., Gavrilov, A. V., Tumskoy, V. E., & Kholodov, A. L. (2004). Permafrost of the east Siberian Arctic shelf and coastal lowlands. Quaternary Science Reviews 23, 1359-1369.

Rozenbaum, G. E., & Shpolyanskaya, N. A. (1998). Late Cenozoic Permafrost History of the Russian Arctic. Permafrost and Periglacial Processes 9, 247-273.

Rutter, N. W., Rokosh, D., Evans, M. E., Little, E. C., Chlachula, J., & Velichko, A. (2003). Correlation and interpretation of paleosols and loess across European Russia and Asia over the last interglacial–glacial cycle. Quaternary Research 60, 101-109.

Schirrmeister, L., Kunitsky, V., Grosse, V., Meyer, H., Kuznetsova, T., Kuzmina, S., Tumskoy, V., Derevyagin, A., Akhmadeeva, I., Syromyatnikov, I. (2000). Quaternary deposits of Bol'shoy Lyakhovsky Island. Reports on Polar and Marine Research 354, 113-168.

Schirrmeister, L., Kunitsky, V., Grosse, G., Kuznetsova, T., Kuzmina, S., & Bolshianov, D. (2001). Late Quaternary and recent environmental situation around the Olenyok Channel (western Lena Delta) and on Bykovsky Peninsula. In: Rachold V, Grigoryev M. (eds.): Russian-German Cooperation “System Laptev Sea 2000” The Expedition Lena 2000. AWI Reports on Polar and Marine Research 388: 85-135.

Schirrmeister, L., Siegert, C., Kunitsky, V. V., Grootes, P. M., & Erlenkeuser, H. (2002a). Late Quaternary ice-rich permafrost sequences as a paleoenvironmental archive for the Laptev Sea Region in northern Siberia. International Journal of Earth Sciences 91, 154-167.

Schirrmeister, L., Siegert, C., Kuznetsova, T., Kuzmina, S., Andreev, A. A., Kienast, F., Meyer, H., & Bobrov, A. (2002b). Paleoenvironmental and paleoclimatic records from permafrost deposits in the Arctic region of Northern Siberia. Quaternary International 89, 97-118.

Schirrmeister, L., Oezen, D., & Geyh, M. A. 2002c. ^{230}Th/U Dating of Frozen Peat, Bol'shoy Lyakhovsky Island (Northern Siberia). Quaternary Research 57. 253-258.

Schirrmeister, L., Grosse, G., Schwamborn, G., Andreev, A. A., Meyer, H., Kunitsky, V. V., Kuznetsova, T. V., Dorozhkina, M. V., Pavlova, E. Y., Bobrov, A. A., & Oezen, D. (2003a). Late Quaternary History of the Accumulation Plain North of the Chekanovsky Ridge (Lena Delta, Russia): A Multidisciplinary Approach. Polar Geography 27, 277-319.

Schirrmeister, L., Grosse, G., Kunitsky, V. V., Meyer, H., Derevyagin, A., Kuznetsova, T. (2003b). Permafrost, periglacial and paleo-environmental studies on New Siberian islands, Reports on Polar and Marine Reasearch 466, 195-341.

Schirrmeister, L., Grigoriev, M. N., Kutzbach, L., Wagner, D., & Bolshiyanov, D. (eds.) (2004). Russian-German Cooperation System Laptev Sea: The Expedition Lena-Anabar 2003. Reports on Polar and Marine Research 489, 1-209.

Schwamborn, G., Rachold, V., & Grigoriev, M.N. (2002a). Late Quaternary sedimentation history of the Lena Delta. Quaternary International 89, 119-134.

Schwamborn, G., Andreev, A. A., Rachold, V., Hubberten, H.-W., Grigoriev, M. N., Tumskoy, V., Pavlova, E. Y., Dorozhkina, M. V., & Rachold, V. (2002b). Evolution of Lake Nikolay, Arga Island, western Lena River delta, during late Pleistocene and Holocene time. Polarforschung 70, 69-82.

Sellmann, P. V., Brown, J., Lewellyn, R. I., McKim, H. L., & Merry, C. J. (1975). The classification and geomorphic implications of thaw lakes on the Arctic Coastal Plain. Alaska, US Army CRREL Research Report 344, pp. 21.

Semiletov, I. P., Pipko, I. I., Pivovarov, N. Ya., Popov, V. V., Zimov, S. A., Voropaev, Yu. V., & Daviodov, S.P. (1996). Atmospheric carbon emission from North Asian Lakes: A factor of global significance. Atmospheric Environment 30, 1657-1671.

Sher, A. V., Kaplina, T. N., & Ovander, M. G. (1987). Unified Regional Stratigraphic Chart for the Quaternary deposits in the Yana-Kolyma Lowland and its mountainous surroundings - Explanary note. In: Decisions of Interdepartmental Stratigraphic Conference on the Quaternary of the East USSR, Magadan, 1982. USSR Academy of Sciences, Far Eastern Branch, North-Eastern Complex Research Institute, Magadan, USSR, 29-62. (in Russian).

Sher, A., Parmuzin, I., Bartsov, A. (2000). Ice Complex on Bykovsky Peninsula. Reports on Polar and Marine Research 354, 169-182.

Sher, A. V., Kuzmina, S. A., Kuznetsova, T. V., & Sulerzhitsky, L. D. (2005). New insights into the Weichselian environment and climate of the East Siberian Arctic, derived from fossil insects, plants, and mammals. Quaternary Science Reviews 24, 533-569.

Siegert, C., Schirrmeister, L., Kunitsky, V. V., Meyer, H., Kuznetsova, T., Dereviagyn, A., Kuzmina, S., Tumskoy, V., & Sher, A. (1999). Paleoclimate signals of ice-rich permafrost. Reports on Polar and Marine Research 315, 145-259.

Siegert, C., Schirrmeister, L., & Babiy, O. (2002). The sedimentological, mineralogical and geochemical composition of Late Pleistocene deposits from the Ice Complex on the Bykovsky Peninsula, Northern Siberia. Polarforschung 70, 3-11.

Slagoda, E. A. (1991). Microstructure features of the deposits of Ice Complexes in Northern Yakutia (by the example of Bykov Peninsula). In: Gilichinskiy, D. A. (ed.). Soil cryolithology (Kriologiya pochv). IPFS PNTs AN SSSR, Pushchino. 38-47. (in Russian).

Slagoda, E. A. (1993). Genesis and microstructure of cryolithogenic deposits at the Bykovsky Peninsula and the Muostakh Island. Unpublished dissertation thesis. Russian Academy of Science, Siberian Branch, Permafrost Institute Yakutsk. pp. 218. (in Russian).

Slagoda, E. A. (2004). Cryolithogenic deposits of the Laptev Sea coastal plain: Lithology and micromorphology (Bykovsky Peninsula and Muostakh Island). Publishing and Printing Centre, Tyumen. pp. 120. (in Russian).

Smith, L. C., MacDonald, G. M., Velichko, A. A., Beilman, D. W., Borisova, O. K., Frey, K. E., Kremenetski, K. V., & Sheng, Y. (2004). Siberian peatlands – a net carbon sink and global methane source since the Early Holocene. Science 303, 353-356.

Soloviev, P. A. (1973). Thermokarst Phenomena and landforms due to frostheaving in Central Yakutia. Biuletyn Peryglacjalny 23, 135-155.

Stow, D. A, Hop,e A., McGuire, D., Verbyla, D., Gamon, J., Huemmrich, F., Houston, S., Racine, C., Sturm, M., Tape, K., Hinzman, L., Yoshikawa, K., Tweedie, C., Noyle, B., Silapaswan, C., Douglas, D., Griffith, B., Jia, G., Epstein, H., Walker, D., Daeschner, S., Petersen, A., Zhou, L., & Myneni, R. (2004). Remote sensing of vegetation and land-cover change in Arctic Tundra Ecosystems. Remote Sensing of Environment 89, 281-308.

Stratigraphy of the USSR. (1982). Quaternary System, volume 1. Moscow. Nedra. pp. 443. (in Russian).

Stratigraphy of the USSR. (1984). Quaternary System, volume 2. Moscow. Nedra. pp. 556. (in Russian).

Strelkov, S. A. (1959). Stratigraphy of Quaternary deposits of the Laptev and the western part of the East-Siberian Sea coasts. Reports of the inter-ministerial commission for standardisation of the Far-East stratigraphic scheme. Magadan Publishing House, Magadan. 468-471. (in Russian).

Stromquist, L. (1985). Geomorphic impact of snowmelt on slope erosion and sediment production. Zeitschrift für Geomorphologie 29, 129– 138.

Stuiver, M., Reimer, P. J., Bard, E., Beck, J. W., Burr, G. S., Hughen, K. A., Kromer, B., McCormac, G., van der Plicht, J., & Spurk M. (1998). INTCAL98 Radiocarbon Age Calibration, 24000-0 cal BP. Radiocarbon 40, 1041-1083.

Svendsen, J. I., Alexanderson, H., Astakhov, V. I., Demidov, I., Dowdeswell, J. A., Funder, S., Gataullin, V., Henriksen, M., Hjort, Ch., & Houmark-Nielsen, M., Hubberten, H.-W., Ingólfsson, Ó., Jakobsson, M., Kjær, K. H., Larsen, E., Lokrantz, H., Lunkka, J. P., Lysså, A., Mangerud, J., Matiouchkov, A., Murray, A., Möller, P., Niessen, F., Nikolskaya, O., Polyak, L., Saarnisto, M., Siegert, C., Siegert, M. J., Spielhagen, R. F., Stein, R. (2004). Late Quaternary ice sheet history of northern Eurasia. Quaternary Science Reviews 23, 1229-1271.

Tappan, G. G., Hadj, A., Wood, E. C., & Lietzow, R. W. (2000). Use of Argon, Corona, and Landsat Imagery to Assess 30 Years of Land Resource Changes in West-Central Senegal. Photogrammetric Engineering & Remote Sensing 66, 727-736.

Thiede, J., Bauch, H. A., Hjort, C., & Mangerud, J. (2001). The late Quaternary stratigraphy and environments of northern Eurasia and the adjacent Arctic seas - new contributions from QUEEN. Global and Planetary Change 31, 1-474.

Thiede, J., Astakhov, V., Bauch, H., Bolshiyanov, D. Y., Dowdeswell, J. A., Funder, S., Hjort, C., Kotlyakov, V. M., Mangerud, J., & Pyramikov, S. M. (2004). What was QUEEN? Its history and international framework--an introduction to its final synthesis issue. Quaternary Science Reviews 23, 1225-1227.

Toll, E.v. (1895). Die fossilen Eislager und ihre Beziehungen zu den Mammuthleichen. Wissenschaftliche Resultate des Yanalandes und der Neusibirischen Inseln; Mem. Acad. Imper. Sci. St.-Petersbourg, VII Serie, 17, 13, St.-Petersbourg, 1-86. (in German).

Tomirdiaro, S. V. (1970). Eolian-cryogene origin of Yedoma-Complex deposits of North-east USSR. In: Abstracts of the allunion permafrost conference; Moscow, MGU Publishing: 106-107. (in Russian).

Tomirdiaro, S. V. (1980). Loess-glacial formation of east Siberia during Late Pleistocene and Holocene. Moscow, Nauka. pp. 184. (in Russian).

Tomirdiaro, S. V., Arslanov, Kh. A., Chernen'kiy, B. I., Tertychnaya, T. V., & Prokhorova, T. N. (1984). New data on formation of loess-ice sequences in Northern Yakutia and ecological conditions of mammoth fauna in the Arctic during the late Pleistocene. Doklady AN SSSR 278, 6. 1446-1449. (in Russian).

Tomirdiaro, S. V., & Chernenky, V. I. (1987). Cryogenic deposits of East Arctic and Sub Arctic. AN SSSR Far-East-Science Center. 1-196. (in Russian).

Tommervik, H, Hogda, K. A, & Solheim, I. (2003). Monitoring vegetation changes in Pasvik (Norway) and Pechenga in Kola Peninsula (Russia) using multitemporal Landsat MSS/TM data. Remote Sensing of Environment 85, 370-388.

Töyrä, J., Pietroniro, A., Hopkinson, C., & Kalbfleisch, W. (2003). Assessment of airborne scanning laser altimetry (lidar) in a deltaic wetland environment. Canadian Journal of Remote Sensing 29, 718–728.

Treshnikov, A. F. (1985). Atlas Arktiki (Atlas of the Arctic). National Commission of Hydro-Meteorology and Environmental Protection, Major Department of Geodesy and Cartography, USSR. Moscow. pp. 204. (in Russian).

Vandenberghe, J., & Pissart, A. (1993). Permafrost changes in Europe during the last glacial. Permafrost and Periglacial Processes 4, 121-135.

Vasil´chuk, Y. K. (1991). Reconstruction of the paleoclimate of the late Pleistocene and Holocene on the basis of isotope studies of subsurface ice and waters of the permafrost zone. Water Resources 17, 640-674.

Velichko, A. A. (ed.) (1999). Climate and environment changes during the last 65 million years (Cenozoic: From Paleocene to Holocene). GEOS. Moscow, pp. 260. (in Russian).

Vereshchagin, N. K., & Baryshnicov, G. F. (1982). Paleoecology of the mammoth fauna in the Eurasian Arctic. In. Hopkins, D. M., Matthews jr. J. V., Schwerger, C. S., & Young, S. (eds.) Paleoecology of Beringia; Academic Press. 267-279.

Virtanen, T., Mikkola, K., & Nikula, A. (2004). Satellite image based vegetation classification of a large area using limited ground reference data: a case study in the Usa Basin, north-east European Russia. Polar Research 23, 51-66.

Vollossovitch, K. A. (1914). Mammoth of the Bolshoy Lyakhov Island (Novosibirsk Islands). Geological essay. Zapiski Imperial Mineral. o-va, ser.2, t. 50, Petrograd, Tipo-litografiya Birkenfel'da: 305-338. (in Russian).

Vtyurin, B. I.; Grigoryev, N. F., & Katasonov, E. M. (1957). Local stratigraphic scheme of Quaternary deposits at the Laptev Sea coast. Leningrad, Reports of the inter-ministerial commission for standardisation of the Siberian stratigraphic scheme, 1956. 564-572. (in Russian).

Wagner, D., Kobabe, S., Pfeiffer, E. M., & Hubberten, H.-W. (2003). Microbial controls on methane fluxes from a polygonal tundra of the Lena Delta, Siberia. Permafrost and Periglacial Processes 14, 173-185.

Walker, D. A. (1999). An integrated vegetation mapping approach for northern Alaska (1:4 M scale). International Journal of Remote Sensing 20, 2895-2920.

Walsh, S. J., D. R. Butler, & Malanson, G. P. (1998). An overview of scale, pattern, process relationships in geomorphology: a remote sensing and GIS perspective. Geomorphology 21, 183-205.

Washburn, A. L. (1979). Geocryology: A survey of periglacial processes and environments. Edward Arnold, London. pp. 406.

Washburn, A. L. (1980). Permafrost features as evidence of climatic change. Earth Science Reviews 15, 327-402.

Wilkinson, T. J., Bunting, B. T. (1975). Overland transport of sediment by rill water in a periglacial environment in the Canadian High Arctic. Geografiska Annaler 57A, 105–116.

Woolard, J. W., & Colby, J. D. (2002). Spatial characterization, resolution, and volumetric change of coastal dunes using airborne LIDAR: Cape Hatteras, North Carolina. Geomorphology 48, 269-287.

Wulder, M. A., S. E. Franklin, White, J. C., Cranny, M. M., & Dechka, J. A. (2004). Inclusion of topographic variables in an unsupervised classification of satellite imagery. Canadian Journal of Remote Sensing 30, 137-149.

Yershov, E. D. (1998). General Geocryology. Studies in Polar research. Cambridge University Press, Cambridge. pp. 580.

Yoshikawa, K., & Hinzman, L. D. (2003). Shrinking thermokarst ponds and groundwater dynamics in discontinuous permafrost near Council, Alaska. Permafrost and Periglacial Processes 14, 151-160.

Yurtsev, B. A. (2001). The Pleistocene "Tundra-Steppe" and the productivity paradox: the landscape approach. Quaternary Science Reviews 20(1-3): 165-174.

Zhang, T., Barry, R. G., Knowles, K., Heginbottom, J. A., & Brown, J. (1999). Statistics and characteristics of permafrost and ground-ice distribution in the Northern Hemisphere. Polar Geography 23, 132-154.

Zimov, S. V., Voropaev, V. V ., Semiletov, I. P., Davidov, S. P., Prosiannikov, S. F ., Chapin, F. S., Chapin, M. S., Trumbore, S., & Tyler, S. (1997). North Siberian lakes: a methane source fuelled by Pleistocene carbon. Science 277, 800-801.

Acknowledgements

First, I would like to thank Prof. Dr. Hans-Wolfgang Hubberten for the possibility to conduct this work under his general supervision and for his availability, when there was need for discussion. Additionally, I would like to thank him the unique chance of doing field work at exciting places in Siberia, and for his support for my participation in oversea conferences and a DAAD-funded research stay in Edinburgh.

The research for this work was conducted within the German-Russian research co-operations "System Laptev Sea 2000" and "Dynamics of Permafrost" supported by the German Federal Ministry of Education and Research (BMBF).

Many thanks go especially to Dr. Lutz Schirrmeister, who was mentoring me in a wide variety of scientific aspects during this Ph.D. work. I joined him on several Siberian expeditions, and we together survived several adventures in Northern and Central Yakutia. And of course, the discussions with him arising during these field trips, and also after the field season, were most fruitful and contributed a lot to the final picture of this thesis.

Special thanks go to Dr. Viktor V. Kunitsky, who guided Lutz and me through several of the above mentioned Siberian adventures and was thus an experienced and instructive field partner for many scientific and non-scientific tasks.

Another special thank goes to Dr. Christine Siegert, for providing her several decades of Siberian field knowledge and laboratory experience whenever it was necessary to solve problems concerning basic questions in permafrost research.

I also would also like to thank the German Academic Exchange Service (DAAD) for a grant which enabled a four-month research visit to the School of Geosciences, University of Edinburgh, Scotland. During this period atmospheric correction methods and first remote sensing classification approaches for the work described in chapter 4 were evaluated together with my supervisor Dr. Tim J. Malthus.

Many thanks also to all other co-authors in the presented research papers for providing ideas or contributing field data (Drs. Alexander Y. Dereviagyn, Andrei A. Andreev, Elena A. Slagoda). More thanks go to all the other members of the field teams that I joined. They often provided generous help for various tasks in the field and discussions during the long Siberian Polar days.

Furthermore, I highly appreciate the friendly working atmosphere and the generally low level of hierarchy at the AWI Potsdam, both which provided a good stage for most productive discussions. All the other AWI geo- and bio- Ph.D. students I would like to thank for creative scientific and non-scientific discussions, and friendships.

Thanks to Prof. Dr. Hugh M. French and the PPP editorial board for their review and suggested changes to the first paper. Marco Lack, Rene Schmid, and Anne Morgenstern is thanked for their efforts as students in digitising the topographic maps of several investigation sites in Northern Siberia.

I further would like to thank Alexander Kholodov for providing previously unpublished data from some boreholes from the Ivashkina Lagoon on the Bykovsky Peninsula for the inclusion in the cryolithological field database described in chapter 4.

Last but not least many thanks to Dr. Martin Antonow and Dr. Matthias R. Krbetschek who introduced me to German Polar Research during my studies at the Mining Academy and Technical University of Freiberg during 1998-2001.

Other more personal thanks are obvious and thus not particularly mentioned.